

**TRANSPORT AND KINETICS OF AROMATIC HYDROCARBONS INTO
MICRON-SIZED LIQUID DROPLETS:
WITH APPLICATIONS TO ATMOSPHERIC CHEMISTRY**

A Dissertation

Submitted to the graduate faculty of the
Louisiana State University
Agricultural and Mechanical College
in partial fulfillment of the
requirements for the degree of
Doctor of Philosophy

in

The Interdepartmental Program in Engineering Science

by

Suresh Raja

B.Tech. in Chemical Engineering, University of Madras, India, 1998

M.S. in Nuclear Science and Engineering, Louisiana State University, 2001

M.S. in Chemical Engineering, Louisiana State University, 2003

August 2005

ACKNOWLEDGEMENTS

I would like to thank my major professor Dr. Valsaraj for guiding me and supporting me throughout my program here at Chemical Engineering. This work would not have been possible without his constant encouragement and supervision in all aspects of this project. I would like to thank him for giving me the freedom in making decisions related to the various details in this project, which has made me feel capable of performing independent research.

I would like to thank Dr. Ravikrishna for helping in both the fieldwork and lab work. I would like to thank Dr. Reible and Dr. Thibodeaux for their valuable suggestions in the first part of the project. I would like to thank Dr. Wornat for giving me valuable suggestions and insights into this project and for serving in my dissertation committee. I would like to thank Dr. Thompson for teaching me fluid mechanics and transport phenomena and for serving in my dissertation committee. I would like to thank the committee members Dr. Constant at the Department of Civil Engineering and Dr. Gupta at the Department of Petroleum Engineering for serving in this committee.

During the course of this project I sought and received help from various departments in this university. I would like to thank Dr. Kermit Murray at the Chemistry department for help with droplet generator systems. I would like to thank Dr. Caprio and Shane Rolen at the department of biological science for letting me use their capillary puller to design glass nozzle assemblies. I would like to thank the SEM and Electron Microprobe Laboratory at the Geology department for help with use of their equipments. I would like to thank Dr. Collett, Dr. Xiao-Ying Yu and Taehyoung Lee at Colorado State University for their help in field sample collection and use of their equipment.

I would like to thank and acknowledge the constant encouragement and love and support of my mom, brother and sister towards the completion of my degree and during the course of my stay here in the United States. I would like to thank my late dad for being a constant source of inspiration and encouragement. I would like to thank my fiancé Kalpana for being a source of encouragement and support.

I would like to acknowledge the funding provided by the United States National Science Foundation (U.S. N.S.F.) (ATM- 0082836 and ATM-0355291).

TABLE OF CONTENTS

ACKNOWLEDGEMENTS	ii
LIST OF TABLES	vi
LIST OF FIGURES	viii
ABSTRACT.....	xi
CHAPTER 1. INTRODUCTION	1
1.1 Introduction.....	1
1.2 Gas-to-Particle Conversion.....	3
1.3 Analytical Methods in Surface Science	4
1.4 Gas-Liquid Interface	4
1.5 Chemical Species of Interest.....	7
1.6 Sources of Polycyclic Aromatic Hydrocarbons.....	9
1.7 Objective of This Work	11
1.8 Organization of This Dissertation.....	12
CHAPTER 2. FATE AND TRANSPORT OF CHEMICALS IN THE ATMOSPHERIC ENVIRONMENT	14
2.1 Introduction.....	14
2.2 Deposition Pathways.....	14
2.2.1 Dry Deposition.....	14
2.2.2 Wet Deposition	14
2.3 Classification of Atmospheric Reactions.....	16
2.3.1 Homogeneous Gas-Phase Reactions.....	16
2.3.2 Heterogeneous and Multiphase Reactions.....	17
2.4 Gas Uptake Phenomenon of Liquid Droplets	19
2.5 Henry's Law Equilibrium	20
2.6 Effect of Organic Matter.....	22
2.7 Effect of Adsorption at the Air-Water Interface.....	23
2.8 Transport Phenomena of Gas Phase Molecules into Droplets.....	24
2.9 Laboratory Methods to Study Interface Dynamics.....	27
2.9.1 Flow Tube Methodologies.....	27
CHAPTER 3. EXPERIMENTAL METHODOLOGY – DROPLET TRAIN APPARATUS	31
3.1 Introduction.....	31
3.2 Experimental Setup.....	32
3.2.1 Benzene Vapor Generation	32
3.2.2 PAH Vapor Generation.....	32
3.2.3 Droplet Generator	33
3.2.4 Droplet Size Measurement.....	34

3.2.5 Droplet Spacing	35
3.2.6 Droplet Train Apparatus (DTA)	36
3.2.7 Gas Phase Analysis (Benzene and Naphthalene).....	37
3.2.8 Gas Phase Analysis (Phenanthrene).....	38
3.2.9 Liquid Phase Analysis (Naphthalene and Phenanthrene)	38
3.3 Experimental Procedure.....	39
CHAPTER 4. GAS PHASE UPTAKE STUDY:	
RESULTS AND DISCUSSIONS	41
4.1 Uptake of Organic Compounds	41
4.2 Gas-Liquid Mass Transfer Dynamics	43
4.3 Effect of Droplet Diameter on Gas Uptake.....	44
4.4 Effect of Temperature on Mass Accommodation.....	49
4.5 Effect of Dissolved Organic Carbon.....	54
4.6 Summary	56
CHAPTER 5. EXPERIMENTAL METHODOLOGY TO STUDY	
HETEROGENEOUS KINETICS IN LIQUID DROPLETS.....	57
5.1 Introduction.....	57
5.2 Experimental Setup.....	59
5.3 Analytical Chemistry	61
5.4 Experimental Procedure.....	62
CHAPTER 6. HETEROGENEOUS SURFACE REACTIONS: RESULTS AND	
DISCUSSIONS.....	65
6.1 Modeling Mass Transfer and Reaction Kinetics.....	65
6.1.1 Derivation of Overall Mass Transfer Coefficient With Surface Reaction... 68	
6.2 Ozone Reaction With Naphthalene Vapor on Water Droplets	72
6.3 Surface Reaction and Gas Uptake.....	73
6.4 Estimation of Langmuir-Hinshelwood Parameters.....	76
6.5 Effect of Organic Surrogate on Ozone Kinetics	78
6.6 Reaction Products Due to Heterogeneous Oxidation of Naphthalene by Ozone 80	
6.7 Summary	83
CHAPTER 7. MATERIALS AND METHODS IN MONITORING FOGWATER	
CHEMISTRY	84
7.1 Introduction.....	84
7.2 Formation and Deposition Cycle of Fog.....	85
7.3 Previous Work in this Area.....	87
7.4 Types of Fog Collector	89
7.5 Description of Fog Collection Equipments Used in This Work.....	90
7.5.1. High Volume Atmospheric Fog Collector.....	90
7.5.2. Caltech Active Strand Cloudwater Collector (CASCC).....	92
7.6 Analysis of Fog-Water Samples	94
7.7 Data Analysis	95

CHAPTER 8. FOGWATER CHEMISTRY: RESULTS AND DISCUSSIONS.....	97
8.1 Environmental Conditions During Fog Collection	97
8.2 Fogwater Composition.....	101
8.3 Ion Concentration.....	102
8.3.1 Ammonium	102
8.3.2 Sulfate	103
8.3.3 Nitrate	107
8.3.4 Chloride.....	109
8.4 Metal Species Concentrations.....	109
8.5 Organic Species in Fogwater	113
8.5.1 Organic Species: Results of First Fog Collection Campaign.....	113
8.5.2 Organic Species: Results of Second Fog Collection Campaign	114
8.5.2.1 Aromatics and Derivatives.....	114
8.5.2.2 Alkanes and Derivatives	119
 CHAPTER 9. CONCLUSIONS AND POSSIBLE FUTURE DIRECTIONS.....	 122
8.1 Conclusions.....	122
8.2 Possible Future Directions	123
 REFERENCES.....	 125
 VITA.....	 138

LIST OF TABLES

Table 1.1. Henry's Constant and K_{IA} of Benzene, Naphthalene and Phenanthrene at 298 K.....	6
Table 1.2. Physicochemical Properties of Aromatic Hydrocarbons.....	9
Table 4.1. Characteristic Times for Mass Transfer Dynamics in the DTA.....	46
Table 4.2. Interface Partition Constant as Function of Temperature.....	50
Table 4.3. Mass Accommodation Coefficient, Enthalpy, Entropy of Accommodation and Excess Enthalpy of Solution for the Compounds.....	52
Table 6.1 Calculated Mass Transfer Coefficients and Overall Pseudo-First Order Surface Reaction Constant for 55 μ m Droplet Diameter. (At 296 \pm 1K And \sim 760 Torr).....	74
Table 6.2. Influence of Droplet Size on Transport and Kinetic Parameters.....	75
Table 6.3. Langmuir – Hinshelwood Parameters for Ozone at the Droplet Surface for Various Sizes.....	78
Table 6.4. GC/MS Characteristics of the Reaction Products Identified in Liquid Phase.....	81
Table 6.5. Concentration of Identified Liquid Phase Reaction Products.....	81
Table 7.1 Properties of Atmospheric Aerosols (Valsaraj, 2000).....	87
Table 8.1a Description of Conditions During Fog Collection (March 2002 to March 2004).....	98
Table 8.1b Description of Conditions During Fog Collection (November 2004 to February 2005).....	99
Table 8.2 Comparison of the General Characteristics of Fogwater Collected in Baton Rouge and Other Parts of the United States and World. (Collected Between 2002-2004).....	101
Table 8.3. Comparison of Ion Concentrations (μ M) for Fogwater from Baton Rouge and other Parts of United States and the World. (Collected Between 2002-2004).....	103
Table 8.4. Comparison of the Total Metal Concentrations (μ M) in Fog Water in Baton Rouge and other Parts of the United States and the World. (For Samples Collected Between March 2002 to March 2004).....	112

Table 8.5a. Aromatics and Derivatives: Average and Range Fogwater Concentrations	115
Table 8.5b. Aromatics and Derivatives: Average and Range Air Concentrations.	117
Table 8.5c. Comparison of Henry's Constant with K_{DV} Computed Based on Field Data.....	118
Table 8.5d. Scavenging and Dilution Effect of Fogwater on the Gas Phase Pollutants with Time	119
Table 8.6a. Alkanes and Derivatives: Average and Range Fogwater Concentrations ...	120
Table 8.6b. Alkanes: Average and Range Air Concentrations.	121
Table 8.6c. Comparison of Henry's Constant with K_{DV} Computed Based on Field Data (For Alkanes)	121

LIST OF FIGURES

Figure 1.1 Illustration of Processes in Atmospheric Aerosol Particles	2
Figure 1.2. Illustration of Gas-Liquid Partitioning at its Interface	5
Figure 1.3. Molecular Structure of Polycyclic Aromatic Hydrocarbons (PAHs).....	8
Figure 2.1. Schematics of Transport Gas Molecule into Aerosols Resulting in Uptake, Heterogeneous and Multiphase Reactions	18
Figure 2.2. Electrical Circuit Analog for the Gas-Uptake Governed by Gas Phase Diffusion, Mass Accommodation and Bulk Phase Solubility and Reactivity (Shi et al., 1999)	25
Figure 2.3. Schematic of the Various Steps Involved in the Mass Transfer and Uptake Process for an Organic Compound from the Gas Phase to an Aqueous Droplet in Air ...	26
Figure 3.1. Piezo-Ceramic Actuated Droplet Generation Assembly.....	33
Figure 3.2. Glass Capillary Tube Embedded with Piezo-Ceramic Tube (Ulmke et al., 2001).	34
Figure 3.3. Schematic of the Droplet Train Apparatus (DTA) Apparatus Used to Measure the Uptake and Mass Transfer to Water Droplets and Study Organic Compound Interaction with Ozone.....	36
Figure 3.4. Porous Polymer Bed Used for PAH Vapor Adsorption.	38
Figure 4.1. Modeling Gas Uptake by Micron-Sized Droplets. V_t is the Droplet Velocity and H is the Reactor Height. H/V_t is the Gas-Liquid Contact Time (τ).	41
Figure 4.2. Vapor-Droplet Partition Constants (Measured and Predicted) Versus Droplet Sizes for Benzene, Naphthalene and Phenanthrene Uptake. [Gas/Droplet Contact Time = 52ms for Naphthalene and Phenanthrene and 72ms for Benzene].	45
Figure 4.3. The Effect of the Mass Transfer Coefficient for Phenanthrene and Benzene Vapors on the Gas/Droplet Contact Time in the Reactor.	48
Figure 4.4. The Variation in Mass Accommodation Coefficient for Benzene, Naphthalene and Phenanthrene with Temperature.	51
Figure 4.5. Correlations Between Enthalpy of Accommodation and Excess Enthalpy of Solution for Two Classes of Compounds—Aromatic Hydrocarbons and Aromatic Phenols. Data for Phenols are from Müller And Heal, 2002.	53

Figure 4.6. Effects of (Left) Dissolved SDS and (Right) Dissolved SFA on the Vapor-To-Droplet Partitioning of Naphthalene on a 95 μ m Water Droplet.	55
Figure 4.7. The Effect of Dissolved Organic Carbon (Suwannee Fulvic Acid) in Water on the Droplet-Vapor Partition Constant of Phenanthrene and Benzene. Also Shown is the Change in Surface Tension of Water with Increasing Dissolved Organic Carbon.....	55
Figure 5.1. Schematic of the Modified Droplet Train Apparatus where the Saturated Gas Phase PAH Interacts with Ozone on Micron-Size Water Droplets.	60
Figure 6.1 Transport, Surface and Bulk Reaction Kinetics on Gas-Droplet System.....	66
Figure 6.2. Electric Circuit Analog of the Transport, Surface And Bulk Reaction in a Gas-Droplet System.	68
Figure 6.3. Schematic of the Steps Involved in the Mass Transfer and Multiphase Reactions for a PAH Vapor and Ozone at the Surface of a Falling Water Droplet in the Atmosphere.....	69
Figure 6.4. Typical Evolution of Vapor Phase Naphthalene Concentration in mg/mL....	73
Figure 6.5 The Droplet-To-Vapor Partition Constant of Naphthalene on Different Droplet Sizes with Increasing Gas-Phase Ozone Concentrations. The Solid Lines are Predicted Values Based on the K_s Estimated from Equation 6.14 Using k_{max} and $C_{1/2}$ Obtained from Figure 6.6.	75
Figure 6.6. Langmuir Plot of Equation (6.21) with the Values of k_{max} and $C_{1/2}$ Determined from Equation (6.22) and Given in Table 6.3.	77
Figure 6.7. The Effect of Added Fulvic Acid (FA) on (a) The Droplet-To-Vapor Partitioning and (b) The Pseudo First-Order Surface Rate Constant of Naphthalene with Ozone.	79
Figure 6.8. A Schematic of the Reaction Mechanism for Naphthalene with Gas Phase Ozone.	80
Figure 6.9. A Typical GC/MS Trace of the Liquid Collected at the Bottom Outlet of the Reactor. Note the Intermediates Identified in the Text.	82
Figure 7.1. Number of Fog Events Observed Between 2000 and 2003 with Visibility Ranging from Less than 1/4mile to 3/4mile.	85
Figure 7.2. (a) California Institute of Technology (CIT) Rotating Arm Collector. Fogwater Impacts in the Slots on the Leading Edge of the Rotating Arm. (b) Atmospheric Science Research Center (ASRC) String Collector. These Strings Rotate in the Horizontal Plane; Fogwater is Intercepted by the Nylon Strings.....	89

Figure 7.3. Schematics of High Volume Atmospheric Fogwater Collector.....	91
Figure 7.4. Size Fractionating California Active Strand Cloudwater Collector (CASCCsf).....	93
Figure 8.1. Location of Sampling Site.....	100
Figure 8.2. GC/MS Traces of Fogwater and Air Samples Collected Between 2002-2004.....	116

ABSTRACT

In the natural process of wet deposition, gas-water interfaces play an important role in the transport of chemical contaminants in the atmosphere via fog, rain and cloud drops. Evidences from several other works point out deviations in gas-liquid partitioning as predicted by Henry's law. Uptake and mass transfer of benzene, naphthalene, and phenanthrene was chosen to study in a falling droplet train apparatus. Higher droplet-to-vapor partition constant (K_{DV}) was noted for diameters less than 200 μ m and was attributed to surface adsorption and accumulation. Mass transfer of phenanthrene was dependent on gas-phase diffusion and mass accommodation at the interface, while the mass transfer of benzene was dependent on liquid phase diffusion and mass accommodation. Mass accommodation coefficients showed a negative dependence on temperature, resulting in lower partitioning at higher temperatures.

In order to understand the influence of atmospheric oxidants such as ozone on mass transfer and uptake of organic vapors in water droplets, ozone was introduced into the modified droplet train apparatus. Ozone reacted with PAH vapor at the air-water interface, thereby decreasing the mass transfer resistance and increasing the rate of uptake of naphthalene into the droplet. A Langmuir-Hinshelwood reaction mechanism at the air-water interface satisfactorily described the surface reaction, where the surface reaction rate constant increased with decreasing droplet size. The presence of organic matter in the liquid phase resulted in a higher droplet-to-vapor partition constant due to both presence and absence of ozone in the reactor.

Knowledge and observations from the laboratory scale setup were extended to field fogwater characterization. Various chemical properties and characteristics of

fogwater were determined. Most of the chemical composition and make-up of fogwater was characterized due to near-surface local atmosphere. Concentration of certain pesticides and organic compounds were found in the fogwater far exceeding their aqueous solubility. The calculated K_{DV} for the field samples were several orders of magnitude higher than bulk phase Henry's constant prediction. Higher organic compound concentrations were observed in smaller-sized fogwater than in larger-sized droplets. These conclusions support our laboratory observation of higher partitioning due to surface adsorption and due to presence of organic matter in the aqueous phase.

CHAPTER 1

INTRODUCTION

1.1 Introduction

Aerosols are basically fine sub-micron particles dispersed in the gas phase ([Fuchs, 1964](#)). Atmospheric aerosol dispersions in air may be present either as solid particles or liquid droplets. Solid aerosols include smoke and dust which may be natural or anthropogenic, while liquid aerosols include clouds, fogs and mists. Aerosol particles, solid and liquid, range in sizes from 100nm to 100 μ m. Typical aerosol particle concentrations vary according to the atmospheric layer in question. Aerosol particle concentrations closer to the surface may range from 10^7 - 10^8 particles per cm^3 , while the particle concentration in the troposphere may be up to a 10^3 particles per cm^3 .

Interaction of chemical species in the gas phase with aerosols, both liquid (water and ice) in the form of rain, fog and snow, and with solid aerosol particles, is universal and a cyclic process in our biosphere. These atmospheric aerosols undergo an array of processes as they are subject to deposition, by both dry and wet pathways, from its inception. Ambient solid aerosols, known as condensation nuclei, activate and result in nucleation water molecules to form cloudwater and fogwater (See Figure 1.1). Nucleation also occurs on crystalline water ice particles or extra-terrestrial matter, which is removed as it enters the upper atmosphere.

In general, liquid aerosols are composed of both water-soluble and insoluble components, where the insoluble components, initially serve as sites for heterogeneous nucleation. As a result, partitioning of chemicals takes place between the bulk aqueous and particles in the liquid phase, bulk gas phase and bulk aqueous phase, and between the

bulk gas phase and surface of the liquid aerosol particles. Figure 1 illustrates the various processes of atmospheric aerosol particles. The physical and chemical aging (in Figure 1.1) refers to the changes in size distribution, particle morphology and chemical composition that aerosol particles undergo. Simulation and transport methodologies of aerosol transport in confined spaces ([Sajo and Raja, 2002](#)) and characterization and simulations of ambient aerosols transport based on size, composition and morphology are important to understand atmospheric transformations of gas phase chemical species, as heterogeneous chemistry in aerosol particles are size dependent ([Reynolds et al., 1974](#), [McFarland et al., 1997](#)).

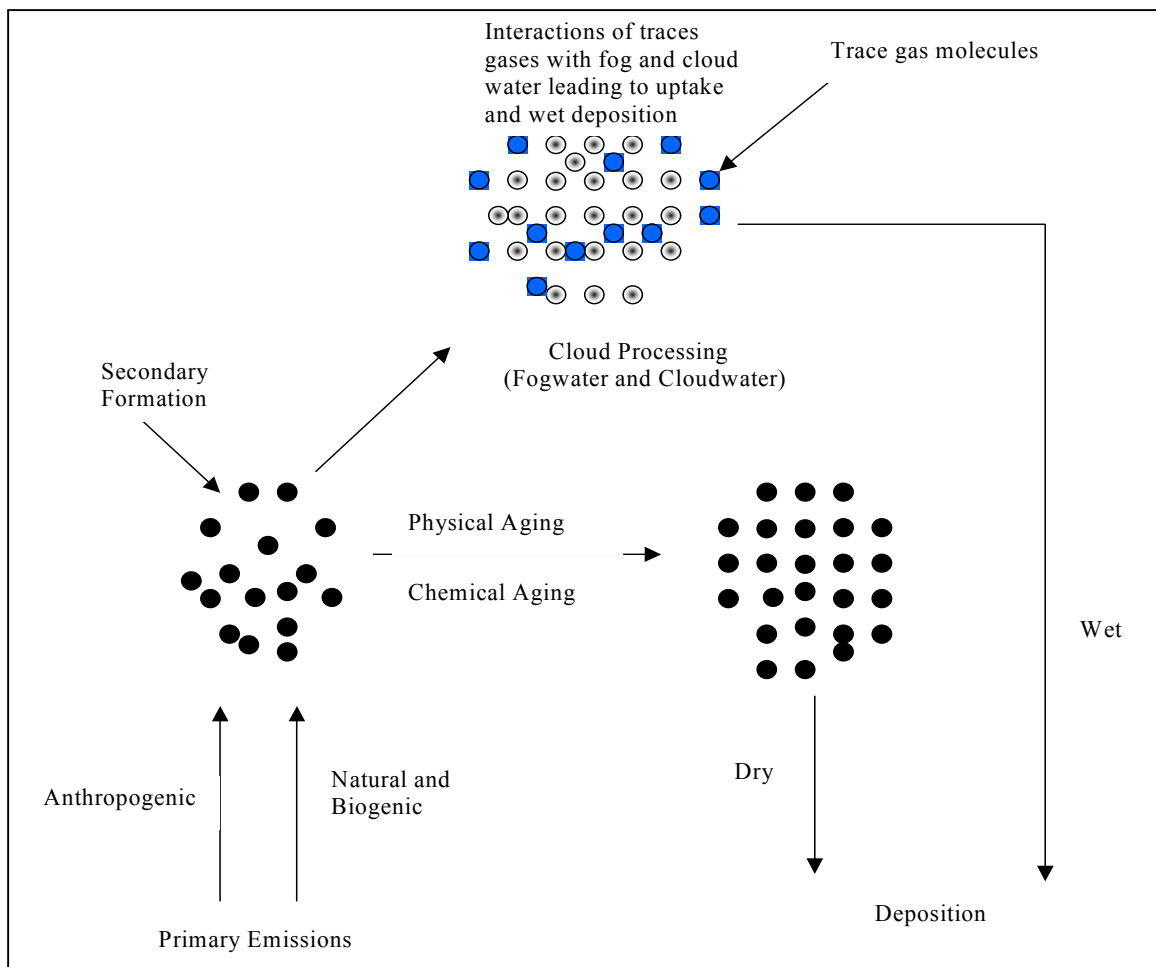


Figure 1.1 Illustration of processes in atmospheric aerosol particles.

The gas phase chemical species that are present in the atmosphere may be both natural and anthropogenic in origin. Changes in size distribution of the cloud droplets take place through condensation of water vapor on the preexisting aerosol particles. Initially, water coated on the solid aerosol particles may re-evaporate before precipitating, whereby the particles are released again to act as nucleation and condensation sites. In certain cases, the aerosol particles grow large enough to form cloud and fogwater droplets.

The so formed cloud droplets remove not only the initial particle that served as the condensation nucleus, but also other particle and gas molecules on its path from the cloud to the earth's surface. This atmospheric process is termed as wet deposition. The mass-transfer of gas molecules to the liquid aerosols (cloud droplets), and in certain cases surface and bulk phase reactions in the droplets, takes place during wet deposition.

1.2 Gas-to-Particle Conversion

The compounds present in the atmosphere exist either in the gas phase or particle phase. Chemical species with high vapor pressures do not form aerosols under atmospheric conditions and hence exist predominantly in the gas phase. The gas-to-particle conversion and partitioning in the atmosphere are dependent on the ambient temperature, the nature and concentration of ambient aerosols, and the interactions between the chemical species and the ambient aerosols. Based on the vapor pressure and the gas-aerosol partition constant ($C_{\text{aer}}/C_{\text{g}}$), chemical compounds are characterized to be present predominantly in the aerosol phase or the gas phase. A certain class of compounds referred to as Semi-Volatile Organic Compounds (SVOC) that include a number of high molecular weight alkanes, polycyclic aromatic hydrocarbons (PAHs),

organochlorine compounds, phthalic acid esters, aldehydes and ketones, and aliphatic and organic acids are present in the gas phase and associated with particles as well.

1.3 Analytical Methods in Surface Science

Thermodynamics and kinetics of adsorption and desorption of gas molecules at a gas-liquid interface can be studied by several methods. Some of the earlier surface adsorption study methods include the Wilhelmy plate method ([Wilhelmy, 1863](#)) and the drop weight method ([Harkins and Brown, 1919](#)). In these methods, by measuring the lowering of surface tension (γ) the free energy per unit area can be obtained. Using these surface tension measurements, a plot of surface tension, γ versus the different concentrations, will yield a slope that is the surface concentration Γ_i , and the suffix i represents a solute. However, these techniques are limited to study of compounds of high vapor pressures.

Other analytical methods available to study gas-liquid interfaces include inverse gas chromatography (IGC) ([Cruickshank et al., 1965](#)). In this method, the mobile carrier gas is used to introduce probes of known characteristics, and the output from the chromatographic analysis, which is the retention time and peak shape, is used to obtain information about the interaction at the interface of the mobile trace gas species and the stationary phase (water film). A part of this project entailed use of IGC to obtain the surface partition constant (K_{IA}) of the gas and aqueous surface film interactions ([Raja et al., 2002](#), [Raja, 2003](#)).

1.4 Gas-Liquid Interface

The gas-liquid interface is an intermediate zone between the two bulk phases, where the transition between the two bulk phases occurs over a thickness of a few

molecular layers. Gas molecules accumulate at the gas-liquid interface on a microsecond time scale and solvate into the bulk liquid, creating a dynamic zone. Interactions, transport kinetics and dynamics of these pollutants (distributed in air) that occur at the interface of fogwater and cloudwater are the interest of this work. Transport and resulting deposition of the various chemical species in the atmospheric environment to various other segments of the biosphere takes place at this environmental interface of air and water.

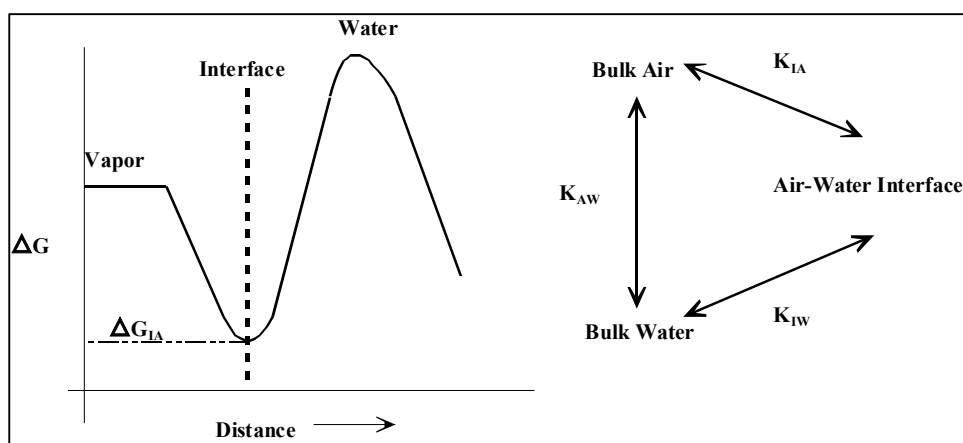


Figure 1.2. Illustration of gas-liquid partitioning at its interface

The Gibbs surface excess, Γ_I identifies the equilibrium concentration at the surface. The partitioning between the air and the surface is defined by the equilibrium constant, $K_{IA} = \Gamma_I/C_A$. Similarly, the equilibrium between the surface and the bulk water phase is defined by another partition constant, $K_{IW} = \Gamma_S/C_W$. Note that, whereas K_{AW} is dimensionless, K_{IA} and K_{IW} have dimensions of length. Thermodynamics dictates that the three constants are related such that $K_{AW} = K_{IA}/K_{IW}$ (Mackay et al., 1991). Figure 1.2 illustrates the free energy profile for an aromatic compound at the gas-water interface.

The free energy minimum shown in Figure 1.2 is connected to the gas, aqueous and the surface concentration through the following equation,

$$\frac{C_1}{C_2} = \exp\left(\frac{\Delta G_{12}}{RT}\right) \quad (1.1)$$

Where the subscripts 1 and 2 represent gas and surface, gas and aqueous bulk phases or a surface and aqueous bulk phase. From [Raja et al., 2002](#), the Gibbs-Helmholtz equation was rewritten as

$$\Delta G_{IA}^0 = -RT \ln \left[\frac{K_{IA}}{\delta_0} \right] \quad (1.2)$$

Substituting equation (1.2) into equation (1.1), we have

$$\frac{C_1}{C_2} = \frac{K_{IA}}{\delta_0} \quad (1.3)$$

Where δ_0 is the standard surface thickness and is the ratio (p_0/π_0), where, p_0 is the standard state pressure equal to 101.325 kPa, and π_0 (=0.06084 mN/m) is the standard state surface pressure given by ([Kemball and Rideal, 1946](#)). The subscripts 1 and 2 in equation (1.3) are for the interface and the bulk gas phase, respectively.

Table 1.1. Henry's constant and K_{IA} of benzene, naphthalene and phenanthrene at 298 K.

Compound	Surface Area [\AA^2]	K_{WA} [-]†	K_{IA} (μm)‡
Benzene	110	4.5 ± 0.1	0.43 ± 0.01
Naphthalene	156	53 ± 4	27.2 ± 1.8
Phenanthrene	198	703 ± 184	1×10^5

† - From [Kochetov et al., 2001](#), [Schwarzenbach et al., 2003](#), [Mackay and Shiu, 1981](#), [De Maagd et al., 1998](#), [Bamford et al., 1999](#), [Staudinger et al., 1981](#) ‡ - From [Raja et al., 2002](#)

At a given temperature (298 K) the value of K_{IA} are such that, phenanthrene > naphthalene > benzene, indicating that the surface adsorption is proportional to the surface area of the molecule. The K_{IA} value for naphthalene obtained at 298 K is nearly 80 times larger than that for benzene and for phenanthrene it is nearly 250,000 times that of benzene. There is ample evidence in the literature that the orientation of aromatic

hydrocarbons on the water surface is parallel to the air-water interface. Therefore the greater the surface area of the molecule the greater will be the interaction energy with the water surface, and therefore the larger the partition constant. From the values of K_{IA} given in Table 1.1, and equation (1.3) we can expect that the accumulation of gas phase phenanthrene will be more pronounced at the gas-water interface than for gas phase benzene.

The transport of gas phase molecules into aqueous droplets is complex and convoluted with diffusion and adsorption of gas molecules on the droplet surface before they are completely solvated in the aqueous phase. The process of physical adsorption of gas phase chemical species at the surface can lead to heterogeneous chemical reactions ([Bertram et al., 2001](#)) at the surfaces of liquid aerosols in addition to the bulk aqueous phase chemical reactions. Generally speaking the size range of liquid aerosols in the environment, such as fogwater and rainwater, are about 1-10 μ m for fogwater and about a tenth of centimeter for rainwater. More on this sub-topic is covered in chapter 2 and in later chapters.

1.5 Chemical Species of Interest

In the class of SVOC present in the atmosphere, the presence of hydrophobic organic compounds such as PAHs, PCBs and pesticides has been reported in fogwater and rainwater ([Glotfety, 1990](#), [Capel et al., 1990](#), [Schomburg et al., 1991](#), [Zhang and Anastasio, 2001](#)). In addition to their presence in the fogwater, deviations in anticipated equilibrium concentrations as predicted by Henry's law has been reported ([Goss and Schwarzenbach, 1999](#), [Gill et al., 1983](#)). The presence of PAHs in fogwater in the

aqueous phase and its suspected carcinogenic nature warrants study of their fate and transport in the atmospheric environment.

Out of the myriad of organic compounds that are present in the atmosphere, most do not form aerosols under atmospheric conditions due to their high vapor pressure. In the class of SVOC, organic compounds further subdivided and known as polycyclic aromatic hydrocarbons (PAHs), are present in both gas phase and aerosol phase. The environmental fate of the PAHs depends partly on their distribution between the particle and gas phase. In this class of compounds (PAHs), certain compounds are more hydrophobic, and have relatively lower vapor pressure and are present exclusively in the gas phase that may be scavenged by wet deposition. While other higher molecular weight compounds are present predominantly in the particle phase and hence scavenged by dry deposition. In this work three compounds were chosen to study the gas-liquid partitioning, namely, benzene, naphthalene and phenanthrene. The properties of the compounds studied in this work are listed in Table 1.2. The rationale in choosing these compounds to study the gas-liquid uptake and interactions can be attributed to their existence predominantly in the gas phase, at 25 °C, due to low gas-aerosol partition constant ($C_{\text{aer}}/C_{\text{g}}$) in the order of 10^{-2} to 10^{-3} . While the other compounds in this class, such as benzo[a]pyrene and chrysene are predominantly in the aerosol phase with higher $C_{\text{aer}}/C_{\text{g}}$ ([Pankow and Bidleman, 1991](#)).

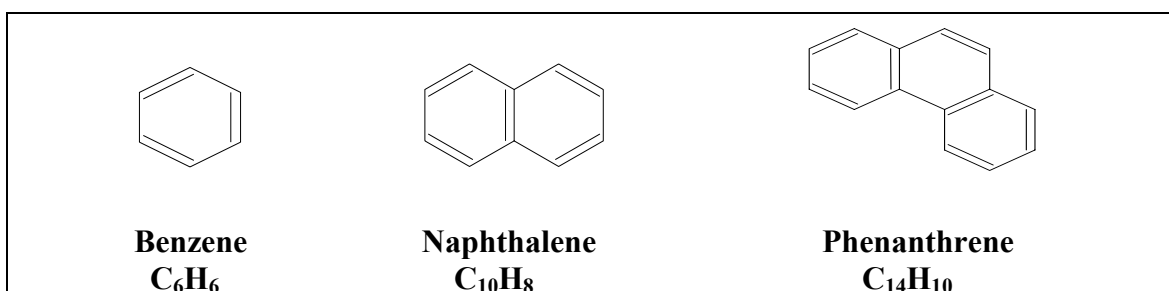


Figure 1.3. Molecular Structure of Polycyclic Aromatic Hydrocarbons (PAHs).

It has also been identified that this class of compounds are ubiquitous ([Saxena, P., Hildemann 1996](#), [Baek et al., 1991](#)) and are identified in the form of bicyclical gas-phase naphthalene to seven or more fused ring species such as coronene.

Table 1.2. Physicochemical properties of aromatic hydrocarbons

Property	Benzene	Naphthalene	Phenanthrene
Molecular weight	78	128	178
Solubility in Water [$\mu\text{g/mL}$]	170	31.7	1.29
Sub cooled liquid vapor pressure, $P_s(l)^\circ$ [kPa]	12.7	0.037	9×10^{-5}
Enthalpy of condensation, ΔH° [kJ/mol]	-34	-58	-75
Enthalpy of solvation, $\Delta_{\text{solv}}H^\circ$ [kJ/mol]	-31	-47	-54

From ([Valsaraj, 2000](#), [Cabani et al., 1981](#))

1.6 Sources of Polycyclic Aromatic Hydrocarbons

The sources of PAHs are mainly anthropogenic, formed during the incomplete combustion of organic matter such as coal, oil, gasoline fuel and wood ([Jenkins et al., 1996](#)). Other sources of PAHs are natural forest fires and volcanic eruptions ([Nikolaou et al., 1984](#)). Sources such as residential heating, industrial processes, open burning, and power generation are estimated to account for roughly 80% of the annual total PAH emissions in the United States with the remainder produced by automobile sources ([Peters et al., 1981](#), [Ramdahl et al., 1984](#)).

The presence of PAHs in water, aquatic sediments and organisms has been recognized for more than 40 years ([Neff, 1979](#)). With the development of sensitive high-resolution techniques for the analysis of PAH in environmental samples, it has become

apparent that extremely complex mixtures of PAHs, including the carcinogenic forms of benzo[a]pyrene, are nearly ubiquitous trace contaminants in aquatic ecosystems. A considerable amount of research has been conducted in recent years on the sources, fates and biological effects of these PAH mixtures in aquatic ecosystems by [Andelman and Sues, 1970](#) and [Andelman and Snodgrass, 1972](#). The sources of PAH found in these aquatic systems are myriad ranging from endogenous to anthropogenic. However, the endogenous sources of PAHs are static and remain in the organism and ecosystem. The anthropogenic sources of PAH reach the aquatic environment by spillage of crude and refined oil, in industrial and domestic effluents, runoff water from land, and by dry or wet deposition in the atmosphere. Hence, it is important to understand the fate and transport dynamics of PAH in the environment.

A twelve-month monitoring program for PAHs and carbonyl compounds were performed in Hong Kong ([Lee et al., 2001](#)). Their studies show highest concentration of Naphthalene ($=993 \text{ ng/m}^3$) and high concentrations of other PAHs, such as phenanthrene, anthracene, and pyrene, in the urban atmosphere of Hong Kong among the other PAHs. Similar studies on PAHs show their presence in Munich ([Schnelle-Kreis et al., 2001](#)). Also, studies done here in metro Baton Rouge area by [Subramanyam et al., 1994](#) characterize their presence in the air.

Table 1 lists the physicochemical properties of aromatic hydrocarbons that were used in this study. Each of these compounds (benzene, naphthalene and phenanthrene) is hydrophobic. The decreasing aqueous solubility and vapor pressure with increase in molecular weight indicate increasing hydrophobic nature of the molecules. Of the three compounds listed, the last two compounds are an important class of compounds known as

Polycyclic Aromatic Hydrocarbons (PAHs) that are ubiquitous in air and due to its hydrophobic nature accumulate in organic rich environments such as lipids, aerosols and soil particles.

With only carbon and hydrogen, PAHs are very stable organic molecules. These molecules are flat, with each carbon having three neighboring atoms much like graphite. Some of the compounds under this class of PAHs are suspected carcinogens and hence their fate and transport in environment is of much interest. The first few studies with respect to the carcinogenic nature of these PAHs were by [Bingham et al., 1979](#). Most of the studies reported by Bingham were of the occurrences of cancer among refinery workers. More recently, [Lewis et al., 1984](#) showed carcinogenic potential of petroleum hydrocarbons on skin.

1.7 Objective of This Work

Gas-water and gas-solid interfaces play significant roles in the fate and transport of contaminants in the environment through dry and wet deposition. Previous studies show that partitioning at the gas-water interface of aerosols (liquid and solid) present as a dispersion with vapor phase is much more important than the bulk air and water phases partitioning. The accumulation of gas molecules at the interface and the resulting droplet-vapor partitioning in fog, mist and bubbles cannot be estimated by Henry's constant, due to deviations in Henry's law prediction.

An intriguing suggestion is that the large variation in aerosol size and adsorption at the large gas-water interfacial area of fog droplets may account for the deviation ([Perona, 1992](#), [Valsaraj et al., 1993](#)). In addition to this, presence of colloidal matter, pH and temperature have also been suggested as reasons for these deviations. Inverse gas

chromatography was used in the first part of this work to determine the interface partition constant, K_{IA} ([Raja et al., 2002](#)). Thermodynamic analysis shows that accumulation of surface-active hydrophobic phenanthrene is more pronounced than less hydrophobic benzene at the gas-water interface.

In order to test the above hypothesis, the gas uptake phenomenon by micron-sized droplets was studied using a falling droplet apparatus. In this experimental apparatus droplet size, temperature and droplet organic carbon concentration were varied to observe the effect on droplet-to-vapor partitioning (K_{DV}). Further experiments were undertaken to test this hypothesis under natural field conditions in the metro Baton Rouge area, by collecting fogwater and air samples.

1.8 Organization of This Dissertation

In this work, the transport parameters of hydrophobic aromatic compounds into aqueous droplets and the associated thermodynamic functions are to be determined using the laboratory scale Droplet-train flow Tube Apparatus (DTA). The effect of droplet uptake of gas-phase species as a function of droplet diameter, due to the presence of organic matter in aqueous phase, and heterogeneous reactions of PAHs on micron-sized droplets by ozone are to be elucidated. The influence of an oxidative species (eg., ozone) on the kinetics and mass transfer of PAHs in droplet-gas interactions and the associated influence on surface kinetics, as a function of droplet diameter are studied in this work. Chapter 2 gives an overview of the supporting materials that was used in this study. General transport phenomena involved in this multiphase system of gas and water are discussed in its entirety. Chapters 3 and 4 involve the experimental methods used in this work to study the uptake process and its results and discussions presented in the

subsequent chapter. Since the heterogeneous kinetics involved a modification to the experimental methodology used for the general uptake study, a separate chapter for the experimental methods and the results and discussions are given in chapters 5 and 6, respectively.

Illustration of the phenomena studied and observed in a laboratory scale setup, and other associated fog-water atmospheric chemistry studied are to be emphasized by field samples of fog-water and air samples collected near an agricultural cultivation field in the Metro Baton Rouge area. Chapter 7 and 8 discuss the experimental methods and results, respectively. Possible future directions and recommendations that may be of interest in the atmospheric chemistry area are discussed in chapter 9.

CHAPTER 2

FATE AND TRANSPORT OF CHEMICALS IN THE ATMOSPHERIC ENVIRONMENT

2.1 Introduction

The fate and transport of a chemical species in the environment is broadly subject to two paths of removal from the atmosphere, namely the dry and wet deposition. The method of scavenging (deposition) and the resulting partitioning of a chemical species depend on the properties of the species in question, atmospheric conditions, and the surface topography.

2.2 Deposition Pathways

2.2.1 Dry Deposition

Dry deposition is the transport of gaseous and particulate matter from the atmosphere onto the surface of the earth in the absence of precipitation. The factors that govern dry deposition of gaseous and particulate matter are the level of atmospheric turbulence, chemical properties of the depositing species, and the nature of the surface. Dry deposition is usually characterized by a deposition velocity, and the amount of species deposited can be calculated if the deposition velocity (dependent on the particle diameter) and the pollutant concentration are known.

2.2.2 Wet Deposition

In the case of wet deposition, the gas molecules are dissolved in cloud, fog rain or snow and these water droplets deposit onto the earth's surface and this is called "wet" deposition. The gas phase uptake by liquid droplets is complex and may include not just transport of the gas molecule resulting in scavenging of the pollutant from the atmosphere. The uptake process may include bulk phase equilibrium and also surface

equilibrium established between the large air-water interface and air. In certain cases, the atmospheric system and the aqueous and/or the gas phase molecules may be reactive, resulting in surface and bulk phase kinetics. The rate of transfer of the air (chemical pollutant), which may comprise both gas and particles into aqueous phase, is defined by the term called washout ratio ([Eisenreich et al., 1981](#)),

$$W = \frac{C_{aq}}{C_{air}}, \quad (2.1)$$

where C_{aq} and C_{air} are the total concentrations of the chemicals in the aqueous phase and air. The wet deposition is relatively complex in comparison to the dry deposition process, primarily due to the involvement of multiple phases. The multiple phases include the three phases, gas, aerosol, and aqueous. In addition, the possibility of the presence of aqueous phase in several other forms, such as fog-water, rain, snow, ice crystals, sleet, and hail, complicates the process even further.

The importance of gas and particle scavenging can be highlighted by the following equation ([Van Ry et al., 2002](#)), $W_T = W_G \cdot (1 - \varphi) + W_P(\varphi)$, where W_G and W_P is the gas phase and particle phase scavenging coefficients, respectively, and φ is the fraction present as atmospheric particles. W_G is the inverse of the compound's Henry's law constant.

The equilibrium of a species between the gas and aqueous phase can be represented by the Henry's law coefficient. The customary units of Henry's law coefficient are mol/L-atm. Henry's law constant can also be defined to dimensionless if the gas-phase concentration is expressed in moles per liter of air and the aqueous phase concentration in moles per liter of water, and their ratio is the dimensionless Henry's law

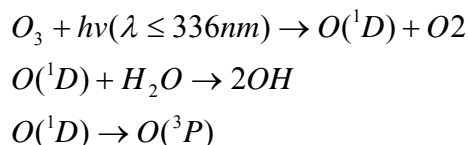
constant. In actuality, the dimension is in liters of air per liters of water. It is important to note that Henry's law is applicable only to dilute solutions.

2.3 Classification of Atmospheric Reactions

The atmospheric reactions may be classified into two categories: (1) homogeneous gas-phase reactions and (2) heterogeneous gas-particle interactions and multiphase reactions. Generally a multiphase reaction occurs on the surface and in the bulk of fogwater or a cloudwater. Typically a fog or cloud is formed by condensation of water on the surface of sub-micron aerosol particles, when the air temperature cools down to its dew point temperature. Generally, chemical reactions on the surface of an aerosol particle and on the surface or the bulk-water of cloud or a fog droplet have higher reaction rate constants in comparison to a reaction rate constant for a homogeneous gas phase or the bulk aqueous phase reaction.

2.3.1 Homogeneous Gas-Phase Reactions

Ozone is the one of the oxidants in troposphere and stratosphere gas phase chemistry in addition to OH free radical and NO_x. In the troposphere, it initiates oxidation through the formation of OH free radical and electronically excited O(¹D). In the following equation only a fraction of the O(¹D) formed generates OH by reaction with water vapor, while the remaining deactivates to ground state.



Typically, the only known reaction to produce ozone in the atmosphere is by photolyses of NO₂ to NO and O, where the oxygen atom combines with O₂ to form O₃, ([Seinfeld, 2004](#)). More information on the ozone production and its role in heterogeneous

and multiphase reactions is presented in chapter 5. Gas phase reactions of volatile chemicals and degradation rates in the atmosphere are modeled based on photolysis frequencies and rate constants of reactions with atmospheric oxidants such as OH radicals, ozone, NO₃ and chlorine. The conversion of gas phase emissions of nitrogen oxides from combustion sources to produce gaseous species such as N₂O₅ and HNO₃ ([Finlayson-Pitts and Pitts Jr., 1986](#), [Seinfeld, 1986](#)).

2.3.2 Heterogeneous and Multiphase Reactions

The heterogeneous chemistry on aerosols (both solid and liquid dispersions) in the atmosphere plays an important role in determining the composition of the gaseous troposphere ([Kolb et al., 1995](#), [Ravishankara, 1997](#)). In the context of atmospheric chemistry, the heterogeneous reactions are those that occur on the surface of the aerosol particles and multiphase reactions are those that take place in the bulk of the liquid phase. Atmospheric reactions in gas-liquid and gas-solid systems include an array of transport processes that results in surface-bound and bulk phase reactions.

The first step in the transport of a gas molecule to the gas-liquid or a gas-solid interface is the transport of gas molecule to the surface. At the interface, the gas molecules either bounce off or are taken up at the surface determined by the gas-surface collision frequency (given by kinetic molecular theory) and the gas phase diffusion coefficient (D_g). The uptake at the interface is defined by the mass accommodation coefficient (α). Resulting accommodation and adsorption of the gas molecule at the interface may result in surface reaction referred to as heterogeneous reaction on the aerosol particle surface. Both the reaction product formed at the interface and the parent molecule solvate into the bulk of the liquid aerosol. In the case of the solid aerosol

particle the reaction is confined to the surface as diffusion in and out of the bulk of the solid is too slow to effect the concentration at the surface. The resulting solvation of the vapor phase molecule and the reaction products was modeled based on the critical cluster theory proposed by Davidovits and coworkers ([Davidovits et al., 1995](#)). Diffusion into the bulk phase is determined by the diffusion coefficient in the liquid (D_L). Based on the nature of the compound, diffusion into the bulk phase is slower than in the gas phase and controls the mass transport of the gas molecule. Aqueous bulk phase reactions occur at a region closer to the surface or in the interior aqueous bulk phase. If the contact time between the gas-liquid systems is sufficiently large, the entire system attains equilibrium and can be predicted by Henry's law constant. Figure 2.1 illustrates the transport process of gas molecules into aerosols. More details on uptake kinetics are discussed in the sections 2.7.

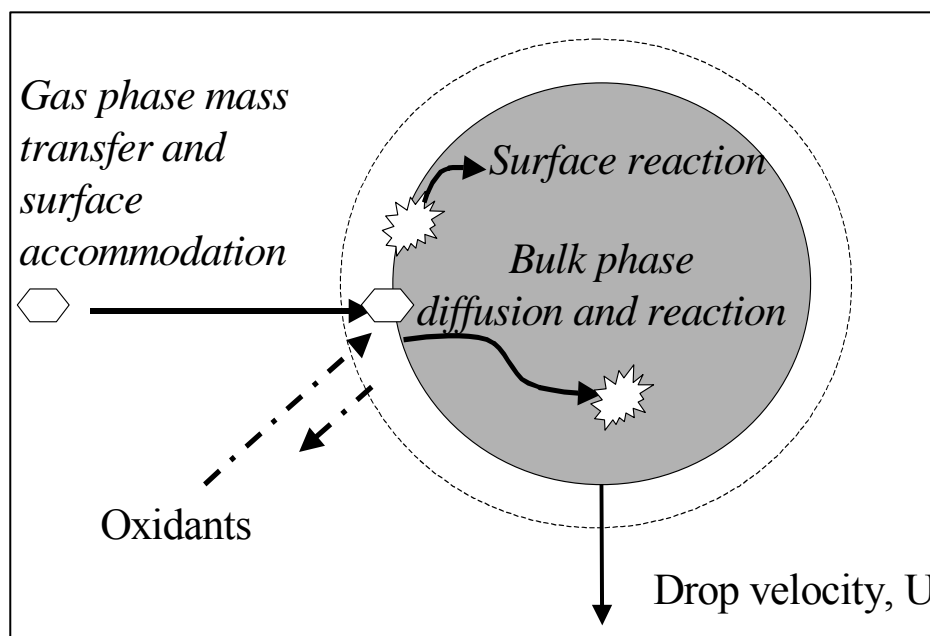


Figure 2.1. Schematics of transport gas molecule into aerosols resulting in uptake, heterogeneous and multiphase reactions.

The current modeling strategy and interest in the atmospheric chemistry community is geared towards being able to quantify the size distribution of aerosols in the atmosphere based on the observed atmospheric composition. During uptake, heterogeneous and multiphase reactions in aerosol particles, changes in atmospheric gas composition occur. It has been suggested that surface bound heterogeneous reaction products may also be released into the gas phase ([Thomas et al., 2001](#)). The ability to predict the atmospheric gas composition will depend on the understanding of microphysics of particle formation ([Ravishankara, 1997](#)).

2.4 Gas Uptake Phenomenon of Liquid Droplets

In general transport of gaseous species into an aqueous droplet can be solved assuming that the droplet does not shrink or swell. Assuming that the surface contains the dissolved species in equilibrium with the bulk gas phase. With an initial zero droplet concentration C and constant bulk gas concentration at all times at $x = \infty$, D_L is liquid phase diffusion coefficient and k is the reaction rate constant, the transport equation is given as

$$\frac{\partial C}{\partial t} = D_L \nabla^2 C - kC \quad (2.2)$$

The appropriate driving force (mass transfer flux) for this transport process of bulk gas phase species into the liquid droplet can be written as, $J = K_C (C_{bulk} - C_{surface})$, where K_C (m/s) is the mass transfer coefficient. In gas absorption by aqueous droplets, Henry's law solubility can be used to define the equilibrium concentrations of bulk gas and liquid. The thickness of the interface with the dissolved species can be estimated by $(D_L t)^{1/2}$.

2.5 Henry's Law Equilibrium

The partitioning of a chemical species between the gas and a condensed phase (water) is calculated assuming equilibrium between the phases and is given by Henry's law ([Schwartz 1986](#), [Seinfeld 1986](#)). Consider a soluble species that exists in a foggy atmosphere or falling raindrops. The rate of transfer of a gas to the surface of a stationary or falling drop (J) is given by

$$\begin{aligned} J &= K_c (C_g - C_{eq}) \\ H &= \frac{C_{aq}}{C_{eq}} \end{aligned} \quad (2.3)$$

Most of the transport models use Henry's law equilibrium for calculating the wet deposition fluxes. The model of atmospheric transport and chemistry, known as MATCH, considers only dissolution of species in the liquid phase, as given by Henry's law ([Crutzen and Lawrence, 2000](#)).

In most of the atmospheric studies, where both the gas and the bulk aqueous phase concentrations has been measured, significant deviations in Henry's law has been observed ([Richards et al., 1983](#), [Munger et al., 1990](#), [Winiwarter et al., 1988](#)). This deviation can be particularly consequential in the case of cloud-water and fog-water samples, which have large surface area to volume ratio. As a result, calculation of gas phase scavenging by cloudwater and fogwater without corrections for the Henry's law deviations will result in significant errors. In order to give a mechanistic explanation to the surface area effect, consider an ensemble of fogwater droplet with a certain size distribution, say 2 μm to 30 μm , in contact with a polluted atmosphere. The concentration of the chemical pollutants observed in the fogwater, and hence the droplet-to-vapor partition due to the gas phase transport will be observed to be higher than the bulk

Henry's constant. Therefore, this enhanced gas uptake phenomena can be characterized to the large surface area available in a foggy atmosphere for the mass transfer process.

Field sampling of bulk cloud and fog-water (1-10 μ m dia.) show deviations from Henry's constant as a result of the uptake of gas phase species by the liquid aerosols ([Glotfelty et al., 1987](#), [Schomburg et al., 1991](#), [Capel et al., 1990](#), [Okochi et al., 2004](#)). There are several reasons for the unexpected enrichment. The presence of colloidal organic matter in the fog and cloud water ([Glotfelty et al., 1990](#), [Schomburg et al., 1991](#), [Capel et al., 1990](#) and [Capiello et al., 2003](#)), the temperature influence on the Henry's law constant, different aqueous phase properties ([Pandis and Seinfeld., 1991](#)), and large specific air-water interfacial area available for adsorption of hydrophobic organic compounds ([Valsaraj et al., 1993](#)) are some of the suggested reasons for these deviations and enhanced uptake in the aqueous phase.

[Pandis and Seinfeld, 1991](#) have put forward theories to explain the "Henry's Law Deviations". Work by others ([Karger et al., 1971](#), [Valsaraj, 1988](#) and [Mackay et al., 1991](#)) have shown the air-water interface to be a significant compartment for species accumulation in this regard. More recently [Hoff et al., 1993](#) have discussed evidence in support of their contentions.

Species accumulation at the interface can be considerable in the case of hydrophobic compounds. The hydrophobic nature of a chemical species is attributed to their chemical property; such as its high activity coefficient and low aqueous solubility. The "solvophobic theory" proposed by ([Franks and Evans, 1945](#)) describes a large decrease in entropy upon dissolution of non-polar compounds in water, due to increased ordering of water molecules around the non-polar molecule. Accumulation of

hydrophobic solute molecules occur at the “the air-water interface” where the least number of water molecules interact with them. Thus, the interface acts as a zone for accumulation of a species, and is particularly pronounced in the case of a hydrophobic solute. Also as discussed in section 1.3, accumulation of solute molecules at the interface increases with increasing interface partition constant K_{IA} . The compounds analyzed in this work are phenanthrene, naphthalene and benzene, with phenanthrene having the lowest vapor pressure and aqueous solubility and is the most hydrophobic and benzene having highest vapor pressure and aqueous solubility and is the least hydrophobic.

2.6 Effect of Organic Matter

Atmospheric cloud water is known to compose largely (~70%) of organic compounds ([Saxena and Hildemann, 1996](#), [Zappoli et al., 1999](#), and [Facchini et al., 1999](#)). Presence of organic compounds that are surface active have been observed by [Gill et al., 1983](#) and [Facchini et al., 2000](#). Decrease in surface tension, higher uptake and surface-active nature of cloud and fogwater have been attributed to the presence of humic-like substances in the solution ([Facchini et al., 2000](#), [Capiello et al., 2003](#)). The presence of organic matter (OM) in cloud and fogwater increases the dissolved concentration of PAHs that associate with OM and adds to the overall load of PAHs in fogwater.

Humic-like substances are natural organic matter present in the environment and can be extracted from soil. There are two types of humic-like substances available; they are humic acids and fulvic acids. Humic acids are not soluble in water under acidic conditions, but are soluble at higher pH values. They can be extracted from soil by various reagents and are brown to black in color. The fraction of humic substances that is

soluble in water under all pH conditions are known as fulvic acid. Fulvic acids are light yellow to yellow-brown in color.

2.7 Effect of Adsorption at the Air-Water Interface

The effect of adsorption of gas phase species can be considered for potentially two scenarios, (1) gas molecule is water soluble and surface active and (2) gas molecule is water insoluble and surface active. It is also obvious that the atmosphere is composed of many types of gas molecules simultaneously, which may include scenarios (1) and (2), as a result the uptake of one species will influence the uptake of other species.

Let us consider a system composed of a droplet, trace gas, and the interface of the droplet and gas. According to mass conservation, we have the following equation:

$$N_{VAP} + N_{SURF} + N_{SOL} = N \quad (2.4)$$

The total droplet concentration can be written as the sum of the surface concentration and the bulk aqueous phase concentration as follows,

$$N = N_{SURF} + N_{SOL} \quad (2.5)$$

$$N_L (mol) = C_g^* (K_{IA} A_W + K_{WA} V_W)$$

Where K_{IA} is the surface adsorbed partition constant at equilibrium (units of length), K_{WA} is dimensionless Henry's constant (C_{Liquid}/C_{Gas}); A_W and V_W are the surface area and the volume of the liquid droplet, respectively, C_g^* is the gas phase concentration in equilibrium with the liquid phase. For the case when K_{IA} is small the total liquid phase concentration is determined by the Henry's law equilibrium constant in equation 2.5. On the contrary, when K_{IA} is large or when the droplet diameter is very small, the liquid phase concentration is determined by both the surface concentration term and bulk equilibrium concentration term. Inverse Gas Chromatography (IGC) was used to

determine the value of K_{IA} (listed in Table 1.1) in the preceding work of this project for the test compounds ([Raja et al., 2002](#)), viz., benzene, naphthalene and phenanthrene. From the values of K_{IA} , we can expect that the surface adsorption term to be more pronounced for phenanthrene than for benzene. Similarly, the surface adsorption is important as the droplet size decreases.

2.8 Transport Phenomena of Gas Phase Molecules into Droplets

Multiphase reactions and/or interactions of the liquid water droplets and gases occur in the various layers of the atmosphere ([Seinfeld, 1986](#)). In this regard, the initial entry of the gas species into the liquid is governed by the mass accommodation coefficient α together with a convolution of other transport processes such as diffusion, surface saturation, solubility and reactivity ([Danckwerts, 1951](#), [Worsnop et al., 1989](#)). The mass accommodation coefficient α is the probability that an atom or molecule striking the liquid surface enters into the bulk liquid phase.

$$\alpha = \frac{\text{no. of molecular entering the liquid surface}}{\text{no. of molecular collisions with the surface}} \quad (2.6)$$

The general processes of mass transfer in a gas/liquid interaction are as follows:

- (1) Diffusion of gas molecules to the liquid surface
- (2) Accommodation of the gas molecule on the surface
- (3) Chemical conversion if any to form a soluble product
- (4) Liquid phase diffusion of dissolved products away from liquid surface

As mentioned earlier, the uptake of gas molecule by the droplet is characterized by the total mass transfer flux to the droplet, as $J = K_C (C_{bulk} - C_{surface})$,

$$\frac{1}{K_C} = \frac{1}{k_g} + \frac{4}{\bar{C} \cdot \alpha} + \frac{1}{\xi K_{WA}} \cdot \sqrt{\frac{\pi \tau}{4D_L}} \quad (2.7)$$

In the above equation ([Seinfeld, 1998](#)), K_C is the mass transfer coefficient that is an ensemble of all the transport processes listed above. The first term on the right hand side of equation (2.7) represents the resistance due to gas-phase diffusion, which is given by $(d_D/2D_g)$. Where d_D is the droplet diameter and D_g is the gas phase diffusion coefficient. The resistance due to mass accommodation is given by the second term and that of solubility is the third term. The schematics of the sequence of steps involved in the uptake process of the gaseous species by a droplet are shown in the Figure 2.3, with the electric circuit analog of the process shown in Figure 2.2. The uptake process is characterized by diffusion of the gas species from the bulk of the gas to the surface of the liquid droplet. At the surface of the droplet the gas-species is subjected to mass accommodation as defined in equation (2) or evaporation. Once the gas phase species is accommodated on the surface, based on the surface saturation limitation that is related to the Henry's law solubility, the gas species is solvated into the bulk liquid.

However, in certain instances with reactive species, such as ozone and hydroxyl radicals (OH), present the surface reactivity may occur faster than the rates they occur in the bulk liquid ([Worsnop et al., 1989](#)). Recent experiments by [Tolocka et al., 2004](#) have shown the importance of reactive uptake and surface kinetics over the transport process entailed in a gas to liquid mass transfer.

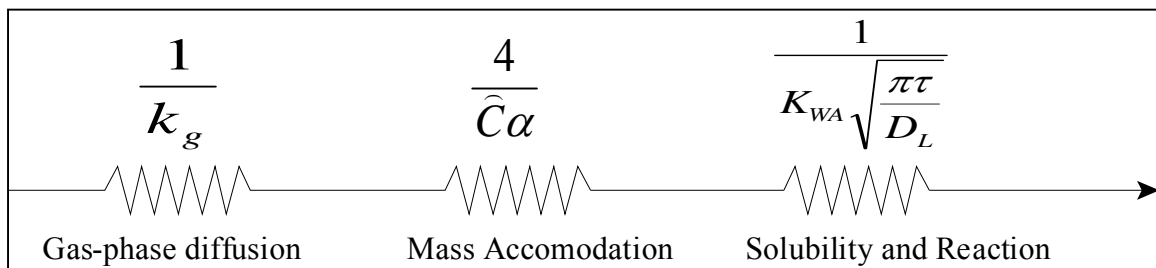


Figure 2.2. Electrical circuit analog for the gas-uptake governed by gas phase diffusion, mass accommodation and bulk phase solubility and reactivity ([Shi et al., 1999](#)).

The total uptake process can be represented as an electrical circuit analog, a resistive model, as shown in Figure 2.2 with the mass transfer coefficient shown in equation 2.7 (Seinfeld, 1986). As shown in Figure 2.2, all the resistances in the uptake processes are hypothesized to occur in series. Figure 2.3 is an illustration of the processes.

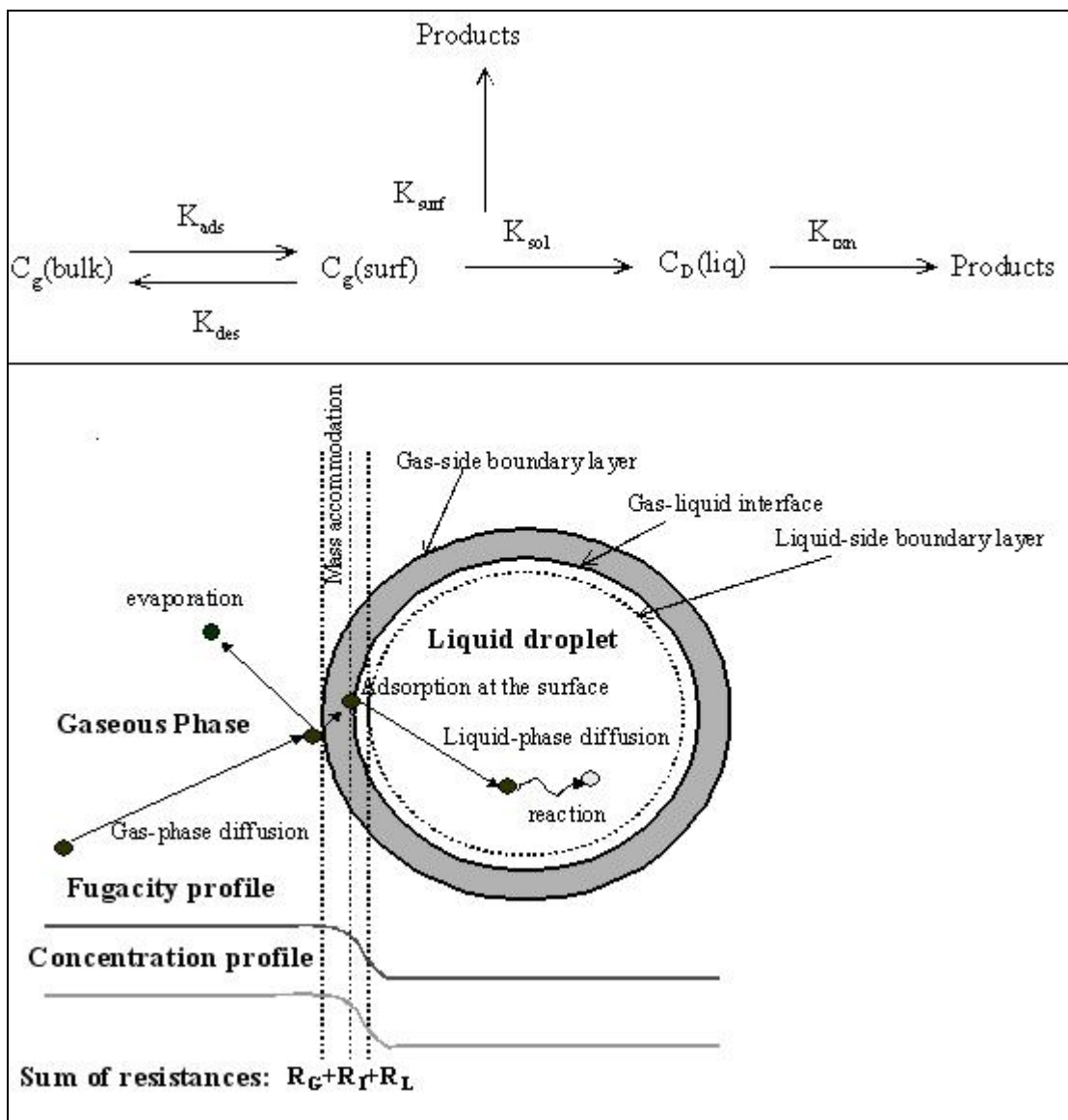


Figure 2.3. Schematic of the various steps involved in the mass transfer and uptake process for an organic compound from the gas phase to an aqueous droplet in air.

The solubility resistance is a function of the contact time of the gas and droplet and is initially zero at time $t=0$. As a result, the solubility resistance increases with increasing contact time, and also the surface saturation of the droplet surface varies depending on the Henry's law solubility of the gas in the aqueous droplet. In order to deconvolute the uptake process, and to study the significance of each transport rate-limiting step a droplet train apparatus that renders control of certain factors that affect the uptake process was developed as discussed in the next chapter.

2.9 Laboratory Methods to Study Interface Dynamics

Currently, the techniques that are used to determine and study the uptake characteristics at the interface are variant forms of the aerosol flow tube apparatus. Most of the earlier works were performed using a Knudsen-cell reactor ([Golden et al., 1973](#), [Iraci et al., 2002](#)), which is essentially a low-pressure chamber with the liquid surface introduced with the test gas phase through an orifice. The uptake of the gas phase species by the liquid surface is estimated from the difference in inlet and outlet concentrations. Currently, there are a lot of work performed in flow tube designs to study interaction of gas molecules with liquid surfaces ([McMurry and Stolzenburg, 1987](#)), and variants of this design can be used to study the interactions of gas with droplets, bubbles or aerosols ([Gardner et al., 1987](#), [Jayne et al., 1992](#), [Katrib et al., 2001](#)).

2.9.1 Flow Tube Methodologies

Interaction of the solid or liquid surfaces with gas species can be performed in a flow tube apparatus by coating the tube walls with the condensed phase materials and introducing the gas phase using a movable injector ([Huff et al., 2000](#)). In most cases coating the flow tube walls is cumbersome, and alternately the condensed phase material

is coated on to a glass plate to study gas phase interactions with surfaces. In a flow tube apparatus, it is possible to simulate low-pressure troposphere and stratosphere conditions and as well as below-cloud atmospheric pressures.

A droplet-train flow reactor ([Shi et al., 1999](#), [Smith et al., 2002](#)), consist of a flow tube in which droplets generated either in a vertical chamber or a coaxial chamber interacts or reacts with a test gas-phase species. In certain cases, the gas can be reactive or inert with respect to the liquid. In this methodology, it is also possible to study liquid droplets or sub-micron particles that can form volatile vapors that react with the gas molecules. The variants of this methodology are called Droplet Train Flow Reactor, Bubble Train Flow Reactor and Aerosol Flow Reactor. Other methodologies include, an aerosol flow tube ([Hanson and Lovejoy, 1996](#)), liquid-jet coaxial flow reactor ([Kirchner et al., 1990](#)) and impinging-flow methods ([Shimono and Koda, 1996](#)), wetted wall flow reactor ([Muller and Heal, 2002](#)) and are in essence similar to the droplet train apparatus. Other novel techniques to study gas-liquid interface are the electrodynamic levitation cell ([Schwell et al., 2000](#)).

[Saylor and Handler, 1997](#), studied gas transport across air-water interface with waves generated on the aqueous surface in the form of capillary waves. The uptake of CO₂ in this interface was studied by observing the change in pH in the water phase while the gas phase CO₂ concentration was maintained constant. The uptake was studied at various capillary wavelengths that are representative of the air/water interface observed in ocean and sea surfaces.

In comparison to all these techniques, the electrodynamic levitation cell is different from the other mentioned above. Here the droplets are generated by a piezo-

actuated droplet generator, and are levitated by applying voltage to the electrodes on the sides of the chamber and hence brought in contact with the gas phase. In this technique, the time dependent optical properties of the droplet surface are monitored to study the gas uptake process in the droplet. The presence of “wall-effects” ([Hanson et al., 2004](#)), an inevitable phenomenon in a flow tube apparatus, is absent in a levitated droplet apparatus ([Schwell et al., 2000](#)). Evidently, there is no consensus in the results obtained from the various methodologies to study surface interactions. Despite the discrepancy in the results, the choice of methodologies is to be made in regards to the nature of problem in hand and the scenario that needs to be simulated.

Study of solid aerosol particle interaction with reactive gas phase species has been studied in a form of aerosol flow tube reactor ([Katrib et al., 2004](#)). In this methodology, the solid aerosol particle is coated with the reactive material and allowed transport through a series of flow tube before it reacts with oxidative species.

In each of these methods used to study gas and liquid interactions, a liquid surface (a film or a droplet) is brought in contact with the test gas-phase species. Accurate information about the surface coverage of the film or surface area of the droplet, the gas phase concentration and its associated system conditions, and the gas-aqueous phase contact times are important to determine the properties associated with the interface dynamics.

The properties associated with the gas-liquid interface kinetics and mass transfer include the gas phase diffusion to the aqueous surface, its accommodation/adsorption at the gas-liquid interface and subsequent dissolution into the bulk liquid and reaction in the

bulk liquid phase. In certain instances, surface reactions ensuing mass accommodation and adsorption is a possibility.

CHAPTER 3

EXPERIMENTAL METHODOLOGY – DROPLET TRAIN APPARATUS

3.1 Introduction

Unlike current microscopic methodologies, such as scanning electron microscope fluorescence microscopy, scanning probe microscope, to study adsorption on surfaces, the heterogeneous and multiphase gas and droplet interaction/kinetics require a system that can eliminate or control certain transport process. Even though transport processes in a multiphase system takes place in the molecular level, observing macroscopic changes (bulk gas and liquid phase concentration) in a multiphase system using a Droplet Train Apparatus (DTA) and by controlling or estimating certain parameters, we can study the transport dynamics involved at a molecular level.

In the experimental setup discussed below, the gas diffusion limitations are reduced by use of micron sized droplets, and low reactor pressure. Saturation of Liquid droplets with gas phase species resulting in desorption of gas molecules from the droplet is avoided by use of low gas molecule concentration. Monitoring the concentration in the liquid and vapor phase at the reactor outlets, the droplet-to-vapor concentration ratio (K_{DV}) is determined. Using K_{DV} we can estimate the overall mass transfer coefficient (K_C) and the mass accommodation coefficient (α). In essence, the gas-liquid interactions is studied by bringing the gas phase molecules in contact with the liquid phase, after a controlled period of interactions the amount of gas molecules dissolved in the liquid phase is measured. The challenge was to limit, control or design techniques (in the DTA) that de-convolute the several processes involved in the overall uptake of the gas and determine the parameters involved in the uptake process. The DTA shown in Figure 3.3

was modeled after [Worsnop et al., 1989](#). In a previous work, Inverse Gas Chromatography (IGC) was used to determine the thermodynamic properties and equilibrium interfacial constant in the adsorption process of hydrophobic compounds, such as Benzene, Naphthalene and Phenanthrene, at a gas-water interface ([Raja et al., 2002](#), [Raja, 2003](#)). Using this data and other parameters that can be defined in this system, it was possible to study the transport of organic vapors into micron-sized droplets. The important parameters in this experiment are the gas-liquid contact time and the surface area of the liquid droplet in contact with the gas.

3.2 Experimental Setup

3.2.1 Benzene Vapor Generation

The benzene vapors were generated by passing helium gas through a porous sparger set inside a glass column filled with about 25mL of benzene. To obtain reproducible carrier gas flow rates in the glass column, a mass flow controller (Sierra instruments Inc., 8100 series) was used to set the helium flow rate to glass column at $55 \times 10^{-6} \text{ m}^3/\text{min}$. The gas concentration obtained in this manner range from 100 to 300 $\mu\text{g}/\text{mL}$. In all the compounds generated in the vapor phase helium was used due to its inert nature.

3.2.2 PAH Vapor Generation

The vapor generator was made of two tubular stainless steel columns (SS 316, 0.762m long, 0.013m o.d.) connected serially and each packed with 15 g of Chromosorb P (60/80 mesh nonacid washed, obtained from Supelco Inc., Bellefonte, PA). The Chromosorb P was mixed with a hexane solution containing pure naphthalene (99.9%, Fisher Scientific Co., St. Louis, MO). Excess hexane was evaporated, thereby obtaining

PAH-coated Chromosorb P. The average loading obtained this way was about 0.02 g of naphthalene per gram of support, and in the case of phenanthrene 0.1 g/g. The coated packing was supported with glass wool on both ends. To obtain reproducible carrier gas flow rates in the chamber a mass flow controller (Sierra instruments Inc., 8100 series) was used to set the helium flow rate to the saturation chamber at $55 \times 10^{-6} \text{ m}^3/\text{min}$. The gas concentrations obtained in this manner ranged from 0.7 to 1.5 ppm_v for naphthalene and 0.1 to 3 ppb_v in the case of phenanthrene.

3.2.3 Droplet Generator

The droplet generation assembly was made of high-density polyethylene (HDPE) with a reservoir volume of $1.16 \times 10^{-4} \text{ m}^3$. The droplets were generated using a commercially available sapphire orifice assembly (O'Keefe Controls Co., Trumbull, CT) with the desired orifice diameter (30-100 μm).

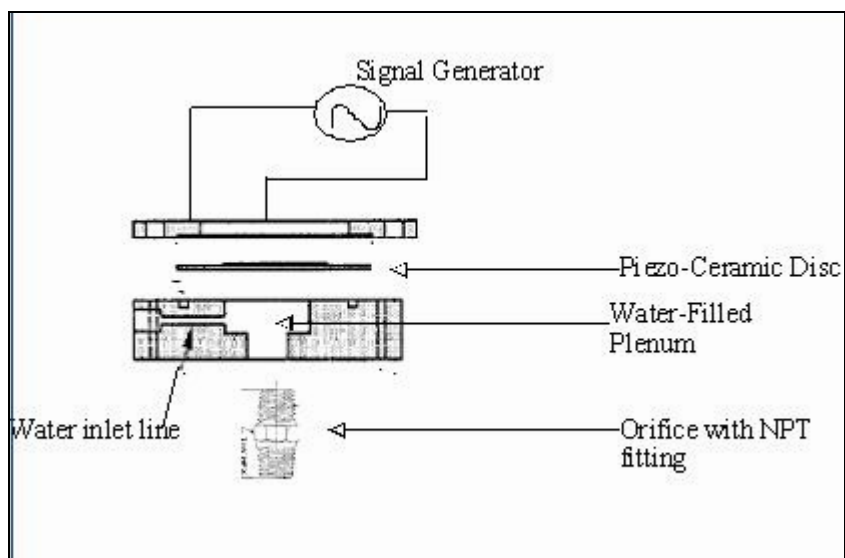


Figure 3.1. Piezo-ceramic actuated droplet generation assembly.

A piezo-ceramic crystal (American Piezoceramics Inc., Mackeyville, PA) placed above the orifice, shown in Figure 3.1, was mechanically vibrated to generate droplets of a given size that depended on the frequency, amplitude and pulse width of the applied

signal, and the orifice diameter (Yang et al., 1997). Distilled, de-ionized water was fed to the droplet generator using a model LGP pump (Graylor Dyneco Co., Cape Coral, FL). In the case of droplets of size lesser than $55\mu\text{m}$, a glass nozzle assembly was used to generate droplets (Ulmke et al., 2001).

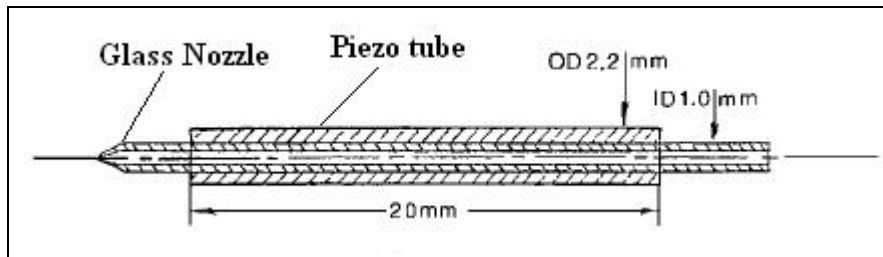


Figure 3.2. Glass capillary tube embedded with Piezo-ceramic tube (Ulmke et al., 2001).

The glass nozzle assembly shown in Figure 3.2 consists of a capillary glass tube of about 1mm internal diameter embedded inside a piezo tube and sealed at the ends with adhesive. A specific diameter glass nozzle was obtained using a capillary puller that consists of a filament heater that softens the glass tube and stretched slowly until break off. The glass tip diameter is reduced to about $20\mu\text{m}$ in the capillary puller and is smoothed and viewed under a light microscope to determine the exact nozzle diameter.

A constant flow of distilled, de-ionized water was fed to the glass nozzle assembly using a syringe pump obtained from KD Scientific. The electric pulse applied to the piezo tube transforms into mechanical vibration and transmitted to the capillary tube, thereby breaking the stream into clearly spaced droplets.

3.2.4 Droplet Size Measurement

The droplet stream was photographed using a Tiffen 62-mm standard hot mirror lens connected to a desktop computer by a 30-frame-per-second interface frame grabber. The pictures were analyzed using OPTIMAS 6.2 version software. The droplet diameters that were quantified in this manner were on an average $1.89d_{\text{orifice}}$, which was in

agreement with the observations of [Shi et al., 1999](#). The droplet diameters can also be determined based on the liquid flow rate and the frequency applied on the piezo-ceramic

disk as follows, $d = \left[\frac{6F}{\pi f_d} \right]^{1/3}$ ([Worsnop et al., 1989](#)), where F is the jet stream flow rate

through the orifice and the f_d is the frequency applied in units of Hertz. For example, for an applied frequency of 15kHz, and a typical average jet stream flow rate of 0.0125cm³/sec the estimated droplet diameter corresponds to about 118.6µm, while photographic measurements show about 94.5µm. The droplet radius determined photographically was used in all the calculations.

3.2.5 Droplet Spacing

In order to obtain widely spaced droplets the pulse generator was operated at different frequencies and the droplet spacing was monitored by illuminating the droplets by use of a laser beam and observed by the naked eye. The smaller the applied frequency, the more widely spaced droplets were obtained. The spacing of the droplets can be quantified using the following equations. The Rayleigh formula ([Rayleigh, 1879](#)) for natural breakup of droplets is given as $f_o = v_d / 4.5d_o$. For example, a 50µm nozzle used for droplet generation would have an average droplet size computed based on frequency applied and by fast photography techniques mentioned above, to be about 98µm. Based on the droplet velocity and the observed droplet size, the droplet spacing (d_c) can be computed as $d_c = v_d / f_o$, to be about 425µm which corresponds to about 4 center-to-center droplets spacing.

3.2.6 Droplet Train Apparatus (DTA)

The DTA has a flow tube where the micron-sized droplets that were generated in the top portion of the reactor, interact with the gas-phase species through a set of two spargers as shown in Figure 3.3. A sparger is a porous frit assembly placed within the reactor in the form of a perforated ring, which yield a fairly uniform concentration distribution of the gas stream along the radial direction of the reactor.

The droplets generated in the top section of the reactor passed through a long cylindrical stainless steel reactor (0.0245m i.d., 0.32m long) and exited the bottom into a collection chamber. In order to limit the gas phase seepage into the liquid collection chamber, a 1400 μ m nozzle was used to connect the liquid collection chamber to the reactor.

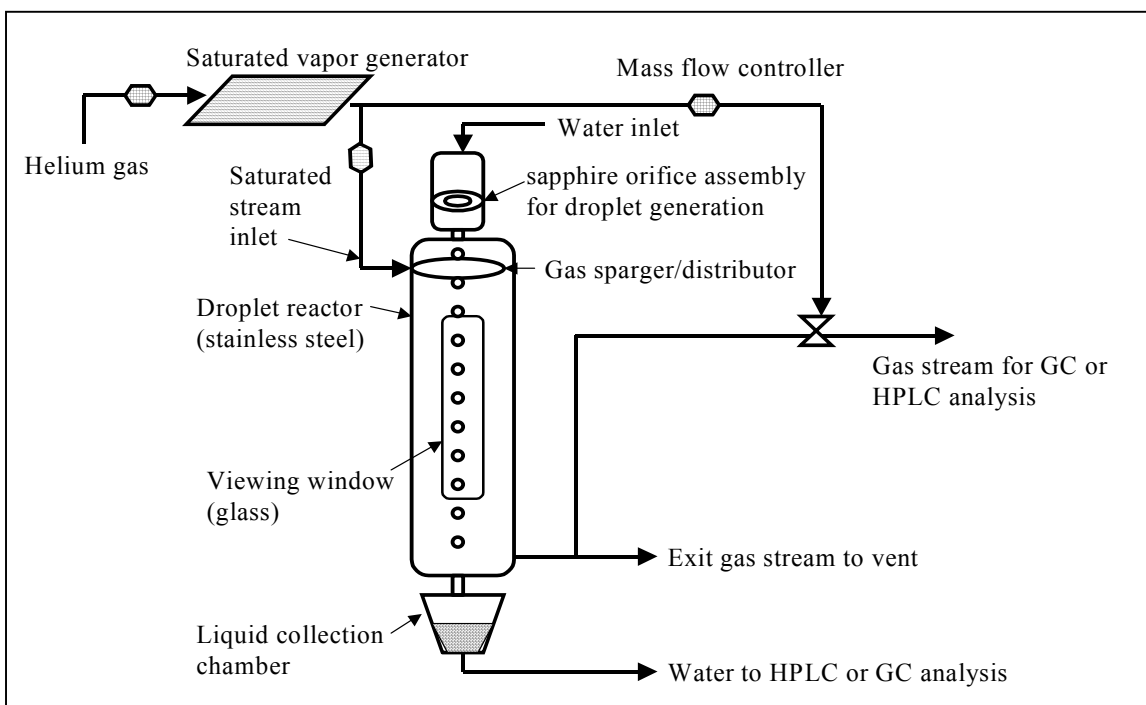


Figure 3.3. Schematic of the Droplet Train Apparatus (DTA) apparatus used to measure the uptake and mass transfer to water droplets and study organic compound interaction with ozone.

The uptake experiment was conducted with a constant gas phase concentration of organic compound fed to the reactor throughout the experiment, whereas the exiting liquid stream composition depended on the residence time and mass transfer to the droplet within the reactor. The liquid from the collection chamber was analyzed using liquid chromatography. The exiting gas stream at the bottom of the reactor was analyzed on-line by directing it to a gas chromatograph through a six-port sample valve. The entire reactor and the flow lines were heat traced using heating coils to maintain a constant temperature within the reactor using temperature controllers (Series 6100 from Omega Engineering Inc., Stamford, CT) and Omega model DT462 temperature indicators. The reactor pressure was maintained at about 760 Torr. The reactor had two vertical glass side ports that could be used to photograph the bubbles and determine their sizes, when desired.

3.2.7 Gas Phase Analysis (Benzene and Naphthalene)

Benzene (vapor and aqueous) and naphthalene vapor was analyzed using a Hewlett-Packard 5890 GC with a flame ionization detector. A stainless steel column (0.023 m long x 0.0063 m i.d.) packed with Chromosorb P was used for chromatographic separation. The carrier gas flow rate in the GC was 70 mL/min and column head pressure was 200 kPa (29 psi) and the outlet pressure was atmospheric. Gas-phase samples were injected into the GC by a manually actuated 6-port injection valve (Valco Instrument Co., Inc., Houston, TX). The injection volume for all vapor phase samples was $1 \times 10^{-6} \text{ m}^3$ through a sample loop. The column temperature was 250 °C. The gas concentrations were analyzed on a Hewlett Packard 5890 GC, using a stainless steel column (0.023 m long x 0.0063 m I.D.) packed with Chromosorb P. The packing had a surface area of (4 to

5) m^2/g , a bulk density of $380 \text{ kg}/\text{m}^3$, and a mean particle density of $230 \text{ kg}/\text{m}^3$. The gas concentration was analyzed at a constant column temperature of 250°C using a flame ionization detector at the outlet of the column.

3.2.8 Gas Phase Analysis (Phenanthrene)

Gas-phase phenanthrene was adsorbed Supelpak porous polymer adsorbent, shown in Figure 3.4, obtained from Supelco Inc. The adsorbed phenanthrene was extracted into acetonitrile and analyzed in liquid chromatography using the same methodology described below for the aqueous phase. The typical time waited for complete extraction of adsorbed PAH into acetonitrile was about 6 to 8 hours.

The concentration of the vapor stream was estimated based on the gas flow rate, the time of flow of gas into the polymer bed and the volume of acetonitrile used for extraction. In most experiments, two polymer traps were used in series to ensure complete removal of gas molecules.

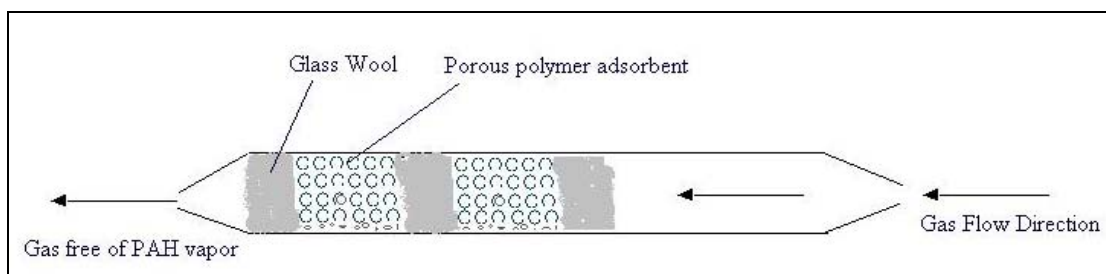


Figure 3.4. Porous polymer bed used for PAH vapor adsorption.

3.2.9 Liquid Phase Analysis (Naphthalene and Phenanthrene)

The liquid samples for the experiments with naphthalene and phenanthrene were analyzed using a Hewlett Packard (Series 1100) liquid chromatograph with a diode array detector, with Envirosep-PP HPLC column (1.25 cm long x 0.0046 m i.d., Phenomenex, Torrance, CA). The collected liquid samples were analyzed in a Hewlett Packard (Series

1100) liquid chromatograph with a Diode Array Detector, using an Envirosep - PP HPLC column (1.25 m cm x 0.0046 m I.D. from Phenomenex, Torrance, CA).

3.3 Experimental Procedure

Starting the vapor generator first and determining the feed concentrations initiated the experiment. The vapor phase concentrations were observed to be constant within 40 minutes of system initiation. At this time, the droplet generator was started and jet flow rate measurements were made to estimate the jet-stream velocity. In order to have trouble free operation of the droplet generator, the nozzle was cleaned in acetonitrile and sonicated to remove any adsorbed dirt in the nozzle. High-pressure air (~50psi) was also used to clean a clogged nozzle. This cleaning procedure was essential to ensure that the droplet stream does not strike the reactor walls and thereby lose droplet surface area. The signal generator was set at 15kHz to ensure same droplet spacing between each experiment. It was observed that, for a given droplet diameter, droplet concentration was uniform between each sample vial when the signal generator was in operation. This observation confirmed the uniform droplet diameter and droplet spacing obtained from the droplet generator.

Simultaneous measurements of the gas phase concentrations were done while the liquid samples were collected. It was essential to have the liquid collection pump running prior to starting the droplet generator to avoid liquid seeping from the reactor exit and thus flowing into the gas chromatography system. Measurements were made to determine the increase in liquid concentration due to gas seepage in the droplet collection chamber and were found to be insignificant in comparison to actual concentration observed in the liquid phase due to the droplet traversing the length of the reactor. From the experiment,

the gas concentration, liquid phase concentration, droplet velocity and diameter, and reactor temperature were determined to study mass transfer and gas uptake phenomena.

CHAPTER 4

GAS PHASE UPTAKE STUDY: RESULTS AND DISCUSSION

4.1 Uptake of Organic Compounds

In general, the flux of chemical species from the gas phase to the surface of the liquid droplet for a moving droplet with low turbulence at the interface is given in terms of a concentration difference (see Figure 4.1), and is written as follows, $J = K_C (C_{bulk} - C_{eq})$. Where, K_C is the overall mass transfer coefficient (m/s), C_{eq} is the gas phase concentration in equilibrium with the liquid phase concentration; C_{gas} is the bulk gas-phase concentration. With equation (2.6) re-written to obtain C_{eq} , we have

$$C_{eq} = \frac{C_D}{(a_V K_{IA} + K_{WA})} \quad (4.1)$$

$$J = K_C \left(C_{gas} - \left[\frac{C_D}{(K_{IA} a_V + K_{WA})} \right] \right) \quad (4.2)$$

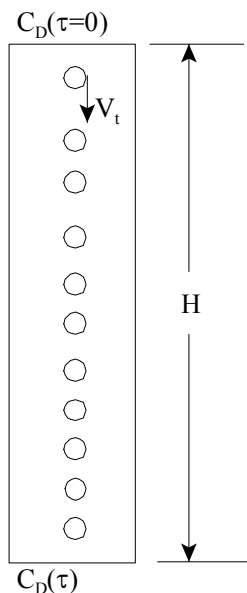


Figure 4.1. Modeling gas uptake by micron-sized droplets. V_t is the droplet velocity and H is the reactor height. H/V_t is the gas-liquid contact time (τ).

The rate of transfer of the gas phase species to the liquid droplet as it traverses the length of the reactor can be given as follows,

$$V_W \frac{dC_D}{d\tau} = K_C \cdot A_W \left(C_{gas} - \left[\frac{C_D}{(K_{IA} a_V + K_{WA})} \right] \right) \quad (4.3)$$

Solving the above differential equation (4.3) with respect to the gas-liquid contact time, τ , we have the following equation,

$$C_D(\tau) = C_{gas} \cdot (K_{IA} a_V + K_{WA}) + \left(\exp \left[-K_C \cdot \frac{1}{(K_{IA} a_V + K_{WA})} \cdot \frac{6}{d} \cdot \tau \right] \right) \cdot C_1 \quad (4.4a)$$

where, a_v is the area per unit volume of the droplet, and is given by $(6/d)$ and K_{IA} interfacial partition constant discussed earlier. Writing $(K_{IA} a_v + K_{WA})$ as ζK_{WA} and the term ζ represents the deviation from bulk-phase partitioning as a result of interfacial adsorption and is given by $\left(1 + a_v \cdot \frac{K_{IA}}{K_{WA}} \right)$ and solving for zero droplet concentration at $t = 0$, the constant C_1 is $C_1 = -C_{gas} \cdot \zeta K_{WA}$. Substituting C_1 in equation (4.4a) and simplifying, we have

$$K_{DV}(\tau) = \frac{C_D}{C_{gas}} = \zeta \cdot K_{WA} \left[1 - \exp \left(-K_C \cdot \frac{1}{\zeta K_{WA}} \cdot \frac{6}{d} \cdot \tau \right) \right] \quad (4.4b)$$

In the above equation d is the droplet diameter, τ is the gas-liquid contact time and K_{DV} is the ratio of the droplet concentration and the gas concentration. The data obtained from the DTA experiment include the droplet-to-vapor partition constant (K_{DV}) which is the ratio of the observed droplet concentration C_D , during the given contact time, to the gas stream concentration C_g , the droplet diameter and its velocity inside the reactor from which the droplet contact time τ is calculated. The parameter K_{IA} in ζ , which is the deviation in Henry's law constant, is known from the previous work ([Raja et al., 2002](#)).

Hence, with all the parameters known, we can calculate the overall mass transfer coefficient, K_C , from the above equation. From equation (2.7), with all other parameter known, it is possible to calculate the mass accommodation coefficient (α).

4.2 Gas-Liquid Mass Transfer Dynamics

The three test compounds, benzene, naphthalene, and phenanthrene, were studied in the DTA with varying droplet sizes and the results of these experiments are discussed next. The average gas-droplet contact time for naphthalene and phenanthrene experiments was 72 ms, and in the case of benzene uptake studies it was 52 ms. In the gas uptake studies done in the DTA, K_{DV} values reported are for the given gas-liquid contact time and not equilibrium Henry's law constant value.

In terms of the characteristic gas diffusion time, the time for liquid diffusion and the time required for phase equilibration at the surface (surface saturation) are given as follows by [Schwartz, 1986](#).

$$\tau_g = \frac{d^2}{4\pi D_G} \quad (4.5)$$

$$\tau_D = \frac{d^2}{8\pi D_D} \quad (4.6)$$

$$\tau_{IA} = D_D \left[\frac{4HRT}{\bar{c}\alpha} \right]^2 \quad (4.7)$$

Using the above equations by Schwartz, we can estimate the various characteristic time involved in the droplet enrichment process. In the above equations, D_D is the liquid phase diffusion constant (m^2/sec), D_G is gas phase diffusion constant (m^2/sec), d is the droplet diameter (m), H is the Henry's Constant ($mol/Pa\cdot m^3$), R and T are the universal gas constant ($Pa\cdot m^3/mol\cdot K$) and temperature (K). The characteristic times for the

diffusion of gas and liquid, and the surface saturation times are shown in Table 4.1. In terms of the diffusion constants, we observe that the liquid diffusion time is about 8 times larger than the gas-liquid contact time in these experiments. This gives us an indication that the liquid droplet will never be saturated completely with the gas species, and hence never approaches the equilibrium Henry's constant for the given gas-liquid contact time. As a result, the change in gas concentration from the inlet stream to the outlet stream will only be marginal, and this was also confirmed by experimental observation. Since, phenanthrene is the most hydrophobic of the three compounds we can also expect that the droplet surface will never be saturated with this gas species (no desorption from the droplet surface). As a result, the overall mass transfer coefficient will be close to the mass accommodation coefficient for phenanthrene but not necessarily true for the other two compounds.

4.3 Effect of Droplet Diameter on Gas Uptake

The droplet enrichment observed for various droplet sizes are shown in Figure 4.2 for the three compounds. The figures clearly show that smaller droplet size have larger droplet-to-vapor partition constant (K_{DV}) than the larger droplet, thereby delineating the importance of surface adsorption.

The overall mass transfer coefficient K_C is calculated from the experimental partition constant K_{DV} , and using the K_C in equation (2.7) with all the other values known except α , one can solve for α . Figure 4.2 also shows simulation curves for two scenarios, one with surface adsorption and the other without surface adsorption. Equation 4.4b was used to predict the K_{DV} for the two scenarios, where ζ was set equal to 1 for the case without adsorption, with all the other parameters in equation 4.4b known.

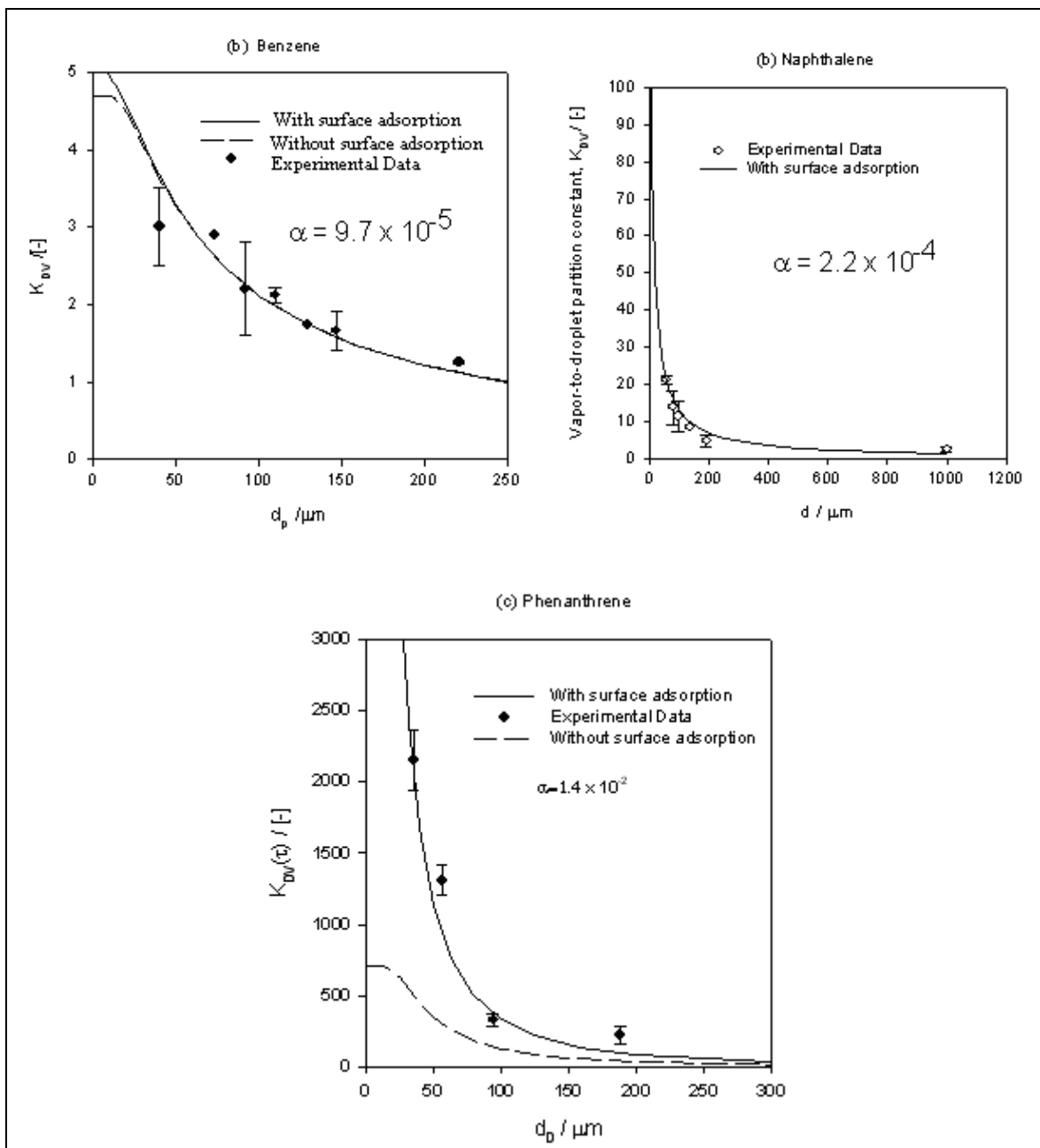


Figure 4.2. Vapor-droplet partition constants (measured and predicted) versus droplet sizes for benzene, naphthalene and phenanthrene uptake. [Gas/droplet contact time = 52 ms for Naphthalene and Phenanthrene and 72 ms for Benzene].

From Figure 4.2, we note that the surface adsorption phenomenon is least important for the least hydrophobic compound (benzene), while it is the most important in the case of phenanthrene (the most hydrophobic compound of the three). Using the

mass accommodation coefficient for the three compounds, now it is possible to compute the characteristic time for the surface saturation.

Table 4.1. Characteristic times for mass transfer dynamics in the DTA

Property[†]	Benzene	Naphthalene	Phenanthrene
D_L (m²/s)	9 x 10 ⁻¹⁰	7 x 10 ⁻¹⁰	5.8 x 10 ⁻¹⁰
D_G (m²/s)	8.8 x 10 ⁻⁶	5.7 x 10 ⁻⁶	4.8 x 10 ⁻⁶
\bar{c} (m/s)	284	222	188
H (mol/Pa-m³)	1.78 x 10 ⁻³	2.04 x 10 ⁻²	2.82 x 10 ⁻¹
K_{WA} [-]	4.5 ± 0.1	53 ± 4	705 ± 184
τ (s)	0.072	0.052	0.052
τ_g (s)	7.49 x 10 ⁻⁵	1.16 x 10 ⁻⁴	1.37 x 10 ⁻⁴
τ_D (s)	0.366	0.471	0.568
τ_{IA} (s)	3.68 x 10 ⁻⁴	1.20 x 10 ⁻²	6.53 x 10 ⁻⁴
τ_{IA}[*] (s)	0.0004	0.0141	0.0713
α [-]	9.7 x 10 ⁻⁵	2.2 x 10 ⁻⁴	1.4 x 10 ⁻²

[†]Data computed for a 91μm droplet diameter at 298K.

Table 4.1 shows the characteristic times for the mass transfer dynamics in the DTA computed for a 91μm droplet diameter. Also, as mentioned earlier the liquid diffusion time τ_D is very large compared to the droplet contact time τ, indicating that the droplet will never be saturated completely with the gas species and achieve the bulk Henry's constant K_{WA}. The characteristic time for surface equilibration show that all the compounds considered in this work attain surface equilibrium at a much shorter time scale in comparison to the gas-liquid contact time. Nevertheless, the surface active nature is a key feature of a compound that is only defined by the surface partition constant K_{IA} and the vapor pressure. In this aspect, phenanthrene is the most surface active of all the

three compounds in this consideration. In the Table 4.1, τ_{IA}^* is the characteristic time for surface equilibration with surface adsorption criterion taken into consideration.

$$\tau_{IA}^* = D_D \left[\frac{4 \left[(HRT) \left(1 + \frac{6}{d} \frac{K_{IA}}{HRT} \right) \right]}{\bar{c} \alpha} \right]^2 = D_D \left[\frac{4 [K_{WA} \zeta]}{\bar{c} \alpha} \right]^2 \quad (4.8)$$

Where, $\zeta = 1 + \left(\frac{6}{d} \right) \left(\frac{K_{IA}}{K_{WA}} \right)$, H is the Henry's law equilibrium, R is gas constant; d is the droplet diameter, K_{IA} equilibrium surface partition constant (m), K_{WA} is the dimensionless bulk air-water Henry's partition constant, while R and T are the universal gas constant and temperature, respectively. With the surface adsorption characteristics taken into account we see that the phenanthrene is the only compound that takes more time than the available experimental gas-liquid contact time to attain surface equilibrium. From Table 4.1, we note that the mass accommodation α is higher for phenanthrene than the other two compounds, indicating a higher probability of collision of a gas molecules at the interface is solvated into the liquid.

From the table, we also see that the surface saturation time is less than the droplet contact time for benzene and naphthalene. This indicates that the calculated uptake coefficient (mass transfer coefficient K_C) is due to the combination of both the mass accommodation (sticking) and also due to re-evaporation (due to the forward and reverse process in the kinetic shown in page 6) for these two compounds. Based on the solubility of the compound in aqueous phase and hence its Henry's law equilibrium value, phenanthrene uptake is dominated by gas diffusion while that of benzene is liquid phase diffusion limited.

From Table 4.1, benzene has the lowest characteristic time for liquid phase diffusion in comparison to naphthalene and phenanthrene. Hence, we can expect a dependence of K_C with gas-liquid contact time for benzene uptake as there is more time for liquid phase diffusion. Similarly, for a compound with no limitation on liquid phase diffusion, K_C should be independent of gas-liquid contact time. Figure 4.3 shows that the mass transfer coefficient is independent of contact time for phenanthrene showing negligible mass transfer diffusion limitation in the liquid phase. On the other hand, change in K_C with gas-liquid contact time for benzene shows that liquid phase diffusion limitation is the controlling process.

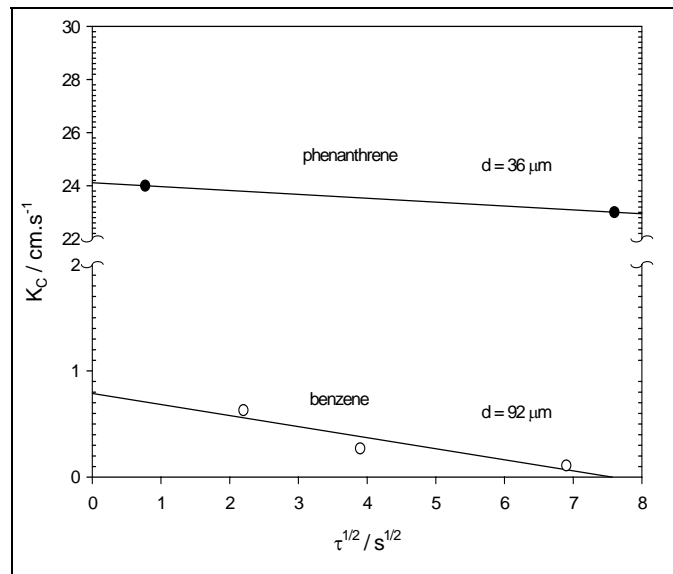


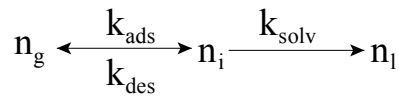
Figure 4.3. The effect of the mass transfer coefficient for phenanthrene and benzene vapors on the gas/droplet contact time in the reactor.

The calculated mass transfer coefficient K_C is a sum of all the resistances as shown in equation (2.7), namely the gas-phase, liquid phase and mass accommodation resistance. In the case of phenanthrene, the liquid phase diffusion plays a minor role in comparison to mass accommodation and gas-phase diffusion. While, for benzene the uptake is dominated by limitations due to the liquid phase diffusion. For phenanthrene

uptake into a 95 μm droplet, 77% resistance is due to gas-phase, 20% due to mass accommodation and 3% due to liquid phase resistance. In a 10 μm droplet, the gas phase resistance for phenanthrene uptake is considerably lesser, and the mass accommodation will account for about 80% of the overall resistance. In the case of benzene uptake into a 95 μm droplet, 92.7% of the resistance is due to liquid phase diffusion, while 0.3% and 7% account for gas phase and mass accommodation resistance, respectively.

4.4 Effect of Temperature on Mass Accommodation

The mass accommodation process can be viewed as a two-step process as shown in the kinetic equation below,



The adsorption rate constant k_{ads} for the above process can be given as $k_{\text{ads}} = n_g c/4$ for a gas molecule striking the liquid surface and accommodated with unit probability. With out liquid surface saturation, the uptake process is given as ([Davidovits, 1995](#))

$$\frac{\alpha n_g c}{4} = \frac{n_g c}{4} - n_g k_{\text{evap}} \quad (4.9)$$

$$\frac{\alpha n_g c}{4} = n_i k_{\text{sol}} \quad (4.10)$$

Solving the above two equations, we get ([Kolb et al., 2002](#))

$$\frac{\alpha}{1-\alpha} = \frac{k_{\text{sol}}}{k_{\text{desorb}}} = \exp\left(\frac{-\Delta G_{\text{obs}}^o}{RT}\right) = \exp\left(\frac{-\Delta H_{\text{obs}}^o}{RT} + \frac{\Delta S_{\text{obs}}^o}{R}\right) \quad (4.11)$$

The above expression is a formulation for observed uptake considering only the process of mass accommodation at the interface, which is known to be a function of temperature.

The accommodation at the gas/liquid interface is theorized according to the critical cluster theory ([Davidovits, 1995](#), [Nathanson et al., 1996](#)). According to the critical cluster theory, the solvation of a gas molecule in the bulk liquid takes place via a critical cluster of water molecule n_s^* formed around a gas molecule. From the development above, we can also consider the kinetic nature to be a competing process between condensation and evaporation, in which a thermodynamic barrier exist for the formation of the surface species n_i from the bulk liquid where accumulation of gas molecules takes at the droplet surface (discussed in section 1.3).

With the mass accommodation coefficient computed (from equation (2.8)) for different temperatures, the Van't Hoff type relationship between α and T in equation (4.11), a nucleation model for uptake into water droplets, can be used to compute the thermodynamic parameters by linear regression. The plot of $\ln(\alpha / 1 - \alpha)$ versus $1/T$ in Figure 4.4 will give the enthalpy from the slope and entropy from the intercept. These thermodynamic functions describe the energy required for cluster formation at the interface between a solute molecule and several water molecules. Also, the plot below shows the negative temperature dependence of α .

Table 4.2. Interface partition constant as function of temperature[†].

T (KELVIN)	Benzene K_{IA} (μm)	Naphthalene K_{IA} (μm)
298	0.43	27.42
308	0.20	15.05
318	0.09	1.22

[†] - From [Raja, 2003](#)

In addition to the influence of α on K_{DV} , the K_{IA} also changes with temperature. Previous measurements of K_{IA} at different temperatures in inverse gas chromatography showed that the K_{IA} decreases with increase in temperature. Therefore, at lower temperatures the K_{DV} increases resulting in higher droplet concentration. Table 4.2 lists the K_{IA} for benzene and naphthalene at different temperatures.

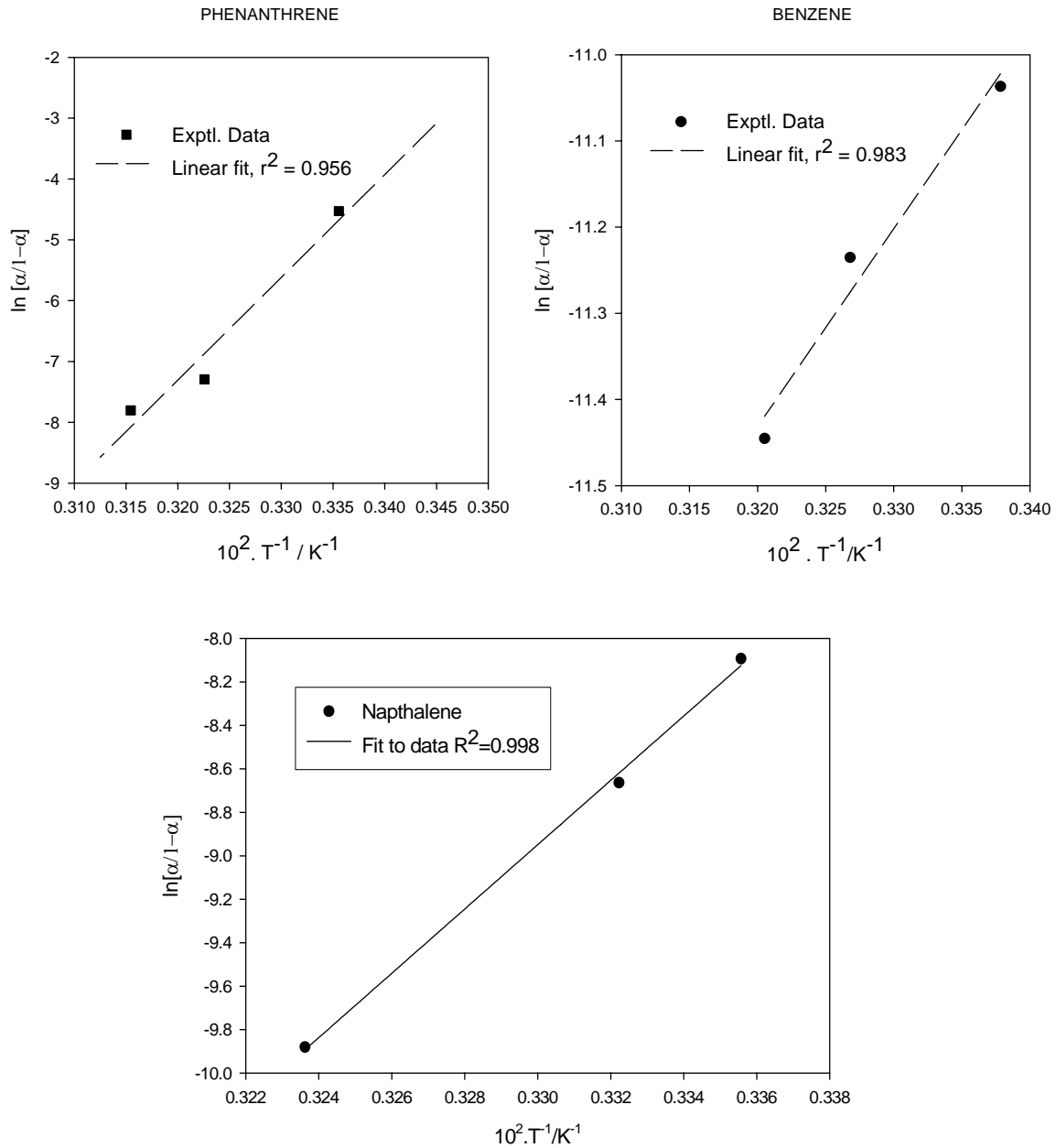


Figure 4.4. The variation in mass accommodation coefficient for benzene, naphthalene and phenanthrene with temperature.

The negative increasing nature of the computed enthalpy and entropy of accommodation for benzene to phenanthrene in Table 4.3, show the hydrophobic nature of the three compounds, and the number of critical cluster required for the subsequent solvation of the gas-phase molecule into the liquid droplet. A large negative value for the enthalpy of accommodation denotes strong exothermic nature of the process. Similarly, a large negative entropic contribution indicates the unfavorable nature of the local structure modifications in the surface water orientation around the solute molecule. Excess enthalpy of solution is also a measure of the solute-solvent interaction. Hence, a comparison of the enthalpy of accommodation to the excess enthalpy of solution can be made.

Table 4.3. Mass Accommodation Coefficient, Enthalpy, Entropy of Accommodation and Excess Enthalpy of Solution for the Compounds.

Compound	α [No Unit]	$\Delta_{\text{obs}}H^{\circ}$ [kJ.mol ⁻¹]	$\Delta_{\text{obs}}S^{\circ}$ [J.K ⁻¹ .mol ⁻¹]	$\Delta_{\text{soln}}H^{\circ}$ [kJ.mol ⁻¹]
Benzene	$(9.7 \pm 1.8) \times 10^{-5}$	- 19	- 157	2
Naphthalene	$(2.2 \pm 0.6) \times 10^{-4}$	- 123	- 482	9
Phenanthrene	$(1.4 \pm 0.4) \times 10^{-2}$	- 140	- 510	17

† - Enthalpy of solutions from [Schwarzenbach et al., 2003](#). Properties shown for 298 Kelvin.

Notice the enthalpies of accommodation values are negative, while the excess enthalpies of solution are positive. Positive enthalpies of solution are indicative of low solubilities and high aqueous-phase activity coefficients for the compounds. Also notably, the highest energy barrier for solvation is evident for phenanthrene due to large negative enthalpy of accommodation among the three test compounds. The excess enthalpy of solution for phenanthrene is the largest, and high energy is needed to dissolve it. It is, therefore, reasonable that it also has the highest enthalpy of mass accommodation at the interface. [Müller and Heal, 2002](#), recently reported values for enthalpies of

accommodation for a few aromatic phenols (phenol, 3-methyl phenol, and 2-nitrophenol) and showed that there is a linear relationship between the enthalpy values. These are plotted (in Figure 4.5) along with those for the three aromatic hydrocarbons from this work.

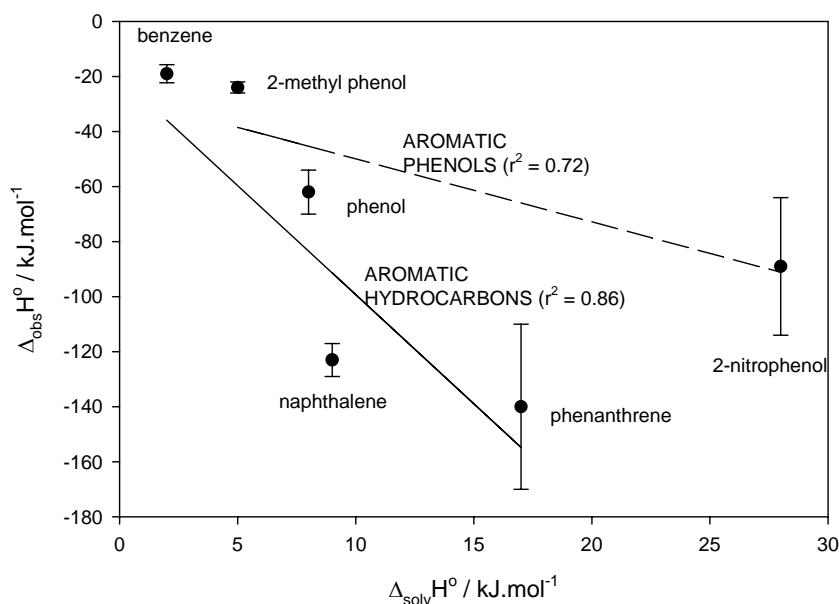


Figure 4.5. Correlations between enthalpy of accommodation and excess enthalpy of solution for two classes of compounds—aromatic hydrocarbons and aromatic phenols. Data for phenols are from [Müller and Heal, 2002](#). (From [Raja and Valsaraj, 2004](#)).

The Figure 4.5 shows a linear relationship for both classes of compound, with a higher slope for aromatic compound than for aromatic phenols. Phenols have a more negative enthalpy of accommodation than the parent compound, benzene. Phenol has an OH group capable of forming hydrogen (H)-bonds with water and, hence, requires less additional water molecules to form the critical cluster ([Davidovits et al., 1995](#)). Also from the Figure 4.5, we can note that with the addition of a methyl group to phenol, enthalpy of accommodation becomes similar to that of a benzene molecule.

4.5 Effect of Dissolved Organic Carbon

As discussed earlier, decrease in surface tension, higher uptake and surface-active nature of cloud and fogwater has been attributed to the presence of humic-like substances in the solution ([Facchini, 2000](#), [Capiello et al., 2003](#)). Although the origin of these surface-active materials is not known, there is an indication that they are formed in the atmosphere by oxidation of gaseous precursors on aerosols ([Kalberer, 2004](#)). The presence of organic matter (OM) in cloud and fogwater increases the dissolved concentration of PAHs that associate with OM and adds to the overall load of PAHs in fogwater. [Capiello et al., 2003](#) showed that Suwannee River fulvic acid was a suitable model compound for the humic (or fulvic) acids, referred to as humic-like substances, present in cloud and fogwater extracts.

In order to describe the effect of dissolved organic carbon in a laboratory scale setup, the water used to generate micron-sized droplets was dissolved with known amount of Suwannee River Fulvic acid. The Figure 4.6 and 4.7a below show the effect of organic carbon on uptake. The Figure 4.7b shows the surface tension of the various concentration of fulvic acid used in the water, measured independently.

The data shown in Figure 4.6 and 4.7a were obtained by performing experiments in the DTA explained in Chapter 3. The experiments were done for a 95 μ m droplet diameter. The droplet-to-vapor partition constant shows a linear increase with increase in organic matter concentration in the droplet. From the surface tension measurements done separately on the organic carbon spiked-water, a constant value of 49mN/m show the surface saturation being attained with respect to fulvic acid. The increased partitioning (K_{DV}) can be due to organic film around the droplet leading to increased surface

concentration of the aromatic compound resulting in a larger K_{IA} value for a surfactant coated surface and secondly due to increased aqueous solubility of the aromatic compound. In the second mechanism of increased solubility, there will be an additional term to ζ given by $C_C K_{CW}$, where K_{CW} is the organic carbon to water partition constant and C_C is the dissolved organic carbon concentration (DOC). Increasing C_C increases the solubility of PAHs in the organic carbon spiked-water.

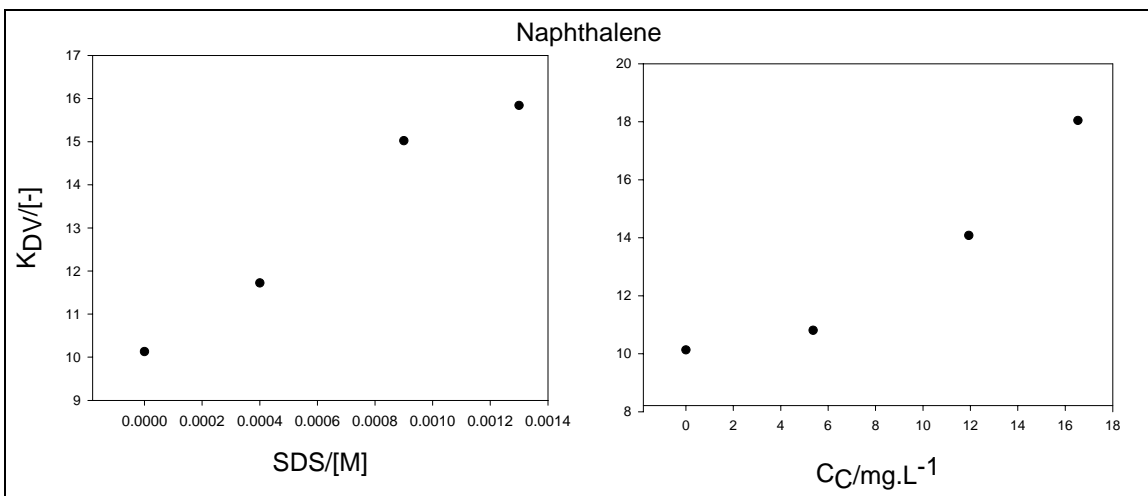


Figure 4.6. Effects of (left) dissolved SDS and (right) dissolved SFA on the vapor-to-droplet partitioning of naphthalene on a 95µm water droplet.

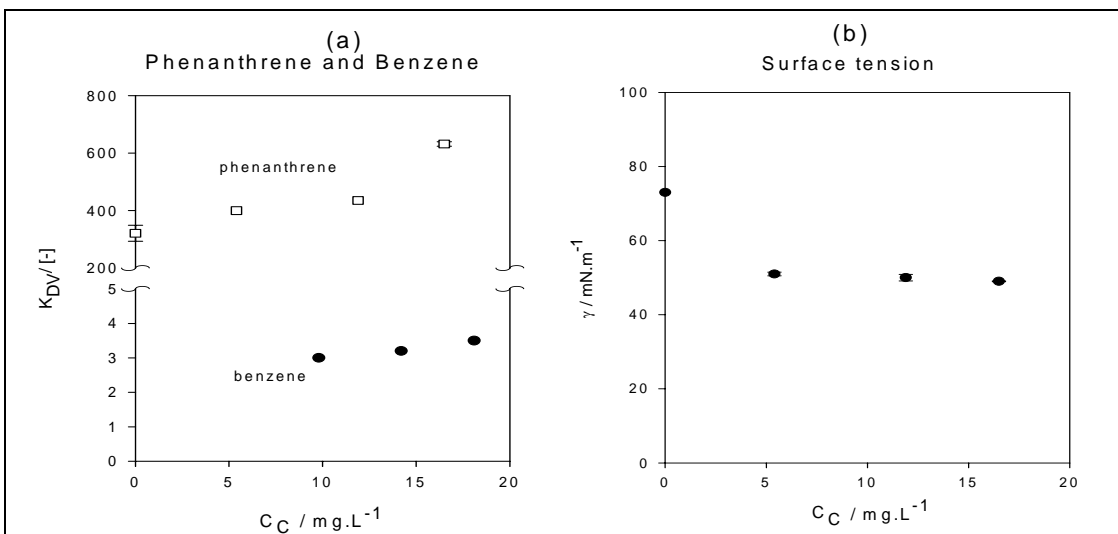


Figure 4.7. The effect of dissolved organic carbon (Suwannee Fulvic acid) in water on the droplet-vapor partition constant of phenanthrene and benzene. Also shown is the change in surface tension of water with increasing dissolved organic carbon.

In order to determine the increase in K_{IA} due to the presence of DOC, inverse gas chromatography experiments may be repeated by coating the gas chromatography packed column with organic carbon spiked-water. However, the present experimental methodology does not allow us distinguish between two hypotheses.

4.6 Summary

The uptake of organic vapors in a droplet train apparatus by micron-sized droplets showed higher partitioning for droplets smaller than $50\mu\text{m}$ than for droplet larger than $200\mu\text{m}$ due to surface adsorption. Surface adsorption was more pronounced resulting in larger droplet-to-vapor partition constant for the most hydrophobic phenanthrene in comparison to less hydrophobic naphthalene and benzene. The mass transfer of benzene to falling water droplets in air is liquid-phase diffusion-controlled, whereas that of phenanthrene is gas-phase diffusion and interface mass accommodation-limited. Uptake experiments were performed at temperatures ranging from 298 to about 320K. Mass accommodation showed a negative temperature dependence resulting in smaller K_{DV} at higher temperature. Mass accommodation was smaller for benzene in comparison to the mass accommodation phenanthrene. The presence of dissolved organic matter increased the droplet-to-vapor partition constant (K_{DV}).

In the next chapter heterogeneous oxidation of PAHs on surface of micron-sized droplet by ozone is discussed. The influence of ozone on uptake of aromatic vapors and the resulting reaction products due to this heterogeneous oxidation are discussed.

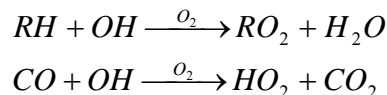
CHAPTER 5

EXPERIMENTAL METHODOLOGY TO STUDY HETEROGENEOUS KINETICS IN LIQUID DROPLETS

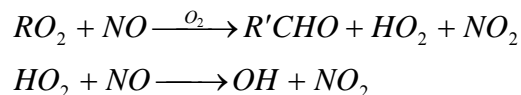
5.1 Introduction

Heterogeneous reactions in the atmosphere refer to multiphase chemistry that occurs on the surface or in the condensed phases that are in contact with the gas phase. These heterogeneous kinetics and reactions confined to the surfaces of aerosols (interfaces of solids and liquid aerosols) have been evidenced to occur faster than homogeneous reactions in the bulk or surface ([Worsnop et al., 1989](#)). Observations of heterogeneous chemistry has been reported by monitoring individual sea salt particles in the troposphere, where replacement of chloride by nitrate in sea-salt particles leading to sodium nitrate production in the particle phase ([Gard et al., 1998](#)). Recently, [Wadia et al., 2000](#) have shown that the reactions of unsaturated phospholipid adsorbed at the air-water interface with ozone occur much faster than the bulk gas phase reaction. Surface limited reactions exhibits higher surface reactivity and the localization of reactions at the surface results in larger concentration of reaction products for smaller droplets with large surface area-to-volume ratios than for larger particle. Evidence by [Sumner et al., 2004](#), show that there are several environmental surfaces that can promote heterogeneous chemistry due to uptake of water.

Ozone is one of the important oxidizing species in the troposphere and is a photolytic precursor to the hydroxyl radical that is responsible for oxidation of hydrocarbons in the atmosphere. The ozone formation begins with reaction of a volatile organic compound or CO with the OH radical. The reactions are as follows,



Reactions of HO₂ and RO₂ with NO lead to formation of NO₂ as follows,



The NO₂ that is formed as shown above, photolyzes to NO and O and the oxygen atom immediately combines with O₂ to form O₃. It is interesting to note that the hydrogen radicals produced in the reactions shown above, OH, NO₂ and RO₂, are removed by reactions that produce peroxides and nitric acid.

The heterogeneous chemistry in the troposphere and stratosphere, confined to the surface of the aerosols (in both liquid and solid particles), lead to secondary organic aerosol formations (in Figure 1.1) and are also known to alter hygroscopic properties of aerosols. The study on heterogeneous and multiphase chemistry leading to transformations of the PAHs adsorbed on atmospheric aerosols are important to understand the kinetics and mechanisms that can be of use in atmospheric chemistry models. Chemical reactions that occur on aerosol particles can transform hazardous Polycyclic Aromatic Hydrocarbons into compounds that are more hazardous than the parent compounds. Consequentially, knowledge and nature of the degradation products due to this heterogeneous chemistry is important to assess health effects. Since fogwater and other fine aerosol particles have considerably high surface-to-volume ratios and large atmospheric residence times they influence changes in atmospheric composition by interactions with gases such as ozone, nitrogen oxides, and OH radicals. Studies of PAHs on solid aerosols by [Pöschl, 2002](#) have shown that degradation products of PAHs are more lethal than the parent compound. The understanding of the degradation products

are important in order to ascertain the chemical makeup of the atmospheric gases resulting from these reactions and the aerosol particles ([Ravishankara, 1997](#), [Thomas et al., 2001](#)).

In this part of the work, oxidation by ozone is considered as an example. The primary oxidants present in the atmosphere include hydroxyl radical, ozone and nitrate radical. The environment in Baton Rouge, Louisiana where extensive fog collection was done (discussed in Chapter 7 and 8) is an oxidative environment due to the predominance of ozone ([U.S. EPA, 2004](#)). In an area such as Baton Rouge, a heavily industrialized and polluted area, ozone is a major air pollution problem as it enters into a variety of heterogeneous reactions in the atmosphere ([Jacob, 2000](#)). Reactions of PAHs in fog droplets can lead to significant reaction due to the large surface area available for reaction, and large residence times of the fogwater in the atmosphere can lead to heterogeneous and multiphase reactions to transform the gas phase compounds.

Oxidation reactions of PAHs on droplets by ozone may be confined on the liquid droplet surface due to low Henry's law partition constant to the bulk liquid phase. As a result, multiphase oxidation reactions by ozone in the bulk liquid may be negligible or absent. Most of the current works on heterogeneous reactions on aerosols are confined to solid aerosol particles ([Pöschl, 2002](#), [Smith et al., 2002](#)). In this scheme of experiments, heterogeneous reactions of PAH vapor on micron-sized liquid droplet surfaces by ozone, were studied in the droplet train apparatus.

5.2 Experimental Setup

The apparatus used in this experiment is a modification of the droplet train apparatus described earlier in Chapter 3. In this work, in addition to the interaction of

micro-sized droplets with aromatic hydrocarbon vapor stream, gaseous phase ozone generated using a unit obtained from Ozone Solutions, Inc., was fed at the top of the droplet flow tube apparatus. The ozone generator uses a corona discharge, where dry oxygen is passed through an electric field, where oxygen molecule (O_2) splits into oxygen atom (O). The oxygen atom reacts with oxygen molecule to form ozone (O_3).

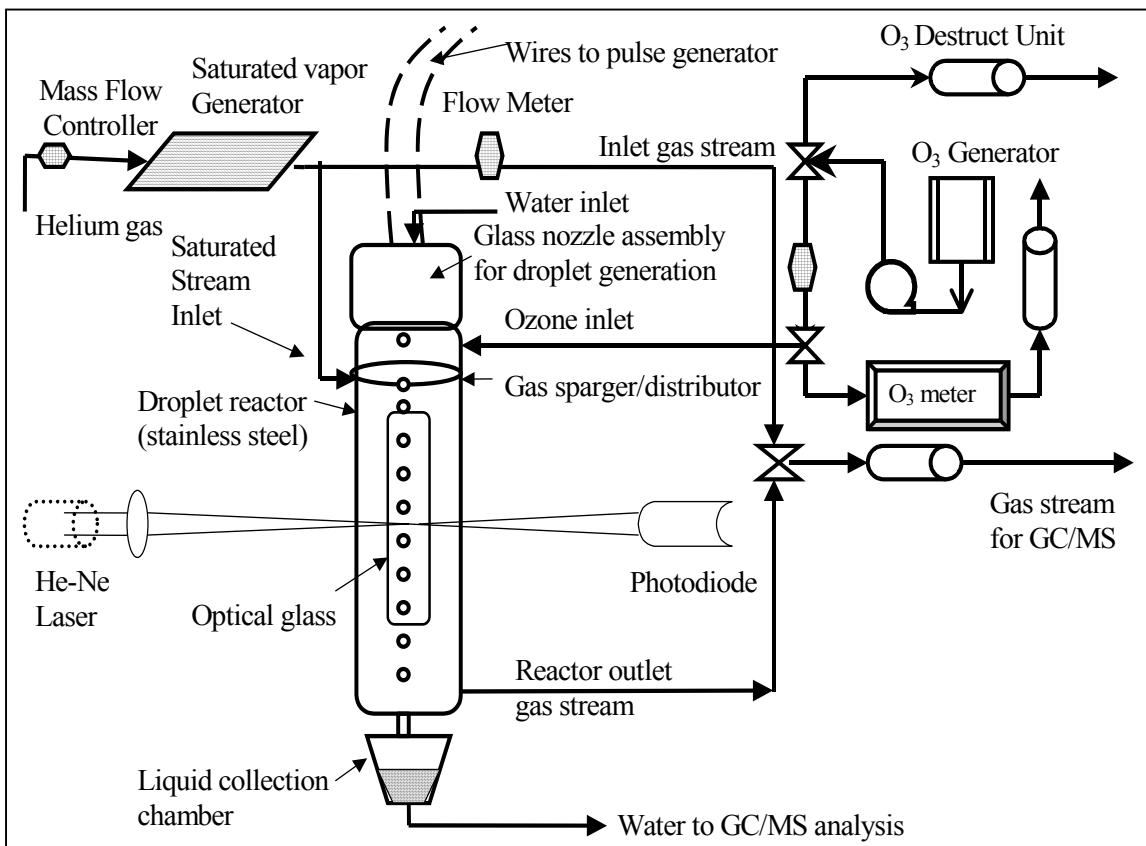


Figure 5.1. Schematic of the modified droplet train apparatus where the saturated gas phase PAH interacts with ozone on micron-size water droplets.

The ozone concentration was measured electrochemically, prior to introduction into the droplet flow reactor, using a handheld ozone sensor obtained from Ozone Solutions Inc. The pure ozone stream flow rate that was fed to the Ozone sensor and subsequently to the reactor was about 15-20mL/min. The droplets generated in this study passed through a cylindrical stainless steel reactor (0.0245m i.d., 1.06m long). The

saturated vapor stream, was generated as described in section 3.2, was fed into the droplet flow tube apparatus using a perforated porous frit sparger.

In addition to the droplet generator described earlier in section 3.2.3, capillary glass nozzle embedded in a piezo-ceramic tube actuated by an electric pulse generator obtained from University of Bremen, Germany was used. Droplets were generated using HPLC grade water fed to the capillary nozzle assembly using a syringe pump (KD Scientific, Model 210). Based on the settings in the electronic pulse generator, desired droplet size was generated ([Ulmke et al., 2001](#)).

5.3 Analytical Chemistry

The gas stream concentration fed to the reactor was recorded periodically using a GC5890 Series II installed with a capillary column (30m long x 0.25mm o.d., 0.5 μ m column i.d.) and detected using mass spectrometry MS5971. The carrier gas flow rate in the capillary column was 0.35mL/min and the column head pressure was about 5psi. The column temperature initially held at 70 $^{\circ}$ C for about 7minutes and then increased at 12 $^{\circ}$ C/min upto 200 $^{\circ}$ C. The gas samples streams split from the inlet and outlet of the reactor stream was fed into the GC using an electronically actuated valve, which was controlled using a digital valve sequence programmer, both obtained from Valco Instrument Co. Inc.

The liquid samples collected from the bottom of the reactor using a FMI Lab Pump (QG-20) was extracted into dichloromethane and concentrated by evaporating dichloromethane using a gentle stream of nitrogen gas to about 100 μ L. The concentrated samples were injected using a 7683 Series injector into a GC6890 installed with a capillary column (30m long x 0.32mm o.d., 0.25 μ m column i.d.) and detected using a

MS5973 for reaction products. The GC methodology used to analyze the aqueous phase samples were similar to that of the EPA method 8270 for PAHs. The column flow rate was about 0.7mL/min and the column head pressure was about 3.2psi. The column temperature was initially set at 40° C and then ramped at 10° C upto 270° C.

During each experimental run, an aliquot of liquid sample was separated and used to determine the dissolved ozone concentration calorimetrically using an instrument supplied by CHEMetric Inc. Model I-2007. In order to study the kinetics and uptake in the droplet flow tube apparatus, the whole experimental apparatus was traced with heating coils and controlled by temperature controllers obtained from Omega Engineering Inc.

5.4 Experimental Procedure

The flow of the carrier gas into the generator column produced the saturated aromatic hydrocarbon vapor stream. Steady state gas phase PAH concentration was usually obtained in about 30 minutes from the start of the vapor generator flow. The saturated vapor concentration was maintained constant and the mass transferred to the water droplet was small such that the exit concentration in the gas stream was nearly the same as that at the inlet. The gas phase ozone concentration obtained from the ozone generator was split and fed to the ozone sensor periodically until a steady ozone concentration was reached. Usually, the steady gas phase ozone concentration was obtained within 15 to 25 minutes from the start of the ozone generator.

The water droplet stream was first fed to the reactor without ozone and collected at the bottom of the reactor. While keeping all the reactor conditions same, the droplet stream was turned off and pure ozone was fed to the reactor at about 20mL/min. Analysis

of gas phase PAH vapors in contact with ozone gases by GC/MS showed no significant reaction of ozone and PAH vapor phase in the absence of the water droplets. At this point, droplet stream was restarted and collected from the droplet collection chamber. The aqueous phase samples collected with and without the presence of the ozone in the reactor was extracted into dichloromethane and analyzed in the GC/MS to determine the reaction parameters and the associated reaction products. Aliquot of the aqueous phase samples reacted with ozone was subsequently analyzed for dissolved ozone

The concentrated aromatic hydrocarbon vapor stream was initiated by starting the carrier gas flow into the saturated vapor generator column. Steady state gas phase concentration usually obtained in about 30minutes from the start of the vapor generator flow. Gas phase concentrations were recorded in the GC/MS Agilent data system Chemstation software. The gas phase ozone concentration obtained from the ozone generator was split and fed to the ozone sensor recorded periodically until a steady ozone concentration was reached. Usually, the steady gas phase ozone concentration was obtained within 15 to 25minutes from the start of the Ozone generator.

Droplets stream were first fed to the reactor without ozone and collected at the bottom of the reactor. While keeping all the reactor conditions same, the droplet stream was turned off and pure ozone was fed to the reactor at about 20mL/min. Analysis of gas phase PAH vapors in contact with ozone gases by GC/MS showed no significant reaction of ozone and PAH vapor phase. At this point, droplet stream of the same specific diameter introduced previously without ozone was fed to the reactor and collected from the droplet collection chamber. The aqueous phase samples collected with and without the presence of the ozone in the reactor was extracted into dichloromethane and analyzed

in the GC/MS to determine the reaction parameters and the associated reaction products. Aliquot of the aqueous phase samples reacted with ozone was subsequently analyzed for dissolved ozone concentration.

CHAPTER 6

HETEROGENEOUS SURFACE REACTIONS: RESULTS AND DISCUSSIONS

6.1 Modeling Mass Transfer and Reaction Kinetics

In the droplet train apparatus, the contact time of the gas and liquid droplet is in the millisecond range. This millisecond range contact time can separate the reactions at the gas-liquid interface from the longer time scale bulk phase reactions that depend on the liquid phase diffusion. In the mass transfer dynamics that include reactions, the various processes and electrical circuit analogue of the transport process are shown in Figure 6.1 and 6.2 below, respectively. The figure shows a surface reactive uptake with bulk phase reaction. Surface reaction occurs parallel to the solubility and reaction in bulk phase. In contrast to the previous mass transfer dynamics (where reaction was not present in equation 2.7), here the uptake is characterized by reactions at the surface and the bulk liquid along with mass accommodation at surface and liquid and gas phase diffusion.

The net flux to the gas-surface interface can be written as follows,

$$\frac{c_g \gamma \widehat{C}}{4} = c_g k_{ads} - c_s k_{des} \quad (6.1)$$

Where, c_g is the concentration of trace gas molecules in the bulk gas phase, and c_s is the mass of trace gas molecules per unit area on the particle surface, K_C is the overall mass transfer coefficient related to the uptake coefficient science literatures as) $K_C = \gamma \frac{\widehat{C}}{4}$, n_s is the number of trace gas molecules on the particle surface per unit area and k_{ads} and k_{des} are the adsorption and desorption rate coefficient.

The steady balance for the number of molecules lost on the surface of the particle can be written as the flux of molecules gas to surface and the flux from the bulk liquid to surface as follows,

$$c_s k_s = c_g k_{ads} - c_s k_{des} + c_D k_{ls} - c_s k_{sol} \quad (6.2)$$

where, c_D is the concentration of trace gas molecules in mass per unit volume just inside the surface of the particle.

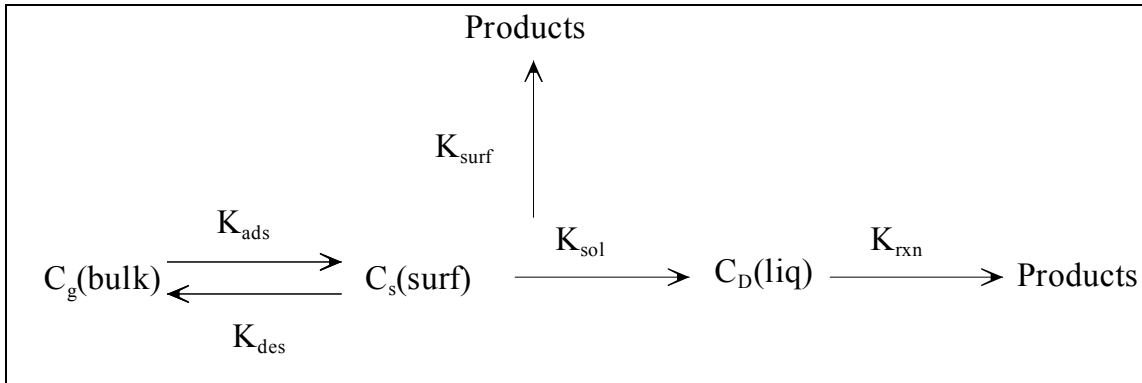


Figure 6.1 Transport, surface and bulk reaction kinetics on gas-droplet system.

The steady state flux of trace gas molecules into the bulk liquid phase is given as follows,

$$c_s k_{sol} - c_D k_{ls} = -D \frac{dn_l}{dz} \quad (6.3)$$

Where the first term on the right hand side is the solvation of the molecules in the bulk liquid phase and the second term is the loss of molecules to the surface from the liquid bulk to the particle surface that is equal to the gradient of n_l evaluated at the particle surface according to Fick's Law.

Adding equations (6.1), (6.2) and (6.3) yields the following,

$$\frac{c_g K_C \widehat{C}}{4} = c_s k_s + (kD)^{1/2} c_D \quad (6.4)$$

$$\gamma \frac{\widehat{C}}{4} = \frac{c_s}{c_g} k_s + (kD)^{1/2} \frac{c_D}{c_g}$$

The overall uptake coefficient is given as follows ([Hanson, 1997](#)),

$$\frac{1}{\gamma} = \frac{\widehat{C}}{4k_g} + \frac{1}{S} + \frac{1}{\gamma_{bulk} \frac{k_{ls}}{k_{ls} + \sqrt{kD}} + \gamma_s} \quad (6.5)$$

In deriving the equation for the overall mass transfer coefficient it is explicitly assumed that the bulk phase reaction is negligible. The experimental measurement for almost negligible ozone concentration in the bulk liquid phase supports this assumption. In addition to this recent work by [Mmerekı et al., 2004](#), on planar water surfaces, in which they showed that gas-phase ozone reaction with PAHs occurs on the surface of water and not in the bulk. The second assumption is that the flux into the bulk liquid phase from the particle surface is equivalent to the flux from the bulk liquid into the particle surface.

This assumption exemplifies that the solvation of the products and the parent compound is almost instantaneous and very fast. That is $k_{ls} \gg (kD)^{1/2}$, with $\alpha=S$. Hence, for negligible bulk phase reaction and by using the following relation, $K_C = \gamma \frac{\widehat{C}}{4}$, equation (6.5) reduces to,

$$\frac{1}{K_C} = \frac{1}{k_g} + \frac{4}{\widehat{C}} \frac{1}{\alpha} + \frac{4}{\widehat{C} (\gamma_{sol} + \gamma_s)} \quad (6.6)$$

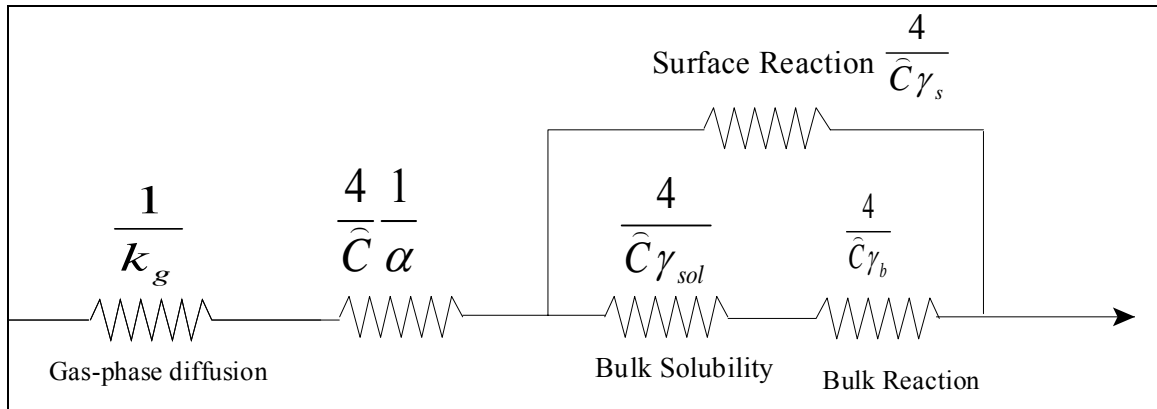


Figure 6.2. Electric circuit analog of the transport, surface and bulk reaction in a gas-droplet system.

6.1.1 Derivation of Overall Mass Transfer Coefficient With Surface Reaction

In this work the surface reaction of species, poly-aromatic hydrocarbon (PAH) and ozone, adsorb to the surface prior to reaction. Such reactions are referred to as Langmuir-Hinshelwood mechanism ([Masel, 1996](#), [Atkins, 1998](#)). Considering the significance of surface reaction as the controlling process, we can incorporate the Langmuir-Hinshelwood mechanism. Similar conclusions were drawn by [Mmereki et al., 2004](#), who observed that gas-phase ozone adsorbed first on the air-water interface according to a Langmuir adsorption isotherm and reacted with the adsorbed PAH via a Langmuir-Hinshelwood mechanism.

In the Langmuir-Hinshelwood mechanism two chemical species A and B first adsorb onto the surface of the surface. The adsorbed A and B reacts to form a reaction product as shown in the Figure 6.3 below. Based on our assumptions to derive the overall mass transfer coefficient presented in section 6.1, the product solvates (dissolves) into the bulk liquid phase instantaneously.

In order to obtain an expression for the surface reaction term (γ_s) with suitable dimensions, the gas phase flux into the particle is determined assuming that the surface

reaction is the sole process governing the uptake ([Worsnop et al., 2002](#)). The rate of loss of a PAH molecule on the droplet surface is given by,

$$-r_A = k'' [O_3]_s [PAH]_s \quad (6.7)$$

where $[O_3]_s$ is the concentration of ozone on the droplet surface, $[PAH]_s$ is the concentration of PAH molecule on the droplet surface in moles/cm² and k'' is the second order surface reaction rate constant.

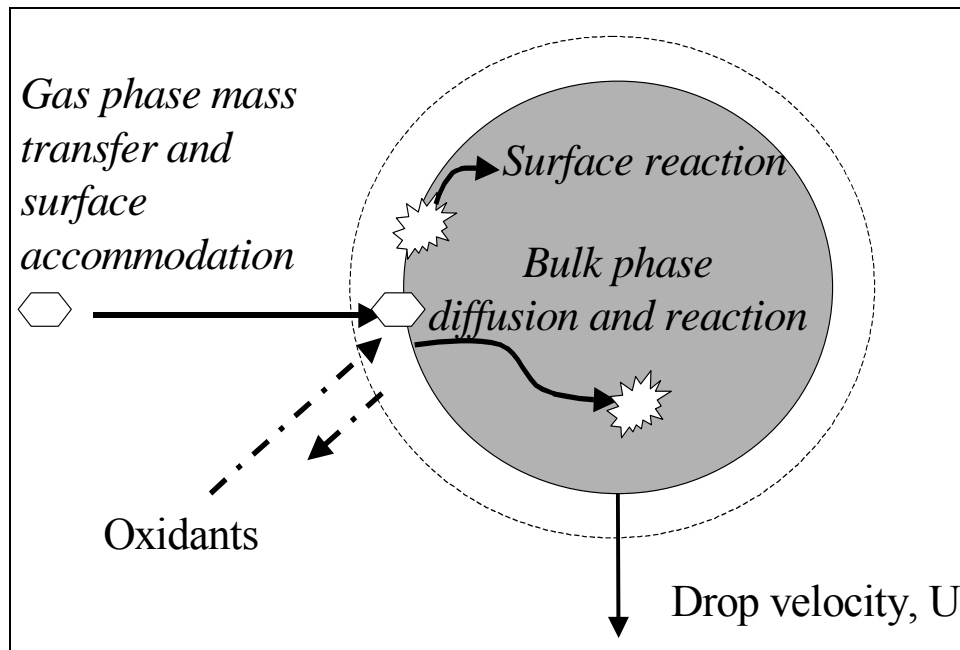


Figure 6.3. Schematic of the steps involved in the mass transfer and multiphase reactions for a PAH vapor and ozone at the surface of a falling water droplet in the atmosphere.

The surface reaction rate depends on the surface concentration of PAH and the ozone surface concentration, where the rate of adsorption and desorption of ozone molecule is given by the langmuir isotherm,

$$[O_3]_s = \frac{S_0 [O_3]_g}{C_{1/2} + [O_3]_g} \quad (6.8)$$

where S_0 is the total number of adsorption sites, $C_{1/2}$ is the ozone concentration in the gas phase when $[O_3]_s$ is equal to $\frac{1}{2}S_0$.

The rate of loss PAH on the droplet surface is then given by,

$$-r_A = k'' [O_3]_s [PAH]_s \quad (6.9)$$

The above equation gives the pseudo first order rate constant for the loss of PAH molecule. The flux of gas phase PAH molecule onto the droplet surface is equated to the surface reaction rate as follows,

$$\frac{[PAH] \widehat{C} \gamma_s}{4} = k'' [O_3]_s [PAH]_s \quad (6.10)$$

Using the definition for $[O_3]_s$ in equation (6.8) and the assumption that $[PAH]_s = K_{IA} [PAH]$, we have

$$\frac{[PAH] \widehat{C} \gamma_s}{4} = \left\{ k'' \left[\frac{S_0 [O_3]_g}{C_{1/2} + [O_3]_g} \right] \right\} \{ K_{IA} [PAH] \} \quad (6.11)$$

Defining k_s as the term in the first parenthesis in the equation (6.11) and simplifying the above equation, the reaction term (γ_s) is given as

$$\gamma_s = k_s K_{IA} \frac{4}{\widehat{C}} \quad (6.12)$$

In the above equation, k_s (1/sec) is the overall pseudo-first order surface reaction constant for PAH on the droplet and K_{IA} with units of length (say microns) is the partition constant for the compound between the gas-water interface and the gas phase and \widehat{C} is the mean average thermal speed of the molecule. The equation for the overall mass transfer coefficient is hence given in the following equation (6.13),

$$\frac{1}{K_c} = \frac{d}{2D_G} + \frac{4}{\bar{C}} \frac{1}{\alpha} + \left(\frac{1}{K_{WA}^* \sqrt{\frac{4D_L}{\pi\tau}} + k_s K_{IA}} \right) \quad (6.13)$$

Each of the terms in the above equation (6.13) represents a resistance to mass transfer. The first term on the RHS is diffusion resistance, the second term is the resistance due to mass accommodation and the last term is the resistance due to bulk phase solubility and surface reaction acting parallel. In addition to the assumptions of negligible solubility and instantaneous solvation rate of surface reaction products into the bulk phase, the Langmuir-Hinshelwood surface reaction is assumed ([Atkins, 1998](#)). In a Langmuir-Hinshelwood mechanism of surface-catalyzed reactions, the reaction takes place between molecular fragments and atoms adsorbed on the surface. In this type of surface reaction mechanism, the ozone adsorbs at the droplet surface and reacts with already adsorbed naphthalene.

As derived in chapter 4, equation (4.4b) for K_{DV} is rewritten here for continuity, where τ^* is a characteristic time for mass transfer into the droplet.

$$K_{DV} = \zeta \cdot K_{WA} \left[1 - \exp\left(-\frac{\tau}{\tau^*}\right) \right] \quad (6.14)$$

In the above equation, τ^* is given as follows, $\tau^* = \frac{1}{K_c} \cdot \frac{d_D}{6} \cdot \zeta \cdot K_{WA}$ for the mass transfer of PAH based on a three step process discussed above. For smaller droplets and at higher ozone concentration, the surface reaction becomes important and the characteristic time for a surface reaction is given as follows,

$$\tau_{surf\ rxn}^* = \frac{d_D}{6} \cdot \frac{1}{k_s K_{IA}} \cdot \zeta \cdot K_{WA} \quad (6.15)$$

The solubility-limited uptake is given by the following equation $\tau_{sol}^* = \frac{d_D}{6} \sqrt{\frac{\pi\tau}{D_L}}$.

The ratio of the characteristic time due to surface reaction and solubility characterizes,

known as the Hatta number, $Ha = \frac{k_s K_{IA}}{\zeta \cdot K_{WA} \sqrt{\frac{D_L}{\pi\tau}}}$, characterizes the importance of surface

reaction and bulk phase solubility. Experimentally, the importance of the surface reaction rate can be delineated by the amount of reaction products for different droplet sizes, wherein the reaction products would be higher for smaller droplets than in comparison for the larger droplets.

6.2 Ozone Reaction With Naphthalene Vapor on Water Droplets

The droplet concentration and the vapor concentrations are measured experimentally at the reactor outlet by the methodologies discussed in the previous chapter. From equation (6.15) we can calculate $\tau_{surf\ rxn}^*$, as all the other parameters are known. The gas-droplet contact time for all the experiments discussed in this ranged from about 0.17 to 0.2 seconds. The gas phase concentration of naphthalene varied from 0.1 to 1 ppm in the experiments. Figure 6.4 below shows a plot of a typical evolution of the naphthalene concentration observed in the vapor phase. Notice the steady vapor phase concentration observed during a six-hour period. The concentration observed during this period (in Figure 6.4) was between $0.252\mu\text{g}/\text{mL}_{\text{He}}$ to $0.354\mu\text{g}/\text{mL}_{\text{He}}$ with a 95% confidence level.

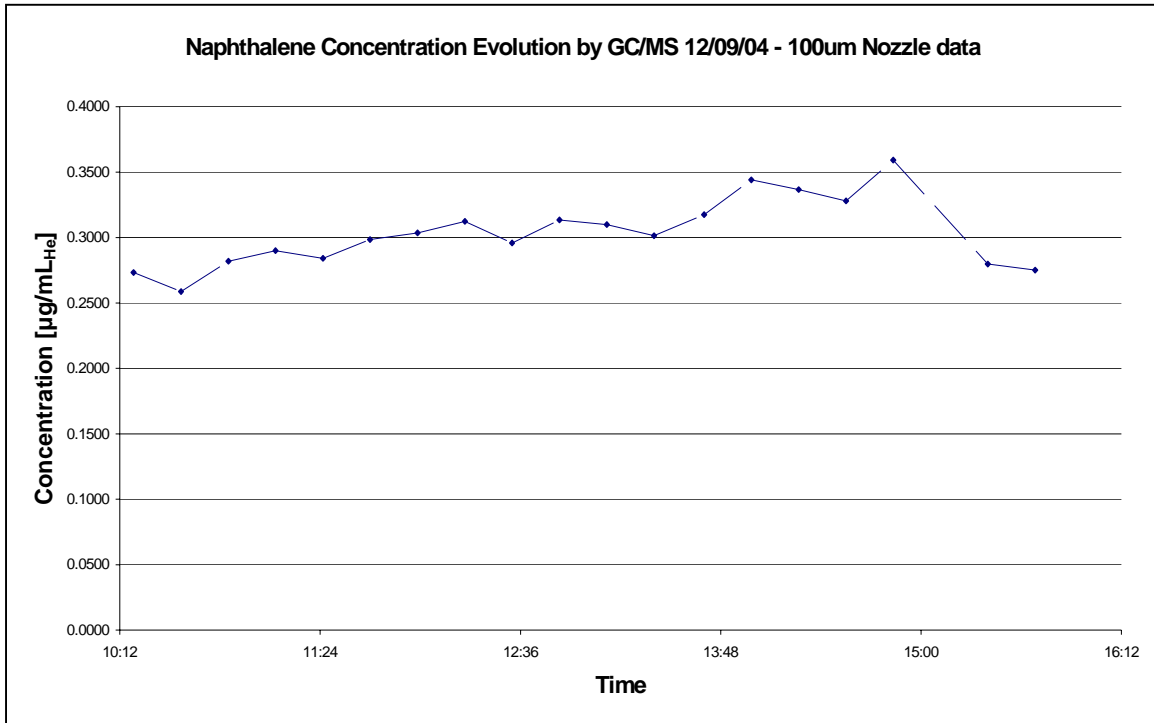


Figure 6.4. Typical evolution of vapor phase naphthalene concentration in µg/mL.

Even though the observed concentration between each consecutive day was different, the concentrations were quite constant during the time period of the experiment. All experiments were conducted at the reactor temperature of 296 ± 1 K and reactor pressure of 760 Torr. All the other relevant parameters listed in Table 4.1 were used directly to compute the characteristic time and the mass transfer coefficient as given in the expression for τ^* . The mass transfer coefficient is used in computing the pseudo-first order surface reaction according to equation (6.14) by trial and error.

6.3 Surface Reaction and Gas Uptake

As shown in the Table 6.1, the overall mass transfer coefficient and the overall pseudo-first order surface reaction constant increases with increasing ozone concentration for a given droplet diameter. With increased reaction rate at the interface, the overall liquid phase resistance decreased and the mass transfer coefficient increased.

Table 6.1 Calculated mass transfer coefficients and overall pseudo-first order surface reaction constant for 55 μm droplet diameter. (At $296 \pm 1\text{K}$ and ~ 760 Torr).

Ozone [molecules/ cm^3]	K_C [m/sec]	k_s [1/sec]
1.7E+12	2.47E-03	104
2.5E+14	4.83E-03	295
6.0E+14	5.05E-03	319
1.3E+15	6.63E-03	562

The Figure 6.5 illustrates the effect of increase in ozone concentration on the measured droplet-vapor partition constant [K_{DV}]. In each of the droplet sizes studied, the K_{DV} reaches an asymptotic value. With clear influence of droplet diameter on the K_{DV} value, the asymptotic value for a 55 μm droplet is about 40, while that of 91 μm is about 30 and a asymptotic K_{DV} value of 15 was observed for a 182 μm droplet diameter. As observed for the uptake studies shown in Chapter 4 the partition constant is larger for small droplet size since the surface effect becomes dominant. It is important to note that these droplet-vapor partition constants are for the specified gas liquid contact time used in this work and not equilibrium values. Table 6.2 shows the influence of droplet size on transport coefficients and other kinetic parameters.

From the data presented in the Table 6.2, we note that the mass transfer coefficient becomes smaller as the droplet size is increased. This decreasing trend in K_C indicates that the overall resistance is lesser for a smaller sized droplet than for a larger 182 μm droplet size. Also from Table 6.1 and 6.2, we note that the rate constant increases with decreasing droplet size and increases with gas-phase ozone concentration. The calculated Hatta number of greater than 2 indicates that surface reaction rate is much faster than diffusion into the bulk of the liquid droplet. For a larger 182 μm droplet, the surface reaction rate is not quite profound and is indicative from a rather constant K_{DV}

value (in Figure 6.5) for all the ozone concentrations studied. The gas phase resistance is smaller and the liquid phase resistance is smaller for a 55 μm droplet than for 182 μm droplet, which emphasizes the extent of surface reaction in a smaller droplet.

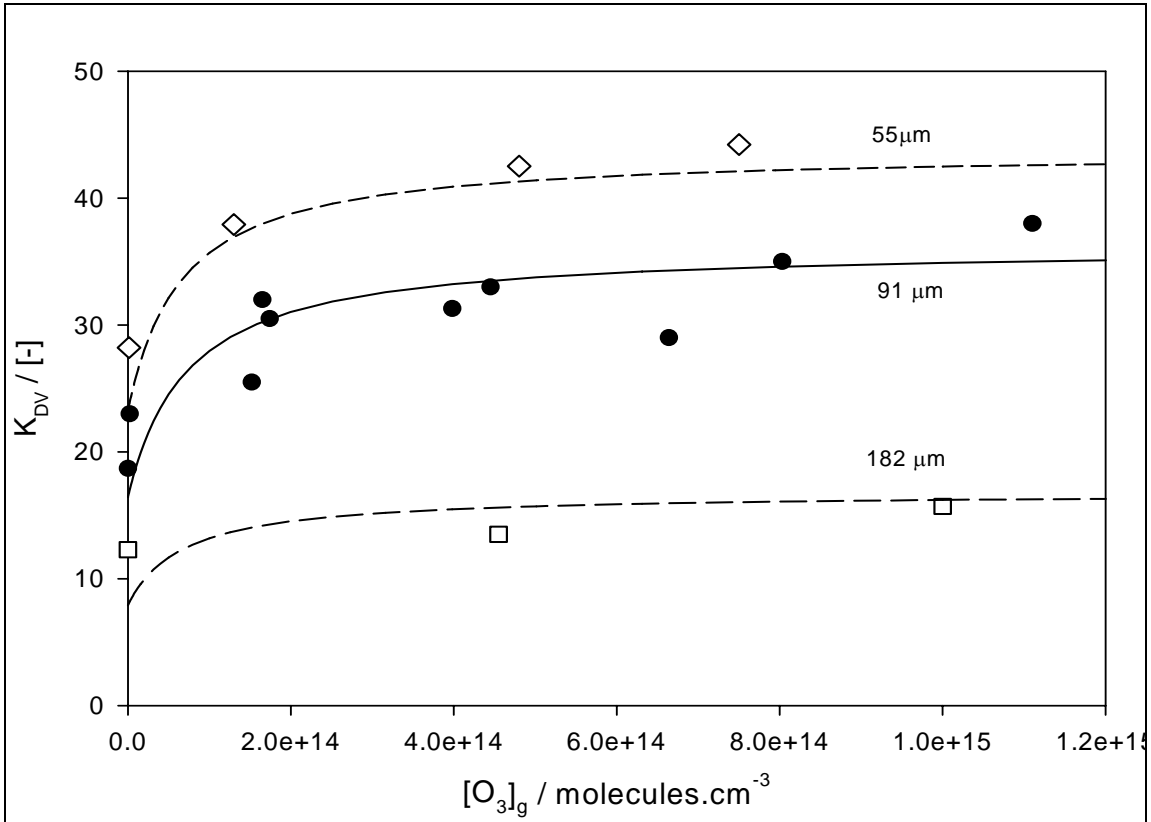


Figure 6.5 The droplet-to-vapor partition constant of naphthalene on different droplet sizes with increasing gas-phase ozone concentrations. The solid lines are predicted values based on the k_s estimated from Equation 6.14 using k_{max} and $C_{1/2}$ obtained from Figure 6.6.

Table 6.2. Influence of droplet size on transport and kinetic parameters*.

Droplet Size	K_C [m/sec]	k_s [1/sec]	Resistances [%]			Hatta Number
			Gas Phase	Mass Accom.	Liquid Phase	
55 μm	5.05×10^{-3}	392	2.4	41.4	46	4.9
91 μm	4.44×10^{-3}	235	3.5	36.3	60	2.6
182 μm	3.93×10^{-3}	141	6.3	32.2	62	1.7

* - Average O_3 concentration 6.58×10^{14} [molecules/cm³]

There are various lines of evidence pointing to the significance of the surface reaction in determining the overall uptake into droplets. Molecular dynamics simulations by [Vacha et al., 2004](#) show a surface minimum free energy deeper than oxygen and nitrogen. That corresponds to a sevenfold increase in the ozone concentration at the gas-water interface in comparison to the gas phase. This is attributed to a combination of its low solubility in water ($K_{WA} = 3.2$) but significant polarizability (2.85 \AA^3). As mentioned earlier the observed negligible bulk phase uptake of ozone in the droplet even at the highest gas-phase ozone concentration is in support to these measurements. Our earlier work, presented in Chapter 4, clearly showed that benzene, naphthalene and phenanthrene accumulates at the air-water interface on small water droplets compared to the bulk phase. The non-linear dependence of the partition constant, K_{DV} in Figure 6.4 and the rate constant, k_s in Figure 6.5 on the gas-phase ozone concentration is another important evidence for the surface reaction of ozone with naphthalene.

6.4 Estimation of Langmuir-Hinshelwood Parameters

As discussed in section 6.2 of this chapter, the pseudo-first order reaction rate constant k_s was computed by trial and error method for all the experimentally measured droplet-vapor partition constant K_{DV} , measured for different ozone concentrations and different droplet sizes studied (55 μm , 91 μm , 192 μm). As we noted earlier from the tabulated values of the rate constant in Table 6.1 and 6.2 increases with increasing concentration and decreasing droplet size, the Figure 6.6 below shows that k_s reaches an asymptotic value similar to the measured K_{DV} (shown in Figure 6.5). The non-linear change in the rate constant indicates that the surface reaction was the controlling process.

From equation (6.11), the expression for the overall pseudo first order surface reaction constant for a PAH (k_s) with units of sec^{-1} is given as follows,

$$k_s = \frac{k^{\max} [\text{O}_3]_g}{C_{1/2} + [\text{O}_3]_g} \quad (6.21)$$

Where k^{\max} is the maximum (asymptotic) value of the rate constant and is given by $k^{\text{II}}S_0$, the product of the second-order surface reaction rate constant ($k^{\text{II}} / \text{cm}^2 \cdot \text{s}^{-1}$) and the surface concentration of ozone adsorption sites on the surface (S_0 / cm^{-2}). $C_{1/2}$ is the ozone concentration in the gas phase at which $k_s = (1/2) k^{\max}$ and is related to the rates of surface desorption to adsorption of ozone. Re-writing equation (6.21) in a linearized form, we obtain equation (6.22)

$$\frac{[\text{O}_3]_g}{k_s} = \frac{1}{k^{\max}} \cdot [\text{O}_3]_g + \frac{C_{1/2}}{k^{\max}} \quad (6.22)$$

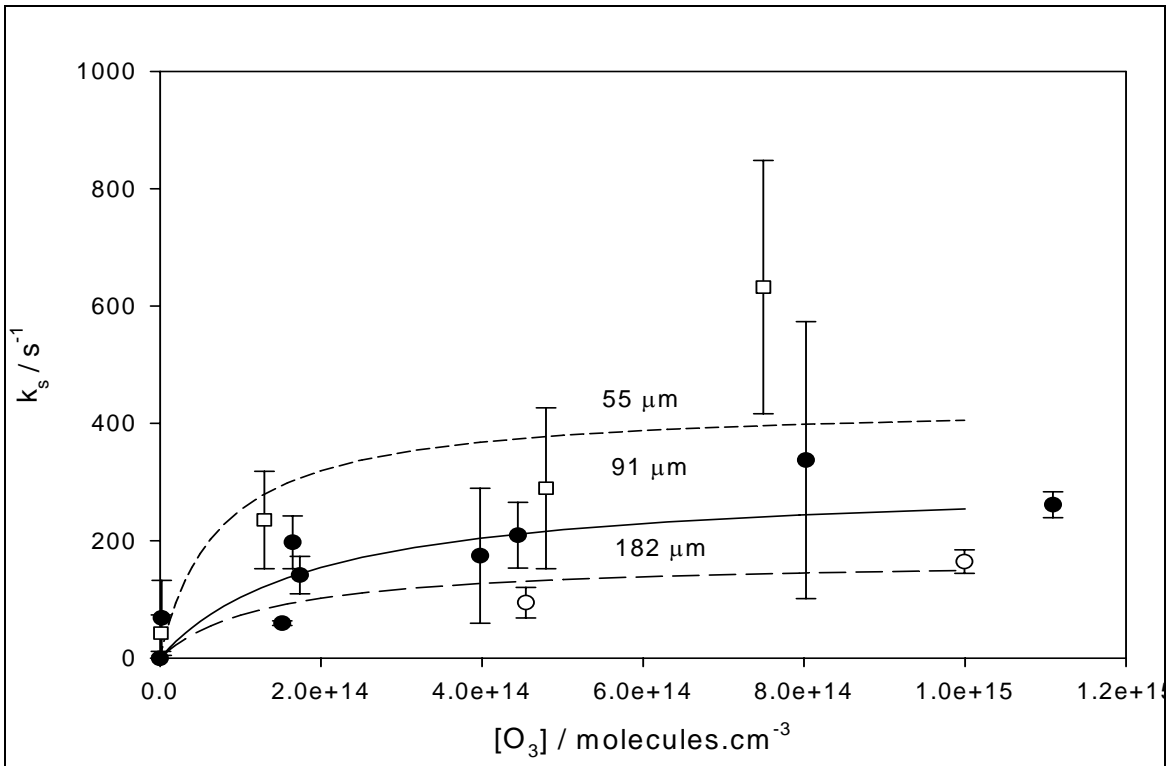


Figure 6.6. Langmuir plot of Equation (6.21) with the values of k_{\max} and $C_{1/2}$ determined from Equation (6.22) and given in Table 6.3.

Table 6.3. Langmuir – Hinshelwood parameters for ozone at the droplet surface for various sizes.

Droplet size	k^{\max}/s^{-1}	$C_{1/2}/\text{molecule.cm}^{-3}$	N	R^2
55 μm	435	7.21×10^{13}	4	0.81
91 μm	303	1.92×10^{14}	10	0.85
182 μm	169	1.31×10^{14}	3	0.80
	1429 (with 0.029 g/L FA)	2.8×10^{13} (with 0.029 g/L FA)	3	0.96
	1400 (with 0.021 g/L FA)	4.3×10^{13} (with 0.021 g/L FA)	4	0.98

Note: N is the number of data points. R^2 is the correlation coefficient for the linear fit to Equation (6.22) and FA is Fulvic Acid (an organic carbon surrogate).

A linear regression of the above equation for each droplet size using the computed k_s value, by trial and error, Langmuir-Hinshelwood parameters were obtained as shown in the Table 6.3 below for experiments performed at 298 Kelvin. The value of k^{\max} increased with decreasing droplet size and $C_{1/2}$ increased with increasing droplet size as shown in the table.

6.5 Effect of Organic Surrogate on Ozone Kinetics

In chapter 4 influence of organic surrogate such as Fulvic Acid on uptake of aromatic compounds were shown. In this section, the influence of fulvic on the ozone kinetics and organic compound uptake is considered. Fulvic acid (FA) is a known surrogate that exhibits properties similar to the surface-active organic carbon in fog droplets ([Cappiello et al., 2003](#)). The presences of surface-active organic materials have been documented in fog-water to cause substantial enrichment hydrophobic toxic substances such as pesticides and PAHs ([Glotfelty, et al., 1987](#), [Zhang and Anastasio, 2001](#)). In addition to altering surface tension, they can affect the movement of materials across aqueous interfaces, change the solubility of compounds in environmental aqueous systems, and also alter size distribution of aerosols ([Andrews and Larson, 1993](#),

[Cappiello et al., 2003](#), [Latif and Brimblecombe, 2004](#)). In chapter 4, it was shown that the surface tension of water decreased from 70 to 51mN/m with 0.029 g/L of FA indicating saturation of the droplet surface with fulvic acid.

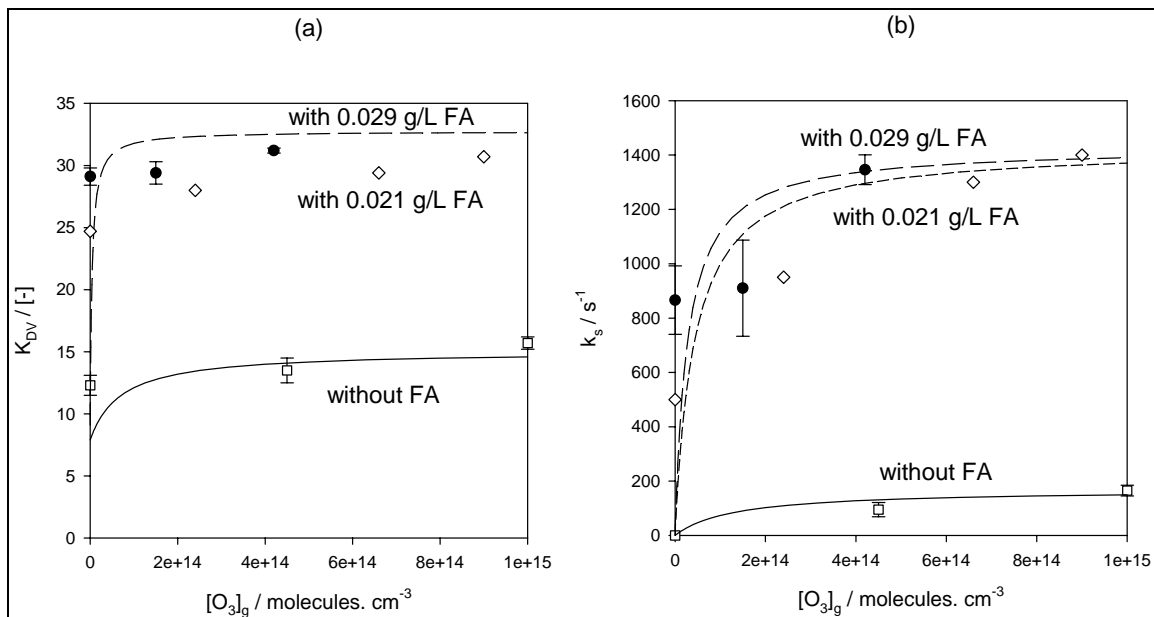


Figure 6.7. The effect of added fulvic acid (FA) on (a) the droplet-to-vapor partitioning and (b) the pseudo first-order surface rate constant of naphthalene with ozone.

Figure 6.7 shows the effect of adding 0.021 and 0.029 g/L of fulvic acid (equivalent to 12 and 17 mg of Carbon/L respectively) to the water droplet on the naphthalene partitioning and ozone reaction for a droplet of 182 μ m size. The fact that FA-covered surface is conducive to the trapping of ozone and naphthalene and decreasing the mass transfer resistance at the surface is evident from the 2 to 3 fold increase in K_{DV} and the 9 to 10 fold increase in k_s as seen in Figure 6.7. Similar increases in ozone and anthracene trapping efficiency on planar water surfaces have been noted by [Mmereki et al., 2004](#) in the presence of an organic compound. Approximately an order of magnitude increase in both k^{max} and $C_{1/2}$ for ozone was observed in the presence of fulvic acid

(Table 6.3). Thus, organic-coated surfaces of water droplets can show much higher ozone reactivity with adsorbed PAH molecules.

6.6 Reaction Products Due to Heterogeneous Oxidation of Naphthalene by Ozone

As naphthalene is transferred to the droplet, its reaction with ozone at the air/water interface will lead to several reaction products that can be identified in the aqueous phase collected at the outlet of the reactor. Figure 6.9 is a typical GC/MS trace where three main products were identified by their mass spectra (Table 6.4). These were 1,2-benzenedicarboxaldehyde (**2**), 1-naphthalenol (**3**) and 1,4-naphthalenedione (**4**). These are also well known intermediates of ozone oxidation of naphthalene in the bulk aqueous phase ([Bailey, 1982](#)).

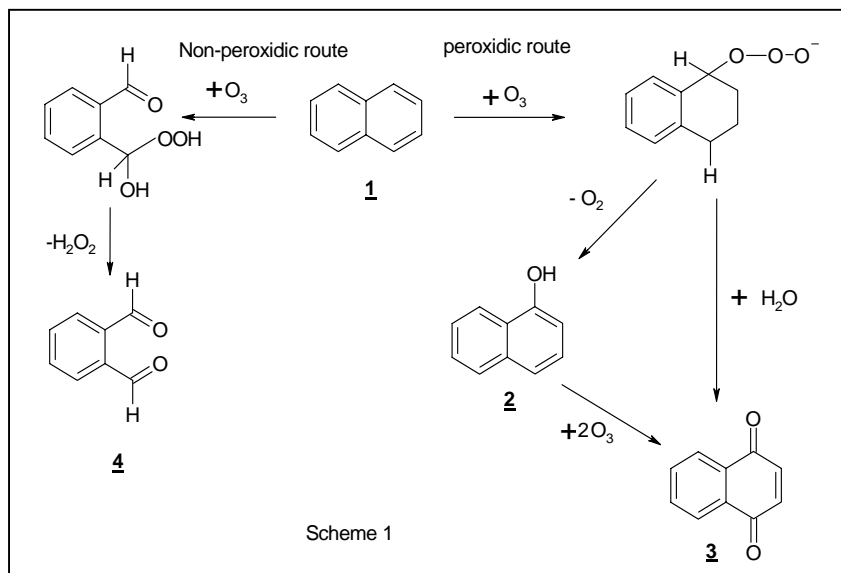


Figure 6.8. A schematic of the reaction mechanism for naphthalene with gas phase ozone.

As shown in Figure 6.8, both **3** and **4** are produced as a consequence of a peroxidic route and **2** are produced via a non-peroxidic route. Both involve attack by ozone on carbon in position number 1 of the 1,2-bond in the naphthalene molecule, which has the lowest bond delocalization energy. In the peroxidic route the elimination of oxygen molecule leads to **3** whereas the addition of water to the peroxide or the addition

of ozone molecules leads to **4**. In the non-peroxidic route the elimination of a hydrogen peroxide molecule leads to the product **2**.

Table 6.4. GC/MS characteristics of the reaction products identified in liquid phase.

Compound	Retention time/ min	Molecular weight	Ion Peaks, m/z
Naphthalene (1)	13.76	128	51,75,102,128
1,2-Benzenedicarboxaldehyde (2)	14.53	124	51,77,106,134
1-Naphthalenol (3)	18.10	144	57,89,115,144
1,4-Naphthalenedione (4)	16.90	158	50,76,102,130,158

The reaction products shown in the Figure 6.9 were quantified for the three droplets size studied. From the Table 6.5, we see the significance of surface reaction in a smaller size droplet (55 μ m) in comparison to a larger sized droplet. In the case of 182 μ m droplet size the concentration of the reaction product were below the detection limit, while an increasing concentration of reaction product with decreasing droplet size for droplets smaller than 182 μ m. This increase in concentration of the reaction product emphasizes the significance of surface reaction in micron-sized droplet in comparison to larger droplets.

Table 6.5. Concentration of identified liquid phase reaction products.

Droplet Size	(1) – Gas	(1)	(2)	(3)	(4)
55 μ m	0.14ppm	6.19ppm	0.1ppm	0.024ppm	0.996ppb
91 μ m	0.26ppm	8.01ppm	0.01ppm	0.016ppm	0.588ppb
182 μ m	0.31ppm	8.65ppm	<d.l.	<d.l.	<d.l.

(**1**)-Naphthalene; (**2**)-1,2-Benzenedicarboxaldehyde; (**3**)-1-Naphthalenol; (**4**)- 1,4-Naphthalenedione; <d.l.-lower than detection limit. Note: Detection limit depends on component mass present in liquid sample.

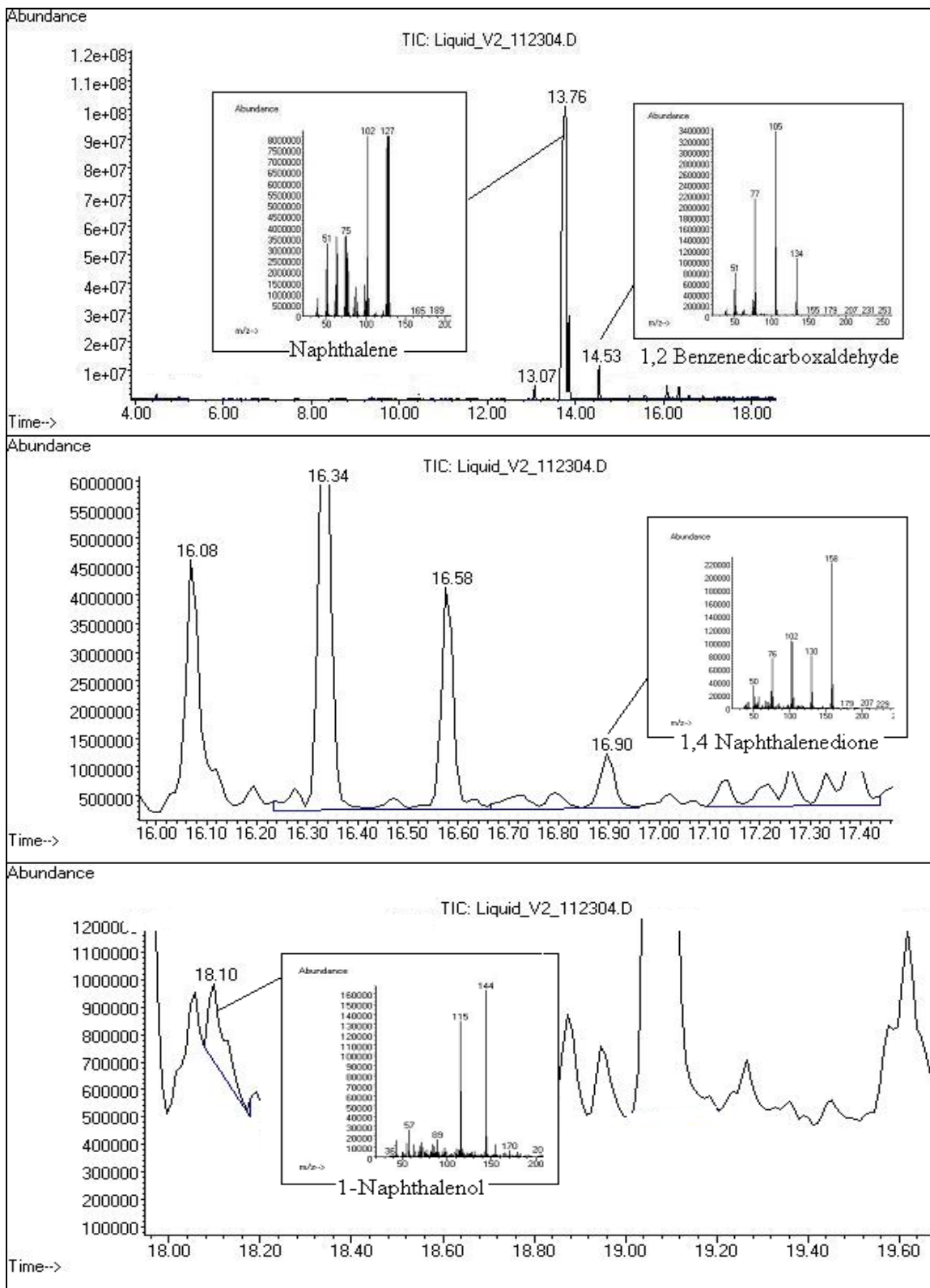


Figure 6.9. A typical GC/MS trace of the liquid collected at the bottom outlet of the reactor. Note the intermediates identified in the text.

6.7 Summary

Heterogeneous oxidation of PAH vapor on micron-sized droplet was studied in a droplet train apparatus. Presence of ozone in the flow tube reactor increased the mass transfer of PAH vapor into the droplet, thereby increasing the droplet-to-vapor partition constant. The pseudo-first order rate constant for the surface reaction of ozone with adsorbed PAH vapor was modeled using the well-known Langmuir-Hinshelwood mechanism. Three reaction products for naphthalene and phenanthrene were observed for the heterogeneous oxidation by ozone on the droplet surface. The reaction products due to heterogeneous oxidation by ozone on micron-sized droplets may be more toxic than the parent compound. Concentration of reaction products observed in the droplets for a 55 μm droplet were significantly higher in concentration while no reaction products were observed for a 182 μm droplet. This signifies the importance of surface reaction presenting a micron-size droplet.

In order to extend and verify the knowledge and observations in a laboratory scale droplet-gas system to atmospheric fogwater, field sampling of fogwater in metro Baton Rouge area was undertaken. The experimental methodology and results are presented in the following chapter.

CHAPTER 7

MATERIALS AND METHODS IN MONITORING FOGWATER CHEMISTRY

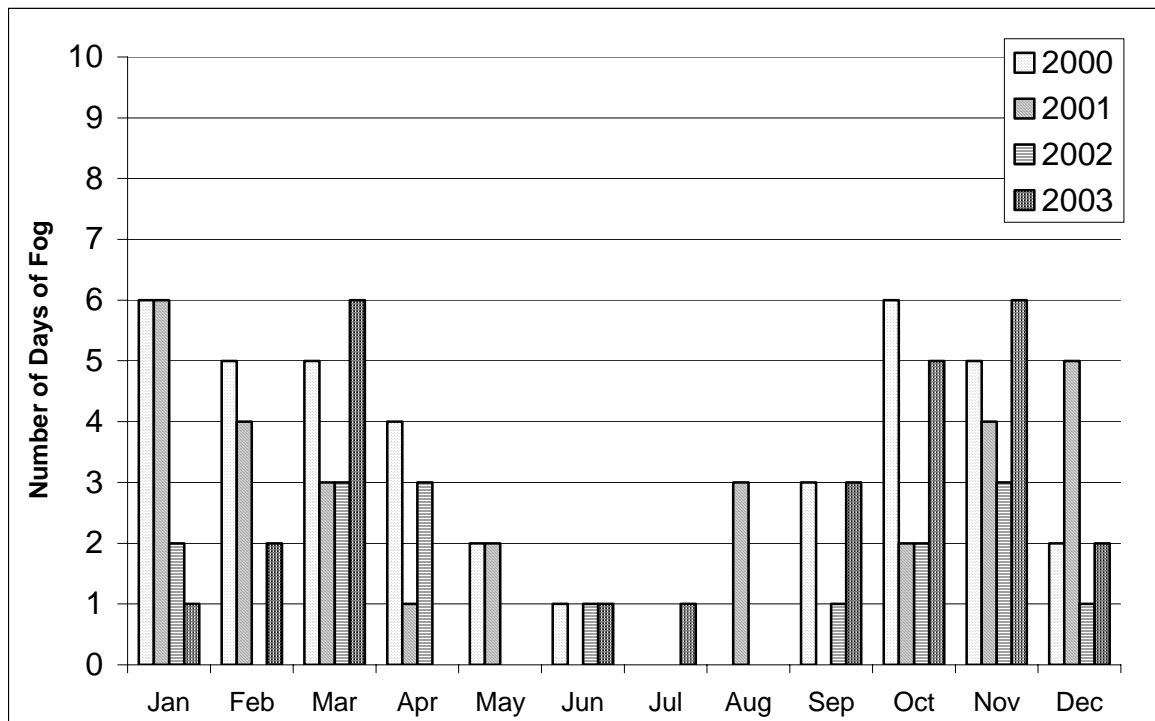
7.1 Introduction

Transport of airborne contaminants takes place through wet and dry deposition. Presence of fogwater in polluted atmosphere can influence atmospheric chemistry and air quality. The mechanisms that are important in controlling fogwater compositions involve the interaction of fogwater droplets with aerosols and gases. Atmospheric aerosols provide nuclei for the growth of fog droplets (Figure 1.1). Chemicals adsorbed on the surface of cloud condensation nuclei (aerosols) may partially solvate in the fog droplets contributing to the chemical composition of the fog droplet. Knowledge gained from laboratory studies about mass transfer and kinetics of gas and micron-sized droplet interactions are to be validated and confirmed by analyzing fogwater and air samples that are in contact in the field.

Interactions of cloud and fogwater with atmospheric gases and aerosols in the heavily industrialized area of the Gulf Coast region of Louisiana provides an excellent zone for studying these multiphase and heterogeneous interactions, where most of the world's recognizable chemical and petrochemical companies are situated ([Petersen, 1999](#), [Burby, 2000](#)). In particular, the area between metro Baton Rouge and New Orleans along the banks of the Mississippi river is of interest, since it is alleged to be a highly polluted region ([Allen, 2003](#)). Louisiana is also typical of a predominantly agricultural area in the northern parishes where various pesticides are in use. Atmospheric sampling from this laboratory in the metro Baton Rouge atmosphere have shown petrochemical markers

such as aliphatic and aromatic hydrocarbons, and agricultural markers such as pesticides ([Subramanyam et al., 1994](#)).

This region of the country also sees its share of dense fog events during the fall season. Fog frequency averages 40 days during the year in the Louisiana Gulf Coast region ([Ahrens, 2000](#)). Extremely low visibilities created by dense fog have contributed to several multi-vehicle accidents resulting in injuries and fatalities. Figure 7.1 shows a histogram of the number of fog events observed between 2000 and 2003 with visibility ranging from less than ¼ mile to about ¾ mile.



* - (Station: Metro Baton Rouge Airport; Source: <http://www.NOAA.org/>)

Figure 7.1. Number of fog events observed between 2000 and 2003 with visibility ranging from less than 1/4mile to 3/4mile.

7.2 Formation and Deposition Cycle of Fog

Typically, a fog or cloud is formed by condensation of water on the surface of sub-micron solid aerosol particles, known as cloud condensation nuclei, when the air temperature cools down to its dew point temperature in the near-surface atmosphere.

Typically fog droplet dimensions range from 1 to 50 μm . There are various types of fog formed in the atmosphere; these are classified as radiation fog, precipitation fog, advection fog, slope fog and valley fog. Table 7.1 lists some of the properties of typical atmospheric aerosols.

Radiation fog forms during a clear calm night and high-pressure conditions when the ground surface cools by loss of heat by radiation along with the presence of a shallow moist air near the surface. In this type of fog, cooling due to radiation allows the temperature to drop to the dew point resulting in fogwater formation. Such a fog may appear at sunset or at night and disappear after sunrise. Formation of fog in Baton Rouge is predominantly by radiation fog.

Advection fogs are formed due to transport of generally warm-humid air on cold surfaces, thereby rapidly reaching the dew point temperature. This type of fog is long lasting and reaches higher altitudes than radiation fog. Advection fog also forms due to transport of cold air on relatively warm river or lake waters. Upslope fog occurs when a parcel of air ascends up a slope and thereby expands and cools to the dew point temperature. This type of fog formation requires strong winds to move the parcel of air upslope.

Table 7.1 lists some of the physical properties of atmospheric aerosols. Typically, aerosols and fogwater have size between a tenth of a micron to about 10 μm . While cloud drops, rain drops and snow flakes have larger size, usually in millimeter range. Smaller particles, such as aerosol and fogwater, have large residence times. Larger snowflakes, rain drops and cloud drops have shorter residence time, due to gravitational settling.

Aerosols and fogwater also undergo change in size distribution due to Brownian coagulation, generally observed in micron-sized particles in suspension.

Table 7.1 Properties of atmospheric aerosols ([Valsaraj, 2000](#))

Nature of droplet	Size range [μm]	Surface Area [m²/m³]	Liquid Water Content [m³/m³]	Residence Time
Aerosols	0.01-10	~1 x 10 ⁻³	10 ⁻¹¹ -10 ⁻¹⁰	4-7 days
Fogwater	1-10	8 x 10 ⁻⁴	5 x 10 ⁻⁸ – 5 x 10 ⁻⁷	3 hours
Cloud Drops	10-10 ²	~ 2 x 10 ⁻¹	10 ⁻⁷ – 10 ⁻⁶	7hours
Rain Drops	10 ² -10 ³	5 x 10 ⁻⁴	10 ⁻⁷ – 10 ⁻⁶	3-15min
Snow Flakes	10 ³ -10 ⁵	0.3		15-50min

The fog thus formed in the atmosphere undergoes chemical exchanges with the dispersed air. Organic and inorganic chemicals distribute between the vapor and aqueous phases and between the particles present in both vapor and the aqueous phase, with a possibility of surface and bulk phase reactions. As the weather conditions change, such as increase in temperature, the fog dissipates and the chemicals contained in the fogwater will deposit on the surfaces contacted by the fog. This cycle of formation, deposition, and dissipation cycle is a mechanism in which atmospheric pollutants are introduced into the terrestrial and aquatic environments ([Waldman et al., 1985](#)).

7.3 Previous Work in this Area

Fogwater characteristics have been explored in various locations particularly in the non-urban, agricultural environments and a few in the more urban environments. The characteristics of the fog formed in urban environments can be different considering the fact that they occur in the more polluted urban atmosphere.

The deposition of fog-water promotes the atmospheric processing of sub-micron particles, organic molecules and inorganic ions. Typical characteristics of fog such as pH,

conductivity and ion composition have been studied for a number of locations ([Waldman et al., 1982](#), [Millet et al., 1996](#), [Pruppacher and Klett, 2003](#)). Fogwater has been a much-researched area for sometime ([Jacob et al., 1985](#), [Glotfelty et al., 1986](#)).

[Capel et al., 1991](#) obtained concentrations of n-alkanes, polycyclic aromatic hydrocarbons (PAHs) and polychlorinated biphenyls (PCBs) in fogwater in an urban area in Zurich, Switzerland. In many samples, the concentrations of individual alkanes and PAHs exceeded their water solubility and were attributed to the presence of colloidal organic matter.

Though much is known regarding the fog processing of particles and ions much less information exist on organic molecules in fog ([Munger et al., 1983](#), [Herckes et al., 2002](#)). A handful of compounds such as low molecular weight carboxylic acids, linear alkanes, pesticides and polycyclic aromatic hydrocarbons have been identified in some fog samples ([Decesari et al., 2000](#); [Limbeck and Puxbaum, 2000](#), [Collett et al., 1999](#), [Capel et al., 1991](#), [Glotfelty et al., 1987](#)). More recent efforts have concentrated on the surface-active components in fog ([Capiello et al., 2003](#)). Much of the extensive fogwater characterization data in the United States are in the California Central Valley, Los Angeles Basin and the northeast Atlantic coast regions where fog is a frequent occurrence ([Collett et al., 2002](#)). Although the Gulf Coast region of Louisiana experiences fogs several times during the year, the literature data on the fogwater characteristics is non-existent. In addition to this, in this work a direct observation of enrichment of fogwater in chemical species higher than that predicted by Henry's law is sought.

A series of fog collection campaigns were performed to obtain the baseline data on fog. In particular we were interested in (i) understanding whether fog in the heavily

industrialized corridor along the Gulf Coast differs from other urban areas of the U.S. and the world and, (ii) elucidating the possible sources of various species in the fog in this area. This study was in preparation for a more concentrated effort at size-fractionated, time-series analysis of fog composition to test the theory we have advanced that small fog droplets are enriched in many organic compounds as a result of surface adsorption ([Valsaraj et al., 1993](#), [Raja and Valsaraj, 2004a,b](#)).

7.4 Types of Fog Collector

There are a wide range of fogwater samplers/collectors available. Most of the fogwater collectors use impaction and interception to collect the fogwater droplets. A rotating rod collector manufactured by AeroVironment Inc. (see [Hering et al., 1987](#)), collects by impaction on a Teflon coated rod rotated at about 3450rpm. There are two rods, outer and inner rods of 1.6mm and 19mm, respectively. The size cuts obtained in these collectors are about $2.5\mu\text{m}$ (outer rod) and $10\mu\text{m}$ (inner rod).

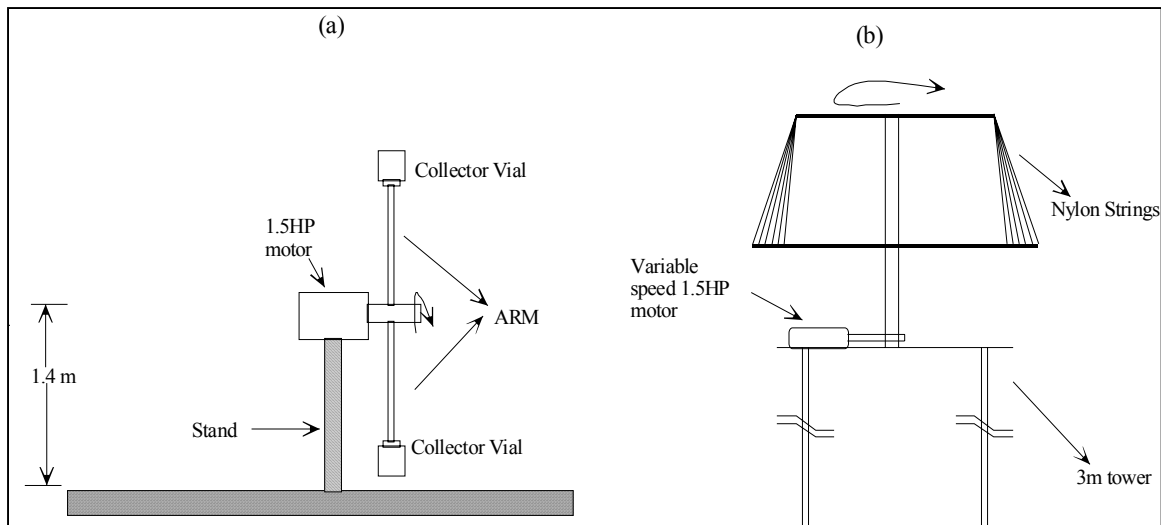


Figure 7.2. (a) California Institute of Technology (CIT) rotating arm collector. Fogwater impacts in the slots on the leading edge of the rotating arm. (b) Atmospheric Science Research Center (ASRC) string collector. These strings rotate in the horizontal plane; Fogwater is intercepted by the nylon strings.

The California Institute of Technology (CIT) rotating arm collector, in Figure 7.2(a), contains an external impactor that rotates at high velocity and is used for collecting large fogwater particles. These collectors contain deflectors that prevent water that impacts the solid part of the arm from being collected. Other types of collector that are available include the Desert Research Institute linear jet collector which is based on jet impaction principle, where fog is drawn through three rectangular jets at a total flow rate of 20 L/sec. This impaction type collector has a sharp cutoff on collection diameter of about 5 μ m.

An Atmospheric Science Research Center (ASRC) string collector, in Figure 7.2(b), contains 150 strings of 0.41mm each. The strings rotate at about 1000rpm and the Fogwater impacts the strings to collect in the traps on bottom plate. This collector requires manual transfer of sample into bottles.

7.5 Description of Fog Collection Equipments Used in This Work

7.5.1. High Volume Atmospheric Fog Collector

In the first series of fog collection campaigns, between March 2002 and March 2004, a modified form of the high volume atmospheric fog sampler ([Jacob et al., 1985](#), [Schomburg, 1991](#)) as shown in Figure 7.3 was used. The fog collector, depicted by the schematic in Figure 7.3, primarily consists of a fan that draws air through a set of screens enclosed in an aluminum cylindrical chamber. The screens were axially attached to a motor that can rotate them in either direction. The size of the screens (meshes) that were fitted into the collector was 1200 μ m and 74 μ m. The meshes in this high volume sampler can be removed and reinstalled for cleaning purposes.

The speeds of the fan and the screen rotations were variable using a motor controller. When the fan pulled the surrounding air at a high flow rate ($34.2\text{m}^3/\text{min}$), fog water impinged on the screens and collected in concentric grooves around the screens. A vacuum pump pulled the collected fog water through Teflon[®] tubes into Pyrex[®] sampling bottles. An air sampling tube was fixed in the fog collection chamber behind the screens. The air that was in contact with the fog droplets was sampled at a fixed flow rate ($\sim 0.8\text{ L/min}$) by passing it through an XAD bed that trapped the organics in the air stream. The XAD polymer traps were obtained from Supelco Inc. Sample collection was started a few hours before the anticipated fog event and continued at least after the fog dissipated to get the background air concentrations.

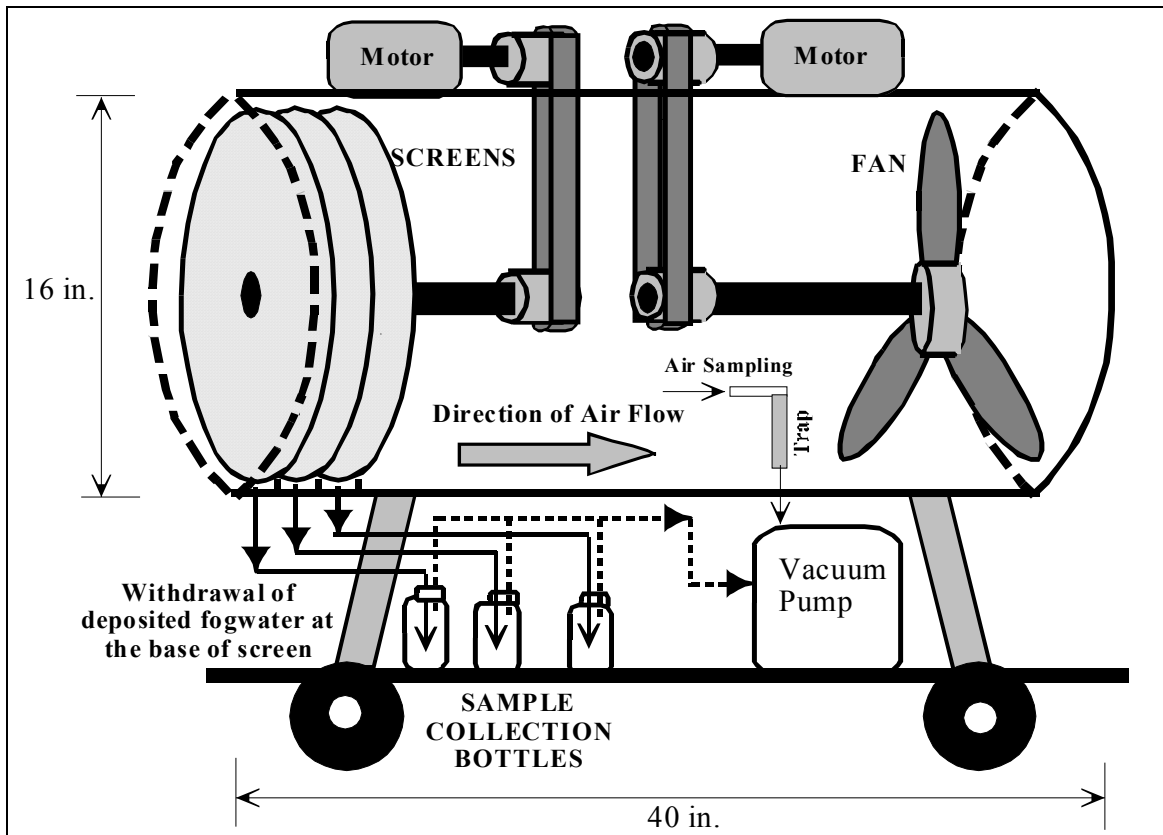


Figure 7.3. Schematics of High Volume Atmospheric Fogwater Collector.

After a fog event, the sample bottles and the XAD traps were sealed and transported back to the laboratory for storage or analysis. The amount of fog water collected varied between 20 – 125 mL depending on the duration of the event. The fog collection equipment was placed in a location facing an open agricultural field, with no tall structures for at least 400 meters in all directions in front of the equipment. Typically, an intensity of fog equivalent to a visibility of $\frac{1}{4}$ mile or less was found to be necessary to collect any fog water. The approximate duration of actual fog collection was estimated from the period of dense fog (visibility $< \frac{1}{4}$ mile) reported by the National Weather Service (NWS) for a nearby area.

7.5.2. Caltech Active Strand Cloudwater Collector (CASCC)

In the second fog collection campaign between November 2004 and March 2005, two-stage sfCASCC, a single stage collector, which is a compact version of the original CASCC design ([Dauble et al., 1987](#) and [Jacob et al., 1985](#)), and a three-stage collector that was designed for this project, was used. The sfCASCC (size fractionated California Active Strand Cloudwater Collector) contains two stages as shown in Figure 7.4. The first stage contains a bank of four rows, each containing eight 12.7mm diameter Teflon rods. Each Teflon rod is offset from those in the front, to avoid rods overshadowing those in the previous rows. Downstream of the inlet is the second stage that contains a bank of six rows containing 102 Teflon strands of 508 μ m spaced 2.3mm part from center to center. The droplets collected with 50% efficiency in the first stage was predicted to be 23 μ m and 4 μ m from the second stage ([Demoz et al., 1996](#)), and thereby, enabling the operator to collect independent large and small droplet size fractions from the sample cloud and fog. The Teflon strands in the CASCC are inclined at 35° from the vertical to

enhance droplet removal by aerodynamic drag. The droplets that are collected by impactions are drawn into the collection vials, through Teflon troughs and tubes, by a combination of gravity and aerodynamic drag.

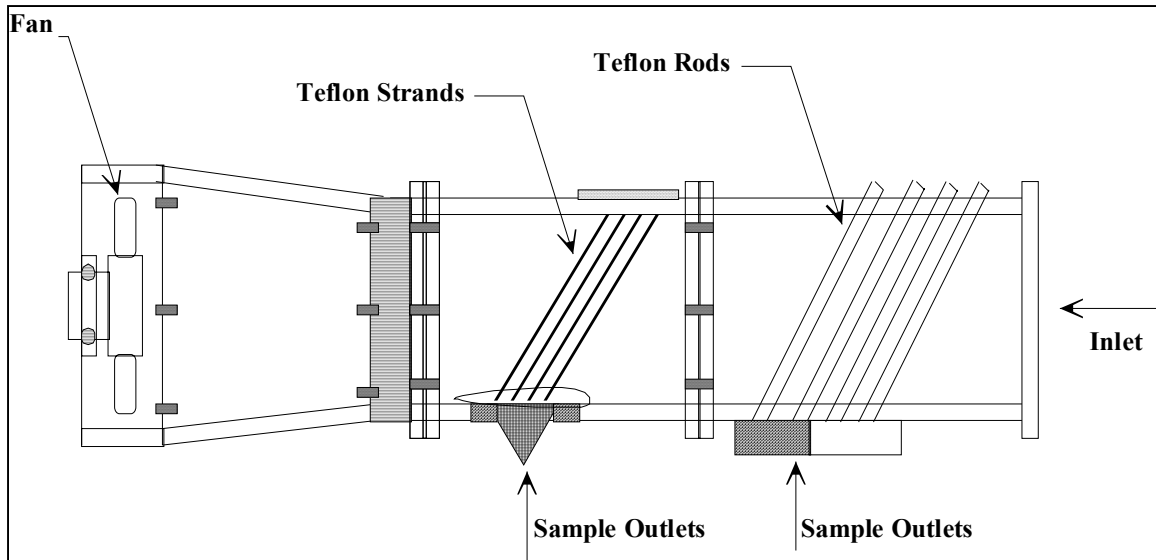


Figure 7.4. Size Fractionating California Active Strand Cloudwater Collector (CASCCsf).

The single stage collector (from here on referred to as CASCC2) collects the bulk cloudwater sample that is representative of the entire fogwater size distribution. In this collector, large droplets are collected by impaction on the Teflon strands (508 μm diameter), while smaller droplets are able to follow the streamlines around the Teflon strands. The droplet size that is collected with 50% efficiency in the single stage collector was predicted to be 3.5 μm (Demoz et al., 1996). The high volume atmospheric fogwater collector was placed at about 2 feet from the ground surface, while the collectors used in the second fog collection campaign was placed at about 10 feet from the ground.

Similar to the methodology described earlier, an XAD (polymer) bed was placed behind the fan in the sfCASCC to sample the air that is in contact with the fog droplets simultaneously. The flow rate of the air flowing through the polymer bed was maintained

at 20L/min. Sample collection was started a few hours before the anticipated fog event. In certain events the air sampling was started at the same time the fogwater collection was started.

[Hering et al., 1987](#) collected fogwater samples, using five different fog collectors simultaneously, to assess differences in measured acidity, analyte concentrations, and liquid water collection efficiencies in fogwater samples from different collectors. Analysis of the collected fogwater samples showed that the acidity measurements and metals concentrations were not affected by the nature of sampling methodology. However, details on the loss of organic compounds in the collected fogwater are not available.

7.6 Analysis of Fog-Water Samples

The fog water samples were filtered using a 0.45 μ m filter cellulose acetate membrane filter as soon as they were brought to the laboratory. The membrane was stored for potential analysis. Liquid sub-samples were isolated for the measurement of pH, conductivity, dissolved organic carbon content (DOC), organic and metals content. The pH and conductivity were measured using Orion[®] Model 210 pH meter and Oakton Model 10 respectively. The analyses of ions were done using a Dionex DX320 Ion chromatograph instrument. The DOC content was analyzed using a Shimadzu 5050A TOC analyzer. For metal analysis a 1mL sub-sample was diluted 10 times with a 2% nitric acid solution. Analysis of selected inorganic elemental analysis was performed according to EPA-SW 846 method 6020 using ICP-MS (Perkin Elmer Model Elan 9000).

The organic analytes were extracted with dichloromethane (DCM) based on EPA method 3510 using a liquid-liquid extraction. The sample and the extraction solvent were

shaken in a sealed bottle for about 25 minutes. The DCM was withdrawn after separation in a separatory funnel. The DCM extract was then concentrated to upto 100 μ l for analysis using a nitrogen blowdown apparatus. The organic analysis was performed based on EPA method 8270 for semivolatile organic compounds using a gas chromatography (Hewlett Packard Model 5890 Series 2) and a mass selective detector (GC-MSD) (Hewlett Packard Model 5971).

The samples collected during the second fog collection campaign were mostly used for organic analysis. Surrogate standards were added to the fogwater and the organics present in the fogwater were extracted into DCM. The DCM extract was then concentrated to about 4-5mL in a Kuderna-Danish apparatus. The sample from the Kuderna-Danish apparatus was further concentrated upto 100 μ L using a gentle stream of nitrogen. The concentration of surrogate standard in the final 100 μ L extract and the actual surrogate concentration added to the fogwater were used to calculate the extraction efficiency. This extraction efficiency was used to correct for the loss of organic compound during extraction and concentration procedures. The organic analysis was performed using gas chromatography (Agilent Technologies Model 6890) and a mass selective detector (GC-MSD) (Agilent Technologies Model 5973) based on EPA method 8270 for semivolatile organic compounds.

7.7 Data Analysis

The chromatograms from the organic analysis were analyzed by selecting compounds present with a spectral match of greater than 90%. Method blanks were analyzed and the organic compounds that appeared in the method blanks were removed from the fog-water organic analytes list. In addition to the method blanks, distilled

deionized water was sprayed on the strands of the fog collector and collected. This was used as fogwater collector blanks. Concentration of organic compounds that appeared in the fogwater collector blanks was deducted in the fogwater sample concentration. This deduction ensured that the reported organic species concentrations were only those present in the fogwater, and not due to the transfer of compounds (during fogwater impaction) adsorbed on the strands into fogwater. A list of commonly occurring analytes was identified and standards were obtained for these. External calibration standards and laboratory control samples (LCS) were used to quantify the GC-MSD analysis results. The concentrations of the final organic extracts were obtained from the chromatographic areas using the external calibration, the recovery percentages from the LCS analysis and the DCM extraction efficiency. The concentrations in the fogwater samples were calculated from the volumes of solvent and the fogwater sample. All other measurements were direct reports of the concentrations in the fogwater and required no calculations.

CHAPTER 8

FOGWATER CHEMISTRY: RESULTS AND DISCUSSIONS

8.1 Environmental Conditions During Fog Collection

Fogwater samples were collected in Baton Rouge, the capital city of Louisiana, which is situated approximately 200 miles inland from the Gulf of Mexico. The Mississippi River makes a bend around the city of Baton Rouge before flowing out into the Gulf of Mexico past New Orleans about 75 miles away. Figure 8.1 shows the location of the sampling site. Fog (generally radiation fog in Baton Rouge), see Figure 7.1, forms during between October and December in the fall and between March and April in the spring. In most cases fog forms during midnight hours and lasts typically through the early morning hours until the sun rises up.

Table 8.1a lists the conditions during first fog collection campaign, for the period between 2002 and 2004, using the high volume atmospheric fogwater collector. Seventeen fogwater samples were collected during this period in the metro Baton Rouge area. Most of the samples were collected during the spring in the month of March and during the fall season in the months of October and November (see Table 8.1). Most of these samples, listed in the Table 8.1, were obtained during the early morning hours in an area in the agricultural farm maintained by the LSU Agricultural Center. Figure 8.1 shows the location of the site. During this work, the atmosphere was in the neutral stability class with wind velocity ranging from 0 to 9 mph and temperature ranging from 45 to 69°F. In most cases, the started at midnight and dissipated in the morning lasting for about 6 to 8 hours.

Table 8.1a Description of conditions during fog collection (March 2002 to March 2004).

Date	Conditions During Fog	Duration of 1/4th mile Visibility (h)	Duration of 1/8th mile Visibility (h)	T (°F)	Range of wind velocity (mph)
3/15/02	Early Morning Fog	3.5	1		
11/11/02	Heavy Cloud Cover	1	1	68	Calm air
11/20/02	Heavy fog following heavy rain	4	2.5	53-58	Calm air
3/5/03	Heavy fog. Fog covered the entire gulf coast. Followed by rain.	8	2	58-61	3.5-5.7
3/14/03	Preceded by rain 24h earlier	2.5	1.5	57-59	4.6-8.0
3/18/03	Dense fog	5.5	1	55-65	3.5-9.2
3/27/03	Dense fog	2	1	60-62	0-5.7
10/25/03	Warm day prior to fog, cool night, clear sky, light fog	2	0	66-69	0-5.7
10/31/03	Warm day prior to fog, cool night, clear sky, heavy fog	5	4	63-67	0-8.0
11/1/03	Patchy fog, clear sky	4	0	63-65	3.5-5.7
11/2/03	Heavy fog, warm day, cool night	3.5	0	60-64	0-5.7
11/6/03	Cloudy sky, heavy fog	1	0.25	62-68	0-5.7
11/12/03	Thick fog, clear sky, cool night preceding	5.5	4.5	60-69	0-3.5
11/17/03	Thin patchy fog	1.5	0	67-68	Calm air
3/19/04	Warm day, cool night preceding fog, clear sky	3.5	1	57-63	Calm air
3/20/04	Hot to warm day, cool night preceding, clear sky	3.5	2.5	57-62	Calm air
3/30/04	Patchy fog	1	0	45-49	Calm air

* - Samples collected using high volume atmospheric fog collector.

Table 8.1b lists the conditions during fog collection, for the period between November 2004 and February 2005, using the two-stage size-fractionated CASCC, single-stage CASCC2 and the three-stage collector discussed in the previous chapter. The fogwater samples collected using these collectors yielded higher sample volume collected than the high volume atmospheric fogwater collector used in the first fog collection campaign. The samples were also cleaner (without insects and large dust particles) in the second campaign as the collectors were placed at about 10 feet from the ground.

Table 8.1b Description of conditions during fog collection (November 2004 to February 2005)

Date	Conditions During Fog	Duration of 1/4th mile Visibility (h)	Duration of > 1/8th mile Visibility (h)	T (°F)	Range of wind velocity (mph)
11/19/04	Overcast	1	0	64-67	3-5
11/21/04	Cloudy with dense fog	3	2	66-67	Calm air
01/09/05	Cloudy with heavy fog	5	0	43-51	3-4
01/10/05	Very Dense fog with overcast sky	2	12	57-58	3.0-5.0
01/11/05	Dense fog with clear to broken clouds	7	2	64-66	3.0-6.0
02/15/05	Fog under a Clear Sky. Cool night followed by hot to warm day.	7	0	62	0 - 5
02/16/05	Patchy fog with overcast sky.	0	0	64-65	5

* - Samples collected using single-stage CASCC, two-stage CASCCsf and a three-stage CASCC. Data obtained from NOAA: <http://cdo.ncdc.noaa.gov/ulcd/ULCD>

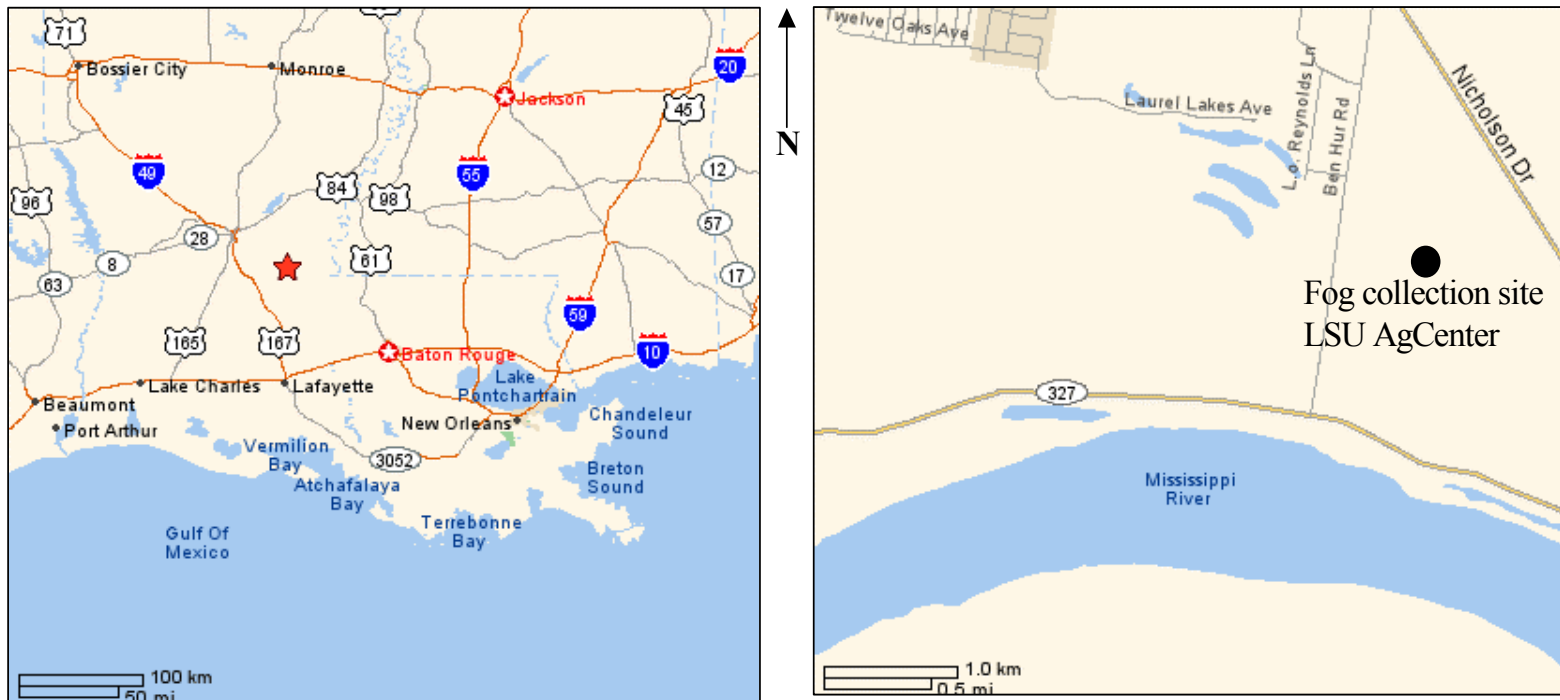


Figure 8.1. Location of sampling site.

8.2 Fogwater Composition

The characteristics such as pH, total organic carbon, total inorganic carbon and conductivity of fogwater are listed in the Table 8.2 below for the samples collected in the first campaign. The samples collected in the second campaign were exclusively used for organic species characterization. The pH of the fogwater averaged between 4.7 and 6.9, was similar to the variation observed in rainwater, between 4.7 and 6.9, in this region ([Braun, 1984](#)). The fogwater and rainwater from this region is not as acidic as in other parts of the United States ([West and Feagley, 1995](#), [NADP, 2004](#)).

Table 8.2 Comparison of the general characteristics of Fogwater collected in Baton Rouge and other parts of the United States and World. (Collected between 2002-2004)

Geographical Location	Urban or Non-Urban	N	pH	Org. C (mg/L)	Inorg. C (mg/L)	Cond. (μ S)	LWC [†] (g/m ³)
Baton Rouge, Louisiana (1)	Urban	15	6.1 (4.8-6.9)	97 (22-548)	6 (1-23)	255 (3-646)	0.020 (0.008-0.04)
Riverside, California (2)	Urban	16	4.3 (2.3-5.7)				
Pasadena, California (3)	Urban	8	(2.9-5.2)				
Corvallis, Oregon (4)	Non-Urban		5.6 (4.5-6.8)	178 (10-507)			0.06 (0.01-0.09)
Dubendorf, Switzerland (5)	Urban		(2.5-6.8)	(78-281)			(0.004-0.089)
Po Valley, Italy (6)	Urban		(2.5-6.8)	(15-108)			(0.1-0.3)
Strasbourg, France (7)	Urban	18	(3.5-4.0)				(0.004-0.05)
New Delhi, India (8)	Urban	43	(6.6-6.7)				

Note: Values within brackets are minimum and maximum. [†]LWC - Liquid Water Content

References: (1) this work (2) [Munger et al., 1983](#) (3) [Waldman et al., 1982](#) (4) [Muir, 1991](#) (5) [Johnson et al., 1987](#), [Capel et al., 1991](#) (6) [Gelencser et al., 2000](#), [Decesari et al., 2000](#) (7) [Millet et al., 1996](#) (8) [Ali et al., 2004](#).

The low pH of 4.7 for two fogwater samples coincided with high ion conductivities and organic carbon in the same samples. The mean organic carbon

concentration in fogwater samples ranged from 97mg/L and varied between 22mg/L and 548mg/L, which is typical of most fogwater samples. The ion conductivity which is an indication of the ion concentration in the samples, varied between 3 and 646 μ S. One of the observations made during the fog sampling was that short duration fog samples (low volume of collection) had more suspended solids than thicker fog samples (higher collection volume).

8.3 Ion Concentration

The ion compositions observed in the fogwater are compared to the other studies in the Table 8.2 below. The principal ions observed were ammonium, sulfate, nitrate and chloride. As in other urban areas, the same three ions (nitrate, sulfates, and chlorides) contribute the most to the overall anion concentration in this study. In addition to this and unlike other areas, ammonium concentrations were observed to be on the high side. The sulfate concentrations are higher than for other urban areas and showed a wide variation among the seventeen fog events in the Baton Rouge samples. The nitrate and chloride were more in line with concentrations from other areas, with notable higher chloride concentration in the Baton Rouge samples.

8.3.1 Ammonium

The observed higher ammonium concentration in the Baton Rouge samples was on the high side with a mean of 5764 μ m. The high concentration of this anion (ammonium) should be anticipated as the fog collection site was near the LSU agricultural farm, which uses ammonia fertilizers at various times during the year. Similar high concentrations of ammonium have been observed in other agricultural areas such as Riverside, California, Po Valley, Italy and Strasbourg, France. To a large extent,

it is possible to say that the large ammonium concentration compensates for the high nitrate and sulfate concentration to result in a near neutral pH of the fogwater in Baton Rouge.

Table 8.3. Comparison of ion concentrations (μM) for Fogwater from Baton Rouge and other parts of United States and the world. (Collected between 2002-2004)

Geographical Location	SO_4^{2-}	NO_3^-	NO_2^-	Br^-	Cl^-	F^-	PO_4^{3-}	NH_4^+
Baton Rouge, Louisiana (1)	1989 (854-4721)	2992 (1467-4962)	386 (76-1404)	24 (14-34)	2740 (360-7183)	50 (29-71)	206 (38-451)	5764 (194-14,118)
Riverside, California (2)	(715-3115)	(7050-28900)	-	-	(100-750)	-	-	(8340-25,800)
Pasadena, California (3)	(240-472)	(1220-3520)	-	-	(480-730)	(180-410)	-	(1290-2380)
Corvallis, Oregon (4)	56 (16-182)	102 (47-216)	-	-	84 (16-164)	-	-	361 (201-528)
Dubendorf, Switzerland (5)	(196-778)	(286-1293)	-	-	(113-11549)	-	-	1160 (336-2793)
Po Valley, Italy (6)	(230-8100)	(165-9250)	(4-510)	-	(0-695)	-	-	(560-12,750)
Strasbourg, France (7)	(2150-5020)	(1240-3410)	-	-	(1880-3110)	-	-	(630-12,640)
New Delhi, India (8)	(125-300)	(10-60)	-	-	(50-140)	(50-100)	-	(300-550)

Note: Values within brackets are minimum and maximum.

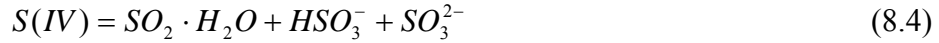
References: (1) this work (2) [Munger et al., 1983](#) (3) [Waldman et al., 1982](#) (4) [Muir, 1991](#) (5) [Johnson et al., 1987](#), [Capel et al., 1991](#) (6) [Gelencser et al., 2000](#), [Decesari et al., 2000](#) (7) [Millet et al., 1996](#) (8) [Ali et al., 2004](#).

8.3.2 Sulfate

The concentration of sulfate, in the aqueous phase, results from the gaseous SO_2 in the atmosphere that converts to sulfate in aerosols and fogwater. Sulfur dioxide gas dissolves in water to set up equilibria as shown in the following equation,



The individual reactions in equation (8.1) to (8.3) are fast ([Martin, 1984](#)). As seen from these equations, dissolved SO₂ contains three chemical species, namely, the hydrated SO₂ (SO₂·H₂O), the bisulfite ion (stable sulfonate form - HSO₃⁻) and the sulfite ion (SO₃²⁻). Due to the above different forms of dissolved SO₂ in solution, the oxidation state (+4) is used to denote these forms of SO₂ taken together as shown below,



The equilibrium constants for the equations (8.1) can be written in terms of the Henry's constant for SO₂ as shown in equation (8.5), and subsequently equilibrium constants for equation (8.2) and (8.3) are written as shown in equation (8.6) and equation (8.7).

$$K_{SO_2} = \frac{[SO_2 \cdot H_2O]_l}{p_{SO_2}} \Rightarrow \frac{1}{K_{SO_2}} = \frac{p_{SO_2}}{[SO_2 \cdot H_2O]_l} = \frac{1}{K_H} \quad (8.5)$$

$$K_1 = \frac{[HSO_3^-]_{l2} [H^+]_{l2}}{[SO_2 \cdot H_2O]_l} = [HSO_3^-]_{l2} [H^+]_{l2} \frac{1}{p_{SO_2} K_H} \quad (8.6)$$

$$K_2 = \frac{[SO_3^{2-}]_{l3} [H^+]_{l3}}{[HSO_3^-]_{l3}} = [SO_3^{2-}]_{l3} [H^+]_{l3}^2 \left[\frac{1}{K_1 p_{SO_2} K_H} \right] \quad (8.7)$$

The total SO₂ concentration that exists in the various forms, [SO₂·H₂O]_l, HSO₃⁻, and SO₃²⁻ in the aqueous phase is given by

$$[SO_2]_T = p_{SO_2} K_H \left(1 + \frac{K_1}{[H^+]} + \frac{K_1 K_2}{[H^+]^2} \right) \quad (8.8)$$

Based on the mean SO₂ air concentrations reported in the Baton Rouge area, it is possible to predict the fogwater S(IV) concentration by rewriting equation (8.8) as follows,

$$\sum [S(IV)]_{fog} = [SO_2]_{gas} RTK_H \left(1 + \frac{K_1}{[H^+]} + \frac{K_1 K_2}{[H^+]^2} \right) \quad (8.9)$$

where K_H (=1.23M/atm) represents the gas-liquid equilibrium Henry's Constant for SO_2 , K_1 (=1.3 x 10⁻² M) and K_2 (=6.6 x 10⁻⁸ M) are the dissociation constants for SO_2 ([Seinfeld and Pandis, 1998](#), [Johnson et al., 1987](#)).

Defining enrichment (ε) of the gas phase species in the aqueous phase as the ratio of the number of moles of the chemical species in the water phase to the total number of moles of the chemical species in the gas phase and water phase as $\varepsilon = \frac{n_w}{n_o}$, with

negligible surface adsorption, we have

$$\varepsilon = \frac{n_w^{SO_2}}{n_o^{SO_2}} = \frac{\left(\frac{V_w}{V_F} \right) \left(\frac{[SO_2]_{tot}}{[SO_2]_{gas}} \right)}{\left[\left(\frac{V_w}{V_F} \right) \left(\frac{[SO_2]_{tot}}{[SO_2]_{gas}} \right) + 1 \right]} \quad (8.6)$$

where V_w/V_F is the liquid water content of the foggy atmosphere (m³/m³) solving the above equation for $[SO_2]_{gas}$ and using equation (8.8) we have for SO_2 in equation (8.5) as,

$$[SO_2]_{gas} = [SO_2]_{tot} \left[1 + RTK_H \theta_L \left(1 + \frac{K_1}{[H^+]} + \frac{K_1 K_2}{[H^+]^2} \right) \right]^{-1} \quad (8.10)$$

The oxidized form of sulfur namely, sulfuric acid and sulfate is in the +6 oxidation state and is referred to as S(VI). The oxidation of S(IV) to S(VI) in the atmosphere is a well-known process and can be promoted by ozone in the atmosphere. Baton Rouge provides a highly oxidative atmosphere, with the concentration of ozone averaging about 80-100µg/m³ (1-hour average).

The Fogwater samples in Baton Rouge show high concentration of sulfate ion and due to the proximity to the Gulf of Mexico it is possible that the sulfate has a marine origin. The ratio of the sulfate to sodium is about 0.12 for seawater, and that of the Baton Rouge fogwater samples it is about 1.64. Absence of such a correlation between sodium and sulfate confirms the lack of marine input.

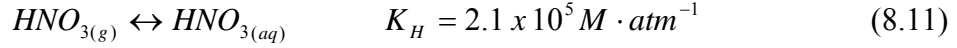
The pH of the droplet plays a critical role in the S(IV) concentrations and in determining which oxidant dominates the S(IV) concentration ([Seinfeld and Pandis, 1998](#), [Finlayson-Pitts and Pitts, Jr., 2000](#)). As the $[H^+]$ increases (or as pH decreases), more and more of SO_2 appears in the solution form, and hence the Henry's constant decreases. At the average pH of 6.45 for the Baton Rouge fogwater $[H^+]$ is 3.57×10^{-7} M. The average fogwater content, θ_L is $2 \times 10^{-8} m^3/m^3$. The predicted value of $S(IV)_{fog}$ from equation (8.5), for 2003 mean $[SO_2]_{tot}$ of $16 \mu g/m^3$ is $217 \mu M$. This prediction is based on the fact that only direct gas transfer of SO_2 to the droplets is considered. The observed value ($854-4721 \mu M$) of sulfate concentration is higher than the predicted value by more than 1 order of magnitude.

Sulfur dioxide emissions in Louisiana result largely from electric power plants, refineries, sulfuric acid production and carbon black production ([LaDEQ, 1999](#)) U.S. EPA estimates 44,924 tons of SO_2 were emitted in the East Baton Rouge Parish in 1999 and is prevalent pollutant at the fog sampling site ([US EPA, 2004](#)). Oxidation of S(IV) to S(VI) in the atmosphere is well known process and can be promoted by ozone. As mentioned earlier, high concentration of ozone observed in the Baton Rouge atmosphere indicates a high photochemical activity and thereby a highly oxidative atmosphere. Hence, with this we conclude that gas-to-particle conversion of SO_2 to SO_4^{2-} occurs

within the fog in the atmosphere to account for the discrepancy between the predicted and measured sulfate ion concentration in the fog water.

8.3.3 Nitrate

Nitric acid is one of the most water-soluble atmospheric gases with a Henry's law constant of 2.1×10^5 M/atm.



The nitric acid in the aqueous phase dissociates into nitrate as follows,



and thereby increasing its solubility. The dissociation constant for nitrate, K_1 , is 15.4M at 298K is given as follows,

$$K_1 = \frac{[NO_3^-][H^+]}{[HNO_{3(aq)}} \quad (8.12)$$

and by Henry's law we have the following relation,

$$K_H = \frac{[HNO_{3(aq)}}{P_{HNO_3}} \quad (8.13)$$

Using the definition for the Henry's constant and the dissociation constant we have the following relation,

$$[NO_3^-] = \frac{K_H K_1}{[H^+]} P_{HNO_3} \quad (8.14)$$

The total dissolved nitric acid [N(V)] is given as follows,

$$[N(V)]^T = [HNO_{3(aq)}] + [NO_3^-] \quad (8.15)$$

The total dissolved nitric acid in equilibrium with the nitric acid vapor can be deduced from the above the three equations (8.13) to (8.15) to equation (8.16) as follows ([Seinfeld and Pandis, 1998](#)),

$$[N(V)]^T = K_H P_{HNO_3} \left[1 + \frac{K_1}{[H^+]} \right] \quad (8.16)$$

Since the dissociation constant K_1 is very large (=15.4M) ($K_1/[H^+] \gg 1$) for a cloud or fogwater of any pH. Thus, $[NO_3^-] \gg [HNO_{3(aq)}]$ for all atmospheric droplets, and we can assume that dissolved nitric acid exists in clouds exclusively as nitrates, as nitric acid being a strong acid dissociates into nitrate ions upon dissolution in water. The total concentration of nitrates in the Fogwater sample is given as,

$$[N(V)]_{fog} = \frac{[NO_x]_{tot}}{\left(\theta_L + \frac{[H^+]}{K_H R T K_1} \right)} \quad (8.17)$$

The high concentration of nitrate in Fogwater represents the direct gaseous input of NO_x and nitrate from aerosols in the Baton Rouge atmosphere. Oxides of nitrogen are known inputs to rivers and streams in the Gulf Coast as reported by a recent survey by USGS (ESA, 1999). NO_x enters the atmosphere not only from agricultural sources in the predominantly agricultural areas of North Louisiana, but also from industrial emissions in Louisiana largely from compressor stations refineries, nitric acid plants and utilities. The total estimated NO_x emissions in the parish were 47,792 tons in 1999. As much as 15-18% of the input of nitrogen into streams of Louisiana have been attributed to atmospheric sources ([Alexander et al., 2000](#)). The LaDEQ has detected nitrogen oxides in the Baton Rouge air with annual mean concentrations of 33 and $30 \mu\text{g}/\text{m}^3$ for year 2002 and 2003, respectively ([US EPA, 2004](#)). From equation (8.17), with all the parameters

known the predicted concentration of nitrate in Fogwater sampled during this period varied between 1543 to 6366 μM . The much higher predicted value of implies that not all NO_x is converted to $[\text{NO}_3^-]$ exist as dissolved species.

8.3.4 Chloride

The chloride to sodium ratio of seawater is about 1.17. From the data in this work, the chloride to sodium ratio was determined to be 2.26. The larger ration of chloride to sodium concentration shows that the source of chloride is not only of marine origin. There are several industries in the Baton Rouge area that use chlorine as the feedstock to produce polyvinyl chloride, plastics and chlorinated solvents. Vinyl chloride is one of the most volatile organic compounds with emissions exceeding 16 tons and atmospheric concentrations in Louisiana ranging from 0.05 to 0.25 ppb_v ([Ford et al., 2000](#), [U.S. EPA, 2004](#)). Vinyl chloride has been shown to degrade to HCL in air with mean atmospheric residence time of 4hours ([Ford et al., 2000](#)). There are several other chlorinated compounds (chlorinated alkanes, chlorinated benzenes, hexachlorobutadiene, etc.) apart from direct chlorine discharges that have also been observed in Baton Rouge ([LaDEQ, 1999](#)). These emissions can also potentially contribute to the evolution of chloride in aerosols and thereby resulting in the fogwater. Refuse incinerators can also be a source of chloride in air, but they are not a major source in this area.

8.4 Metal Species Concentrations

The fogwater samples collected in the first campaign were analyzed for metals. Table 8.4 lists the various metals (total concentration) detected in the fogwater samples. The concentration of metals observed in the metals are similar in magnitude to those observed in other areas. The major ions observed in fogwater were Na, K, Ca, Fe, Al, Mg

and Zn. Of these Na, K, Ca and Mg were the predominant ones with mean concentrations $> 100\mu\text{M}$. There is evidence that sediment and soil composition in Baton Rouge area contain Ca and Mg. Hence, this supports the idea that metals in fogwater result primarily from the aerosol particles derived from the surface soil in the area ([Valsaraj, 2000](#)). Data from aerosol sampling at Baton Rouge further supports this idea ([Subramanyam, 1992](#)). Fe and Al are the two other predominant metals in Baton Rouge soils and sediments and also found in the fogwater. Al, Fe and Zn were present in the samples, at mean concentrations $< 100\mu\text{M}$.

Other metals that were found at smaller concentrations are As, Pb and Mn. Arsenic was observed in fogwater at a mean concentration of $0.32\mu\text{M}$. The likely source of Arsenic is fossil fuel combustion and long range transport. Lead was observed in fogwater at a mean concentration of $0.07\mu\text{M}$. Origin of lead in air can be traced to the use of tetra ethyl lead in gasoline as antiknock. The primary production of tetraethyl lead was in the Baton Rouge area and a known soil contamination of the same has been reported. Also, this region of the country has the largest Bauxite ore processing operation and New Orleans is known to have lead in soil and paints have been shown to be the main cause of higher levels of lead in children. However, lead observed as a minor pollutant in fogwater.

Mean air concentration of As, Pb and Mn in the Baton Rouge area has been reported to be $0.0011\mu\text{g}/\text{m}^3$, $0.0037\mu\text{g}/\text{m}^3$, $0.0012\mu\text{g}/\text{m}^3$ in $\text{PM}_{2.5}$ particulate samples collected as part of the urban air pollutant monitoring program during 82 separate occasions in East Baton Rouge parish during the year 2003 ([U.S. EPA, 2004](#)). Assuming that all of it result as dissolved species in fogwater. The predicted concentration of these

metals As, Pb and Mn in fogwater are As(0.73), Pb(0.89), Mn(1.1) in μM . The observed concentration (μM) of these metals in the fogwater are As(0.32), Pb(0.07), Mn(7.8). Considering the agreement between the predicted and observed concentrations we can conclude that aerosols are the likely sources of these metals in fogwaters in Baton Rouge.

Concentrations of copper observed were small (2 μM) but similar to those reported elsewhere ([Siefert et al., 1998](#)). The main sources of copper are anthropogenic and involve varied sources such as fossil fuel combustion, iron and steel manufacturing, and other nonferrous metal production industries ([Kieber et al., 2004](#)). The presence of heavy metal ions such as Mn and Fe in fogwater can potentially alter the uptake of gaseous species such as SO_2 in the droplet ([Barrie and Georgii, 1976](#), [Behr and Sigg, 1990](#)). Zn is one of those metals not frequently observed in fogwaters from other parts of the country. However it was observed in the present study at a mean concentration of 93 μM , and its source in this area is unknown.

Throughout the duration of this study, in general, higher concentrations for the principal ions and metals were observed for short duration, light, dissipating fog events. This indicates that if fog persists for a lengthy period of time a dilution effect will reduce the concentrations of ions and metals. This behavior has previously been noticed for California fogs ([Munger et al., 1983](#)). Time-series sampling of fog is therefore warranted to further understand the evolution of ion and metal concentrations in the Baton Rouge fogwater.

Table 8.4. Comparison of the total metal concentrations (μM) in fog water in Baton Rouge and other parts of the United States and the World. (For samples collected between March 2002 to March 2004).

Geographic Location	Na	K	Ca	Fe	Al	Mg	Zn	Mn	Pb	As	Cu
Baton Rouge, Louisiana(1)	1212 (304-3913)	328 (23-2359)	1342 (2-3425)	84 (2-223)	61 (1.8-429)	319 (33-1875)	93 (4-815)	8 (0.3-72)	0.07 (0.03-0.16)	0.32 (0.03-1.8)	2.6 (0.26-20)
Riverside, California (2)	(30-188)	-	(53-198)	-	-	(46-206)	-	-	-	-	-
Pasadena, California (3)	(12-500)	(4-53)	(9-265)	(1.7-31)	-	(3.5-180)	-	-	-	-	-
Corvallis, Oregon (4)	28 (5-85)	3 (2-20)	14 (3.5-89)	2.4 (0.1-18)	-	(14(4-40)	1.1 (0.2-4)	0.2 (0.07-0.47)	<0.12	-	-
Dubendorf, Switzerland (5)	(1-35)	(4-63)	(11-975)	-	-	(1-66)	(0.6-28.1)	-	(0.1-5.6)	-	(0.3-10.6)
Po Valley, Italy (6)	(30-765)	(11-145)	(5.5-242)	(0.5-42)	-	(2-120)	-	(0.1-11)	-	-	-
Strasbourg, France (7)	(120-3150)	(45-1260)	(54-3543)	(nd-304)	-	-	-	(nd-4.1)	(nd-24)	-	-
New Delhi, India (8)	(50-200)	(25-50)	(100-300)	-	-	(25-80)	(nd-174)	-	-	-	-

References: (1) this work (2) [Munger et al., 1983](#) (3) [Waldman et al., 1982](#) (4) [Muir, 1991](#) (5) [Johnson et al., 1987](#), [Capel et al., 1991](#) (6) [Gelencser et al., 2000](#), [Decesari et al., 2000](#) (7) [Millet et al., 1996](#) (8) [Ali et al., 2004](#).

8.5 Organic Species in Fogwater

8.5.1 Organic Species: Results of First Fog Collection Campaign

A number of organic compounds were observed in the Fogwater samples collected in this work using GC/MS analysis. These are present both as water-soluble organic compound (WSOC) and particle-associated organic compound (POC). In these samples no distinction was made between the POC and WSOC due to the survey nature of this investigation. Two class of organic compounds were identified in the Fogwater samples collected between 2002 and 2004, viz., linear alkanes and pesticides (shown in the first and third chromatogram in Figure 8.2). Several linear alkanes were observed in the interstitial air samples obtained simultaneously shown in the second chromatogram in Figure 8.2. These linear alkanes are established markers for aerosols in the atmosphere derived from petroleum combustion ([Shauer and Cass, 2000](#)). Hence, we can conclude that aerosols are the predominant source of alkanes in fogwater. In addition to this, several alkanolic acids and pesticides were identified in the Fogwater. Alkanolic acids have been known to result from oxidation of alkanes. The presence of pesticides (Atrazine and Metolachlor) was not surprising as the sample collection was near the LSU Agricultural Farm, which uses pesticides periodically during the year.

In the first fog collection campaigns (between 2002 and 2004) only very few compounds were quantified due to the limited nature of the sample volume and analytical workup. For example, the pesticide atrazine and two linear alkanes (pentadecane and tetratetracontane) were observed in the fog samples at quantifiable concentrations. The observed Fogwater concentration of atrazine varied from 0.39 $\mu\text{g}/\text{mL}$ to 0.89 $\mu\text{g}/\text{mL}$, 0.08 $\mu\text{g}/\text{mL}$ for pentadecane in one sample, and varied from 0.020 to 0.79 $\mu\text{g}/\text{mL}$ for n-

tetratetracontane in two samples. The respective aqueous solubility are 30 $\mu\text{g}/\text{mL}$ for atrazine, $8 \times 10^{-5}\mu\text{g}/\text{mL}$ for pentadecane at 298K, while there are no reported aqueous solubility for n-tetratetracontane. For atrazine the Fogwater concentrations are much less than the aqueous solubility, whereas for pentadecane it is 3 orders of magnitude larger than the aqueous solubility.

Realizing that very little information was derived on the organic compounds constituting the dissolved organic fraction from the first fog collection campaign, a second fog collection campaign (see Table 8.1b) was undertaken, where organic species characterization was the focus. The analytical procedure and other details are described in section 7.6 and 7.7. The organic compounds identified in the second campaign were grouped into three classes, namely, the aromatics and aromatic derivatives, alkanes and alkane derivatives, and the third group of acids, alcohols and amides. Simultaneous collection of air samples that were in contact with the fogwater droplets enables us to characterize the organic composition of the air sample, and also determine the droplet-to-vapor partition constant (K_{DV}). The constant K_{DV} is the ratio of the concentration of droplet and the concentration of vapor phase.

8.5.2 Organic Species: Results of Second Fog Collection Campaign

8.5.2.1 Aromatics and Derivatives

Table 8.5a and 8.5b lists the average and range of concentrations of aromatics and derivatives observed in the fogwater and in the air samples, respectively. Most of the compounds observed in the air and fogwater samples are generally pesticides used in agricultural areas, due to automobile emissions or fossil fuels. For example, 1, 2, 4-trimethylbenzene (TMB) is a component of diesel fuel, present naturally in coal tar and

petroleum crude oil. The compounds such as 1,2,4 trimethyl benzene, 1,2,3 trimethyl benzene, and 1,2,3,4-tetramethyl benzene are insoluble in water ([Weast, 1974](#)). Their presence and solubility in fogwater may be enhanced due to the presence of surface-active organic matter.

Table 8.5a. Aromatics and Derivatives: Average and Range fogwater concentrations.

Compound	Average Fogwater concentration [ng/mL]	Range Fogwater concentration [ng/mL]
1,2,4-Trimethyl Benzene	17.96	12.52 – 23.40
1,2,3-Trimethyl Benzene	0.44	0.166 – 0.718
1,2-diethyl Benzene	<d.l.	<d.l.
1,2,3,4-tetramethyl Benzene	0.07	0.04 – 0.1
Naphthalene	<d.l.	<d.l.
Quinoline	1.21	0.254 – 5.223
2-methyl-Naphthalene	<d.l.	<d.l.
1,6-dimethyl-Naphthalene	<d.l.	<d.l.
Dibenzofuran	<d.l.	<d.l.
1,6,7-trimethyl-Naphthalene	<d.l.	<d.l.
Atrazine	2.32	0.201 – 7.861
Phenanthrene	0.101	0.101
9,10-Anthracenedione	0.115	0.048 – 0.231
1,8-Naphthalic anhydride	0.200	0.083 – 0.368

<d.l.-lower than detection limit. Note: Detection limit depends on component mass present in liquid sample.

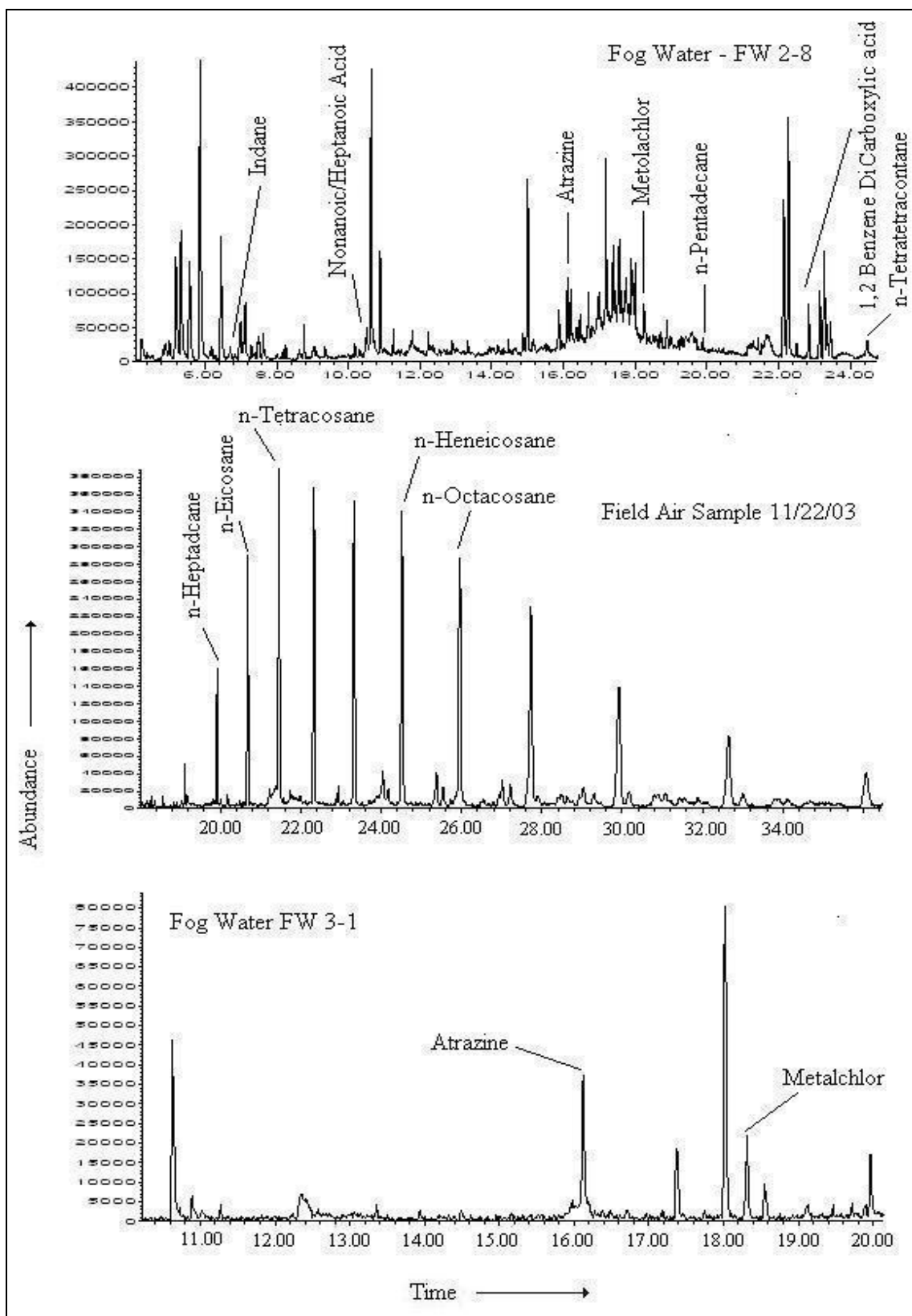


Figure 8.2. GC/MS traces of fogwater and air samples collected between 2002-2004.

Table 8.5b. Aromatics and Derivatives: Average and Range air concentrations.

Compound	Average air concentration [ng/L]	Range air concentration [ng/L]
1,2,4-Trimethyl Benzene	0.276	0.038 – 0.301
1,2,3-Trimethyl Benzene	0.031	0.0116 – 0.043
1,2-diethyl Benzene	0.008	0.008
1,2,3,4-tetramethyl Benzene	0.010	0.002 – 0.022
Naphthalene	0.023	0.008 – 0.069
Quinoline	<d.l.	<d.l.
2-methyl-Naphthalene	0.048	0.009 – 0.14
1,6-dimethyl-Naphthalene	0.008	0.0015 – 0.028
Dibenzofuran	0.0007	0.0009 – 0.001
1,6,7-trimethyl-Naphthalene	0.0009	0.0004 – 0.002
Atrazine	<d.l.	<d.l.
Phenanthrene	0.0034	0.001 – 0.006
9,10-Anthracenedione	<d.l.	<d.l.
1,8-Naphthalic anhydride	<d.l.	<d.l.

<d.l.-lower than detection limit. Note: Detection limit depends on component mass present in liquid sample.

Based on the average concentrations observed in the fogwater and air, the droplet-to-vapor concentrations (K_{DV}) are much larger than given by the equilibrium Henry's constant. Table 8.5c lists the K_{DV} values, computed based on the field data listed in Table 8.5a and 8.5b, for the compounds observed both in the fogwater and air. The higher K_{DV} observed can be characterized due to surface adsorption or enhanced dissolution in the aqueous phase due to presence of surface-active organic matter. For an organic carbon concentration of 16.5mg/L in the water droplet spiked with Fulvic acid in DTA ([see Section 4.5](#)) resulted in a droplet-to-vapor partition constant (K_{DV}) of about 600 for phenanthrene, and the field observed K_{DV} value for phenanthrene was 29,504, for an average organic carbon concentration observed in the fogwater, from this work, was about 97mg/L and ranged from 22mg/L to 548mg/L. Hence, this several fold higher K_{DV}

can be corroborated from our laboratory observation to the presence of organic matter in the Fogwater, in addition to other processes such as surface adsorption.

Table 8.5c. Comparison of Henry's constant with K_{DV} computed based on field data.

Compound	K_{DV}	K_{WA}^*
1,2,4-Trimethyl Benzene	64,949	4.5
1,2,3-Trimethyl Benzene	14,350	7.2
1,2,3,4-tetramethyl Benzene	7,147	5.0
Phenanthrene	29,504	704

* - From [Schwarzenbach et al., 2003](#)

From Table 8.5a and 8.5b, we notice the presence of 9,10-Anthracenedione and 1,8-Naphthalic anhydride exclusively in the aqueous phase, and not present in the vapor phase. [Mmereki et al., 2004](#) observed similar products for anthracene adsorbed at the air-water interface due to heterogeneous reactions. Also in this work, oxidation of naphthalene (discussed in chapter 6) and phenanthrene (not reported in this dissertation) by ozone on the surface of micron-sized droplets showed similar reaction products. Thus, we can conclude that the source of these compounds in the fogwater may be from surface of solid aerosol particles formed due to heterogeneous oxidation of anthracene and naphthalene.

Another objective in this work was to illustrate the importance of surface adsorption and the interface partition constant (K_{IA}) resulting in higher droplet-to-vapor partitioning (K_{DV}). The 50% theoretical size cut (i.e., size of droplets collected with 50% efficiency) for the second stage in the CASCCsf (see chapter 7 for details) is about $4\mu\text{m}$ while the 50% theoretical size cut for the first stage was predicted to be $23\mu\text{m}$ ([Demoz et al., 1996](#)). The concentration of the atrazine observed in the first stage was 2.7ng/mL and a higher concentration of 3.56ng/mL was observed in the second stage. Unfortunately, the K_{DV} could not be computed for this compound, as atrazine was not detected in the air

phase. This can be attributed to the inefficiency of the polymer bed to adsorb atrazine present in the vapor phase. Nevertheless, the observed higher concentration of atrazine in the fogwater droplets collected from the second-stage may be due to surface adsorption phenomena and accumulation of atrazine on the surface of smaller sized fog droplets. Also it was noted that for fog events that lasted longer times, the concentration of the organic compounds reduced with time showing that dilution effect will reduce the concentrations and these results are listed in Table 8.5d. Sample SF1–011005–01 was collected and removed after 2 hours of the fog event, while the sample 02 collection was started at the end of 2 hours and removed at the end of 7 hours, and sample 03 was started at the end of 7 hours and removed at the end of 11 hours, after the fog event. Similar observations of the dilution effect observed in this work for metals and for organics were observed in California fogs by [Munger et al., 1983](#).

Table 8.5d. Scavenging and dilution effect of fogwater on the gas phase pollutants with time. (Concentration of compounds found in fogwater).

Sample i.d.	Tricosane [ng/mL]	Atrazine [ng/mL]
SF1 – 011005-01	1.1	4.47
SF1 – 011005-02	0.8	0.90
SF1 – 011005-03	0.0	0.82

8.5.2.2 Alkanes and Derivatives

Table 8.6a and 8.6b lists the various alkanes and its derivatives observed in the fogwater samples collected during the second fogwater collection campaign. As observed in the first fogwater collection campaign, alkanes ranging from C6 to C44 was observed and the fogwater samples collected in the second campaign was quantitated for the various alkanes as listed in the Table 8.6a. Alkanes present in the air samples were also quantitated and are listed in Table 8.6b.

Most of the alkanes listed are due to fossil fuel combustion and exist as particulates in the atmosphere ([Schauer and Cass, 2000](#)). As mentioned in the earlier, aerosols are dominant sources for alkanes in fogwater. Lack of aerosol sampling in this work precludes further confirmation. Several compounds observed in the fogwater was also observed and quantitated in the air that was in contact with the fogwater. Based on the average concentrations observed in the air and fogwater, K_{DV} values can be computed based on the observed field data for the alkanes and its derivatives. These values are listed in Table 8.6c.

Table 8.6a. Alkanes and Derivatives: Average and Range fogwater concentrations.

Compound	Average Fogwater Concentration [ng/mL]	Range Fogwater Concentration [ng/mL]
Dodecane	n.d.	n.d.
Hexacosene	n.q.	n.q.
Hexadecane	0.88	0.88
Nonadecane	n.d.	n.d.
Pentadecane	n.d.	n.d.
Tetradecane	n.d.	n.d.
Heneicosane	n.d.	n.d.
Octacosane	4.37	1.37 - 7.34
Pentacosane	6.92	1.67 - 15.77
Tricosane	2.34	0.71 - 5.91
2,6,10,14,18,22-Tetracosahexaene	n.q.	n.q.
Eicosane	n.d.	n.d.
Docosane	3.15	3.15
Nonadecene	n.d.	n.d.
Octadecane	10.49	10.49
Hexacosane	2.04	0.53 - 4.94
Nonacosane	9.52	3.75 - 19.702
Tetracosane	6.03	3.06 - 11.97
1,2, - dichlorocyclohexane	n.q.	n.q.
Tricosene	n.q.	n.q.
1-Bromo-11-iodoundecane	n.q.	n.q.

n.d. – not detected; n.q. – not quantitated

Table 8.6c compares the K_{DV} values based on the average concentration of two alkanes observed in the field fogwater samples and bulk phase equilibrium Henry's constant. As observed for aromatic compounds, the deviations from Henry's law are several orders of magnitude, attributed to the presence of surface-active organic matter.

Table 8.6b. Alkanes: Average and Range air concentrations.

Compound	Average Air Concentration [ng/L]	Range Air Concentration [ng/L]
Dodecane	0.067	0.0326 - 0.121
Hexacosene	n.q.	n.q.
Hexadecane	0.004	0.003 - 0.008
Nonadecane	0.003	0.0018 - 0.005
Pentadecane	0.093	0.0316 - 0.206
Tetradecane	0.080	0.035 - 0.172
Heneicosane	0.030	0.0137 - 0.046
Octacosane	2.480	0.0589 - 5.496
Pentacosane	1.534	0.041 - 3.687
Tricosane	0.788	0.281 - 1.294
2,6,10,14,18,22-Tetracosahexaene	n.q.	n.q.
Eicosane	0.026	0.0121 - 0.049
Docosane	0.200	0.0126 - 0.617
Nonadecene	0.002	0.002
Octadecane	0.033	0.0228 - 0.044
Hexacosane	4.457	0.035 - 10.313
Nonacosane	4.546	0.188 - 7.3
Tetracosane	1.385	0.54 - 2.229
1,2, - dichlorocyclohexane	n.q.	n.q.
Tricosene	n.q.	n.q.
1-Bromo-11-iodoundecane	n.q.	n.q.

Table 8.6c. Comparison of Henry's constant with K_{DV} computed based on field data.

Compound	K_{DV}	K_{WA} *
Hexadecane	20,6126	0.21
Octadecane	315,008	0.81

* - From [Schwarzenbach et al., 2003](#)

CHAPTER 9

CONCLUSIONS AND POSSIBLE FUTURE DIRECTIONS

8.1 Conclusions

Mass transfer and uptake of aromatic vapors into micron-sized droplets was studied using a droplet train apparatus. The mass transfer of benzene to falling water droplets in air is liquid-phase diffusion-controlled, whereas that of phenanthrene is gas-phase diffusion and interface mass accommodation-limited. Droplet-to-vapor partition constant for droplet sizes 14 to 200 μm were determined showing higher enrichment for smaller size droplets. This was attributed to surface adsorption and more pronounced surface accumulation of vapor phase chemicals at the gas-water interface of smaller sized droplets. The mass accommodation coefficient, the probability of collision of a gas molecule resulting in solvation, for benzene was much lower than that for phenanthrene. For all the compounds studied accommodation coefficients decreased with increasing temperature.

In order to understand the influence of gas phase oxidant (ozone) on the uptake and mass transfer of aromatic vapors into droplets, a modified form of the falling droplet apparatus was used. The presence of ozone in the gas phase increased the rate of mass transfer into the droplets. The Langmuir-Hinshelwood mechanism was used to model the pseudo first order rate constant for the surface reaction of ozone with the adsorbed PAH molecule. Reaction products observed due to surface reactions were same as the bulk phase ozonolysis.

Knowledge gained from laboratory studies were extended to field fogwater sampling and characterization. Several aromatic compounds such as 1,2,4-trimethyl

benzene, 1,2,3,4-tetramethyl benzene, pentadecane, phenanthrene were found at concentration exceeding their aqueous solubility and in certain cases exceeding the predicted bulk phase Henry's constant. This observation can be attributed to presence of surface-active organic matter in the fogwater. Pesticides, such as atrazine, were found at higher concentrations in smaller sized fog droplets in comparison to larger sized fog droplet. This observation is in line with the laboratory observation signifying the importance of surface adsorption and accumulation at the gas-water interface.

8.2 Possible Future Directions

Atmospheric chemistry entails a complex combination of gaseous, aqueous, and surface processes involving a wide variety of compounds, both organic and inorganic. Knowledge and input from diverse fields such as chemical engineering, fluid mechanics, physics, chemistry, mathematics and atmospheric sciences and meteorology is necessary in order to understand our atmospheric environment better.

In the heterogeneous oxidation on the droplet surface performed in this study, no gas phase reaction products were detected with the analytical methodology used. However, release of surface bound heterogeneous reaction products into the gas phase has been recognized ([Thomas et al., 2001](#)). This release of surface bound reaction products has also been acknowledged to influence the make-up the atmospheric composition. A suitable analysis, such as fluorescence spectroscopy, may be used to probe the release of surface bound reaction products ([Sayer et al., 2003](#)).

Heterogeneous reactions on aerosol particles coated with condensed gas phase chemical species is of interest to researchers in atmospheric sciences ([Morris et al., 2002](#)). These particulates also serve as nucleation sites for the formation of cloud,

fogwater and raindrops and thereby contributing to the chemical composition of fogwater. [Ravishankara, 1997](#) notes that our ability to predict atmospheric composition relies on understanding microphysics of particle formation. Changes in size distribution of these particulate matters due to heterogeneous reactions on particle surface and its resulting influence in microphysics and particle nucleation and formation is a possible area of interest.

In all of these interesting areas of research numerical simulations by solving general constitutive equations and mathematical models can aid in understanding further the details of these complex processes.

REFERENCES

- Adamson, A.W., *Physical Chemistry of Surfaces* (4th Ed.), John Wiley and Sons, 1982.
- Ahrens, D., "Meteorology Today – An Introduction to Weather, Climate and the Environment", Thompson, Brooks and Cole Publishers, New York, 2000.
- Alexander, R.B., Smith, R.A., and Schwarz, G.E., "Effect of stream channel size on the delivery of nitrogen to the Gulf of Mexico", *Nature*, 2000, Vol. 403, pp. 758-761.
- Ali, K., Momin, G.A., Tiwari, S., Safai, P.D., Chate, D. M., and Rao, P.S.P., "Fog and precipitation chemistry at Delhi, North India", *Atmospheric Environment*, 2004, Vol. 38, pp. 4215-4222.
- Allen, B.L., "Uneasy Alchemy: Citizens and Experts in Louisiana's Chemical Corridor Disputes", MIT Press, Cambridge, MA, 2003.
- Andelman, J.B., and M.J. Suess (1970) Polynuclear aromatic hydrocarbons in the water environment. *Bull. Wld. Hlth. Org.* 43: 479-508.
- Andelman and Snodgrass (1972) Incidence and significance of polynuclear aromatic hydrocarbons in the water environment. *CRC crit. Rev. environ. Contr.* 4(1): 69-83.
- Andrews, E., and S.M. Larson, "Effect of Surfactant Layers on the Size Changes of Aerosol Particles as a Function of Relative Humidity", 1993, *Environmental Science & Technology*, Vol. 27, pp. 857-865.
- Atkins, P., "Physical Chemistry", Oxford University Press, New York, 1998, pp.998-1002.
- Baek, S.O., Field, R.A, Goldstone, M.E., Kirk, P.W., Lester, J.N., and Perry, R. (1991) "A review of atmospheric polycyclic hydrocarbons: sources, fate and behavior, *Water. Air soil pollut.* 60, 279-300.
- Bamford, H.A.; Poster, D.L.; Baker, J.E. Temperature Dependence of Henry's Law Constants of Thirteen Polycyclic Aromatic Hydrocarbons between 4 °C and 31 °C; *Environ. Toxicol. Chem.* 1999, 18, 1905-1912.
- Bailey, P.S. *Ozonation in Organic Chemistry, Volume II: Non-olefinic Compounds*, Academic Press, New York, 1982.
- Barrie, L.A. and Georgii, H.W., "An experimental investigation of the absorption of sulfur dioxide by water drops containing metal ions", *Atmos. Environ.*, 1976, Vol. 10, pp. 743-749.

Behr, P. and Sigg, S., "Evidence of redox cycling of iron in atmospheric water Droplets", *Nature*, 1990, Vol. 244, pp. 419- 421.

Bertram, A.K.; Ivanov, A.V.; Hunter, M. Molina, L.T., Molina, M.J. The reaction 12 probability of OH on organic surfaces of tropospheric interest. *J. Phys. Chem. A*. 13 2001, 105, 9415-9421.

Bingham, E., Trosset R. P., Warshawsky D., "Carcinogenic potential of petroleum-hydrocarbons - critical-review of the literature", *Journal of environmental pathology and toxicology*, 1979, 3 (1-2), pp. 483-563.

Braun, R.D., "A study of the pH of rain in Lafayette, Louisiana", *Proc. La. Acad. Sci.*, 1984, XLVII, pp. 42-44.

Burby, R. J., "Baton Rouge: The making (and breaking) of a petrochemical paradise' in Centuries of Change: Transforming New Orleans and Its Environs", Craig Colten (Editor), University of Pittsburgh Press, Pittsburgh, PA, 2000.

Cabani, S.; Gianni, P.; Mollica, V.; Lepori, L., "Group Contributions to the Thermodynamic Properties of Non-Ionic Organic Solutes in Dilute Aqueous Solution", *J. Solution Chem.* 1981, 10, 563-595.

Capel, P.D., Gunde, R., Zuckerman, F., Giger, W., "Carbon speciation and surface tension of fog", *Environmental Science and Technology* 24, 722-727, 1990.

Capel, P.D., Luenberger, C. and Giger, W., "Hydrophobic organic chemicals in urban fog", *Atmospheric Environment*, 1991, Vol. 25A, 1335-1346.

Cappiello, A. et al., "Molecular Characterization of the Water-Soluble Organic Compounds in Fog-water by ESIMS/MS", *Environmental Science and Technology*, 2003, 37, 1229-1240.

Collett Jr., J.L., Hoag, K. J., Sherman, D. E., Bator, A. and Richards, L.W., "Spatial and temporal variations in San Joaquin Valley fog chemistry", 1999, *Atmospheric Environment*, Vol. 33, pp. 129- 140.

Collett, J.L., Bator, A., Sherman, D.A., Moore, K.F., Hoag, K.J., Demoz, B.B., Rao, X., and Reilly, J.E., "The chemical composition of fogs and intercepted clouds in the United States", 2002, *Atmos. Res.*, Vol. 64, 29-40.

Cruickshank, A.J.B., Windsor, M.L., and Young, C.L., *Proc. Roy. Soc., Ser. A* 295, 259 (1965).

Crutzen, P. J. and M. G. Lawrence, "The impact of precipitation scavenging on the transport of trace gases:A 3-dimensional model sensitivity study", *J. Atmos. Chem.*, 37, 81-112, 2000.

Danckwerts, P.V., "Absorption by simultaneous diffusion and chemical reaction into particles of various shapes and into falling drops", Transactions of Faraday society, 1951, Vol. 47, pp. 1014-1023.

Daube, B.C. Jr., Flagan, R.C., and Hoffman, M.R., "Active cloudwater collector", United States Patent No. 4,697,462, 1987.

Davidovits, P., Hu, J.H., Worsnop, D.R., Zahniser, M.S., Kolb, C.E., "Entry of Gas Molecules into Liquids", Faraday Disc., 1995, 100, 65-82.

De Maagd, P.G., Ten Auscher, D.T., Van Den Devil, H., Opperhuizen, A., Siam, D.T.H.M., "Physicochemical Properties of Polycyclic Aromatic Hydrocarbons: Aqueous Solubilities, N-Octanol/Water Partition Coefficients, and Henry's Law Constants", Environ. Toxicol. Chem. 1998, 17, 251-257.

Decesari, S., Facchini, M.C., Fuzzi, S., and Tagliavini, E., "Characterization of water-soluble organic compounds in atmospheric aerosol: a new approach", 2000, Journal of Geophysical Research, Vol. 105, pp. 1481-1489.

Demoz, B.B., Collett Jr., J.L., Daube Jr., B.C., "On the Caltech active strand Cloudwater collectors", Atmospheric research, 41, (1996), pp. 47-62.

Eisenreich, S.J., Looney, B.B., Thornton, J.D., 1981. Airborne organic contaminants in the Great Lakes ecosystem. Environmental Science and Technology 15, 30-38.

Facchini, M.C., Mircea, M., Fuzzi, S., Charlson, R.J., 1999, "Cloud albedo enhancement by surface-active organic solutes in growing droplets", Nature, Vol. 401, pp. 257-259.

Facchini, M.C., Decesari, S., Mircea, M., Fuzzi, S., Loglio, G., "Surface tension of atmospheric wet aerosol and cloud/fog droplets in relation to their organic carbon content and chemical composition", Atmos. Environ., 34, pp. 4853-4857, 2000.

Ford, D. R., Pederson, B., and Thibodeaux, L.J., "Movement of chemical in the industrial corridor: A community-focused summary", TOSC Report, Hazardous Substance Research Center/South & Southwest, Louisiana State University, Baton Rouge, Louisiana, 2000.

Finlayson-Pitts, B.J. and Pitts, J.N. Jr., "Atmospheric Chemistry: Fundamentals and Experimental Techniques", Wiley, New York, 1986.

Finlayson-Pitts, B. J., and Pitts, Jr., J. N., "Chemistry of the upper and lower atmosphere: theory, experiments, and applications", Academic Press, San Diego, 2000.

Franks, H.S., and Evans, M., J. Chem. Phys., 13, 507, 1945.

- Fuchs, N., "The mechanics of aerosols", Pergamon press, New York, 1964.
- Gard et al., "Direct Observations of Heterogeneous Chemistry in the Atmosphere", Science, Vol. 279, 1998, pp. 1184-1187.
- Gelencser, A., Sallai, M., Krivacsy, Kiss, G., and Meszaros, "Voltammetric evidence for the presence of humic-like substances in fog water", Atmos. Res., 2000, Vol. 54, pp. 157-165.
- Gill, P.S., Graedel, T.E., Weschler, C.J., "Organic films and atmospheric aerosol particles, fog droplets, cloud droplets, raindrops and snow lakes", Reviews of Geophysics and Space Physics, 21, 903-920, 1983.
- Glotfelty, D.E., Seiber, J.N., and Liljedahl, L.A., "Pesticides and other organics in fog", in Proceedings of EPA/APCA Symposium on measurements of toxic air pollutants: U.S. EPA/Air Pollution Control Association, 1986, pp.168-175.
- Glotfelty, D. E.; Seiber, J. N.; Liljedahl, L. A., "Pesticides in fog", Nature (1987), 325(6105), 602-5.
- Glotfelty, D. E., Majewski, M. S., Seiber, J. N., "Distribution of Several Organophosphorous Insecticides and their Oxygen Analogues in a Foggy Atmosphere", Environ. Sci. Technol., 1990, 24 (4), 353-357.
- Golden, D.M., Spokes, G.N., and Benson, S.W., " Very Low-Pressure Pyrolysis (VLPP): A versatile kinetic tool," Angew. Chem., Int. Ed. Engl., 1973, 12, pp. 534-546.
- Goss, K.U., and Schwarzenbach, R.P., "Empirical prediction of heats of vaporization and heats of adsorption of organic compounds", Environ. Sci. Technol., 33, pp. 3390-3393, 1999.
- Harkins and Brown, F.E., J. Amer. Chem. Soc., 41, 499 (1919).
- Hanson, D.R., and Lovejoy, E.R., Journal of Physical Chemistry, 1996, 100, 6397-6405.
- Hanson, D.R., "Surface-Specific reactions on liquids", Journal of Physical Chemistry B, 1997, Vol. 101, pp. 4998-5001.
- Hanson, D.R., Sugiyama, M., Morita, A., "Revised kinetics in the droplet train apparatus due to wall loss", Journal of Physical Chemistry, 2004, 108, 3379-3744.
- Herckes, P., Hannigan, M.P., Trenary, L., Lee, T., and Collett Jr., J.L., "Organic compounds in radiation fogs in Davis (California)", 2002, Atmospheric Research, 64, pp. 99-108.

Hering, S.V., Blumenthal, D.L., Brewer, R.I., Gertler, A., Hoffmann, M., Kadlec, J.A., Pettus, K., "Field Intercomparison of Five Types of Fogwater Collectors", 1987, *Environmental Science and Technology*, Vol. 21, pp. 654-663.

Hoff, J. T.; Mackay, D.; Gillham, R.; Shiu, W. Y. Partitioning of Organic Chemicals at the Air-Water Interface in Environmental Systems. *Environ. Sci. Technol.* 1993, 27, 2174-2180.

Huff, A. K., and Abbatt, J. P. D., "Gas-Phase Br₂ Production in Heterogeneous Reactions of Cl₂, HOCl, and BrCl with Halide-Ice Surfaces", *J. Phys. Chem. A* 2000, 104, 7284-7293.

Iraci, L. T., Essin, A. M., and Golden, D. M., "Solubility of Methanol in Low-Temperature Aqueous Sulfuric Acid and Implications for Atmospheric Particle Composition", *J. Phys. Chem. A* 2002, 106, 4054-4060.

Jacob, D.J., Waldman, J.M., Haghi, M., Hoffman, M.R., Flagan, R.C., "An instrument to collect fogwater for chemical analysis", *Rev. Sci. Instrum.*, Vol. 56, pp. 1291-1293.

Jacob, D.J., Waldman, J. M., Munger, J. W., and Hoffmann, M. R., "Chemical composition of fogwater collected along the California coast", *Environmental Science and Technology*, Vol. 19, 1985, 730-736.

Jacob, D. J., "Heterogeneous chemistry and tropospheric ozone", *Atmospheric Environment*, 2000, 34, pp. 2131-2159.

Jayne, J. T., Duan, S. X., Davidovits, P., Worsnop, D. R., Zahniser, M. S., Kolb, C. E., *J. Phys. Chem.* 1992, 96, 5452-5455.

Jenkins, B.M., Jones, A.D., Turn, S.Q., and Williams, R.B., "Particle concentration, gas-particle partitioning, and species intercorrelations for Polycyclic aromatic hydrocarbons (PAH) emitted during biomass burning", *Atmospheric Environment*, 1996, 30, pp. 3825-3835.

Johnson, C. A., Sigg, L., and Zobrist, J., "Case studies on the chemical composition of fogwater: The influence of local gaseous emissions", *Atmos. Environ.*, 1987, Vol. 21, 2365-2374.

Kalberer, M., Paulsen, D., Sax, M., Steinbacher, M., Dolmen, J., Prevot, A.S.H., Fisseha, R., Weingarten, E., Frankevich, V., Zenobl, R., Baltensperger, U., "Identification of Polymers as Major Components of Atmospheric Organic Aerosols", *Science* 2004, 303, 1659-1662.

Karger, B. L.; Castells, R. C.; Sewell, P. A.; Hartkopf, A. Study of the Adsorption of Insoluble and Sparingly Soluble Vapors at the Gas-Liquid Interface of Water by Gas Chromatography. *J. Phys. Chem.* 1971, 75, 3870-3879.

Katrib, Y., Deiber, G., Schweitzer, F., Mirabel, P., George, C., J. Aerosol Sci. 32 (2001) 893.

Katrib, Y. et al., "Products and mechanisms of ozone reactions with oleic acid for aerosol particles having core-shell morphologies", Journal of Physical Chemistry A, 2004, Vol. 108, 6686-6695.

Keiber, R. J., Skrabal, S.A., Smith, C., and Willey, J.D., "Redox speciation of copper in rainwater: Temporal variability and atmospheric deposition", Environ. Sci. Technol., 2004, Vol. 38, pp. 3587-3594.

Kemball, C., Rideal, E. K., "The Adsorption of Vapors on Mercury. I. Non-Polar Compounds", Proc. R. Soc. (London) 1946, A187, 53-73.

Kirchner, W., Welter, F., Bongartz, A., Kaines, J., Schweighoefer, S., Schurath, U., Journal of Atmospheric Chemistry, 1990, 10, 427-449.

Kochetkov, A., Smith, J.S., Ravikrishna, R., Valsaraj, K.T., Thibodeaux, L.J., "Air-Water Partition Constants for Volatile Methyl Siloxanes", Environ. Toxicol. Chem., 2001, 20, pp. 2184-88.

Kolb, C.E., Worsnop, D.R., Zahniser, M.S., Davidovits, P., Keyser, L., Leu, M.E., Molina, M.J., Hanson, D.R., Ravisankara, A.R., Williams, L.R., Tolbert, M.A., "Laboratory Studies of Atmospheric Heterogeneous Chemistry. In Progress and Problems in Atmospheric Chemistry", Baker, J.R., Ed., World Scientific Publishing: Singapore, 1995; Chapter 5, pp. 771-875.

Kolb, C.E., Davidovits, P., Jayne, J.T., Shi, Q., and Worsnop, D.R., "Kinetics of trace gas uptake by liquid surfaces", Progress in Reaction Kinetics and Mechanism", 2002, Vol. 27, pp. 1-46.

Latif, M.T., and Brimblecombe, P., "Surfactants in atmospheric aerosols", 2004, Environmental Science and Technology, Vol. 38, pp. 6501-6506.

Lee, S.C., Ho, K.F., Chan, L.Y., Zielinska, B., Chow, J.C., "Polycyclic aromatic hydrocarbons (PAHs) and Carbonyl compounds in the urban atmosphere of Hong Kong", Atmospheric Environment, 35, (2001) 5949-5960.

Lewis, S. C.; King, R. W.; Cragg, S. T.; Hillman, D. W. Skin carcinogenic potential of petroleum hydrocarbons: crude oil, distillate fractions and chemical class subfractions. Advances in Modern Environmental Toxicology (1984), 6 (Appl. Toxicol. Pet. Hydrocarbons), 139-50.

Li, Y.Q., Davidovits, P., Shi, Q., Jayne, J.T., Worsnop, D.R., Jayne, J.T., Kolb, C.E., Worsnop, D.R., “Mass and Thermal Accommodation Coefficients of H₂O(g) on Liquid Water as a Function of Temperature”, *J. Phys. Chem. A*, 105, 10627-10634, (2001).

Limbeck, A., and Puxbaum, H., “Dependence of in-cloud scavenging of polar organic aerosol compounds on the water solubility”, *Journal of Geophysical Research*, 2000, Vol. 105, pp. 19857-19867.

Louisiana Department of Environmental Quality, OAQRP- Air Quality Information Center, http://www.deq.state.la.us/evaluation/air_indicators/so_2.htm , La DEQ, Baton Rouge, Louisiana, 1999.

Mackay, D., Shiu, W.Y., “A Critical Review of Henry’s Law Constants for Chemicals of Environmental Interest”, *J. Phys. Chem. Ref. Data*. 1981, 10, 1175-1199.

Mackay, D.; Shiu, W. Y.; Valsaraj, K. T.; Thibodeaux, L. J. “Air-Water Transfer- The role of Partitioning” in *Air-Water Mass Transfer*, S. C. Wilhelms and J. S. Gulliver (Editors), ASCE, New York, NY (1991)

Martin, L.R., “Kinetic studies of sulfite oxidation in aqueous solutions”, in *SO₂, NO, and NO₂ Oxidation Mechanisms: Atmospheric Consideration*, Acid Precipitation Series, pp. 63-100, Butterworth, Stoneham, MA, 1984.

Masel, R.I., “Principles of Adsorption and reaction on solid surfaces, John Wiley & Sons, New York, 1st edition, 1996.

McFarland, A. R., Gong, H., Muyschondt, A., Wentz, W. B., Anand, N. K., “Aerosol Deposition in Bends with Turbulent Flow”, *Environmental Science and Technology*, 1997, 31(12), 3371-3377.

McMurry, P.H., and Stolzenburg, M.R., “Mass Accommodation Coefficients from Penetration Measurements in Laminar Tube Flow”, *Atmospheric Environment*, 1987, Vol. 21, pp. 1231-1234.

Middleton, P. et al., “Theoretical estimates of the relative importance of various urban sulfate aerosol production mechanisms”, *Atmospheric Environment*, 14, 1980, 463-472.

Millet, M., Sanusi, A., and Wortham, H., “Chemical composition of fogwater in an urban area: Strasbourg (France)”, 1996, *Environ. Poll.*, Vol. 94, pp. 345-354.

Mmerekki, B.T.; Donaldson, D.J.; Gilman, J.B.; Eliason, T.L.; Vaida, V., “Kinetics and products of the reaction of gas-phase ozone with anthracene adsorbed at the air-aqueous interface”, *Atmos. Environ.*, 2004, Vol. 38, pp. 6091-6103.

Moller, D., “Kinetic model of atmospheric SO₂ oxidation based on published data, *Atmospheric Environment*, 14, 1980, 1067-1076.

Morris, J.W., Davidovits, P., Jayne, J.T., Jimenez, J.L., Shi, Q., Kolb, C.E., Worsnop, D.R., Barney, W.S., Cass, G., “Kinetics of submicron oleic acid aerosols with ozone: A novel aerosol mass spectrometric technique”, *Geophysics Research Letters*, Vol. 29, No. 9, 10.1029/2002GL014692, 2002.

Muir, P.S., “Fogwater chemistry in a wood-burning community, Western Oregon”, *J. Air Waste. Mgmt. Assoc.*, 1991, Vol. 41, 32-38.

Müller, B., and Heal, M. R., “Mass Accommodation Coefficients of Phenol, 2-Nitrophenol, and 3-Methylphenol over the Temperature Range 278-298 K”, *J. Phys. Chem. A* 2002, 106, 5120-5127.

Munger, W. J., Jacob, D.J., Waldman, J.M., and Hoffmann, M.R., “Fogwater chemistry in an urban atmosphere”, *Journal of Geophysics Research*, 1983, 88(C9), 5109-5121.

Munger et al., *Fogwater Chemistry at Riverside, California*, *Atmos. Environ.*, 24(B), 185-205, 1990.

Nathanson, G.M., Davidovits, P., Worsnop, D.R., and Kolb, C.E., “Dynamic and kinetics at the gas-liquid interface”, *J. Phys. Chem.*, 100, pp. 13007-13020, 1996.

National Atmospheric Deposition Program (NSRP-3)/National Trends Network, 2004, NADP Program Office, Illinois State Water Survey, 2204 Griffith Drive, Champaign, IL 61820.

Neff, J. M., “Poly-cyclic Aromatic Hydrocarbons in the aquatic environment, sources fates and biological effects”, *Applied science publishers limited*, 1979.

Nikolaou, K., Masclet, P., and Mouvier, G. (1984) Sources and Chemical reactivity of polynuclear aromatic hydrocarbons in the atmosphere. A critical review, *Sci Total Environ.*, 32, 103-132.

Okochi, H., Sugimoto, D., Igawa, M., “The enhanced dissolution of some chlorinated hydrocarbons and monocyclic aromatic hydrocarbons in rainwater collected in Yokohama, Japan”, *Atmospheric Environment*, 2004, Vol. 38, pp. 4403-4414.

Pandis, S.N., and Seinfeld, J.H., “Should bulk cloudwater and Fogwater samples obey Henry’s Law?”, *Journal of Geophysical research*, Vol. 96, No. D6, pp. 10,791-10,798, 1991.

Pankow, J.F., and Bidleman, T.F. (1991) "Effects of temperature, TSP and percent non-exchangeable material in determining the gas-particle partitioning in organic compounds", *Atmos. Environ.*, 24A, 2695-2698.

Perona, M. J. The Solubility of Hydrophobic Compounds in Aqueous Droplets. *Atmos. Environ.* 1992, 26A, 2549-2533.

Peters, J.A., Deangelis, D.G., and Hughes, T.W. (1981) in *Chemical Analysis and Biological Fate: Polynuclear Aromatic Hydrocabons* edited by M. Cooke and A.J. Dennis Battelle press, Columbus, OH, pp. 571-582.

Petersen, R.W., "Giants on the River – A Story of Chemistry and the Industrial Development on the Lower Mississippi River Corridor", Homewsite Company, Baton Rouge, Louisiana, 1999.

Poschl, U.; Letzel, T.; Schauer, C.; Niessner, R. Interaction of ozone and water vapor with spark discharge soot aerosol particles coated with benzo[a]pyrene: O₃ and water adsorption, benzo[a]pyrene degradation, and atmospheric implications. *J. Phys. Chem. A.* 2001, 105, 4029-4041.

Pöschl, U., "Formation and Decomposition of Hazardous Chemical Components Contained in Atmospheric Aerosol Particles", *Journal of Aerosol Medicine*, 2002, Vol. 15, No. 2, pp. 203-212.

Pruppacher, H.R., and Klett, J.D., "Microphysics of Clouds and Precipitation", Kluwer Academic Publishers, Dordrecht, Germany, pp. 700-791, 2003.

Raja, S., Yaccone, F. S., Ravikrishna, R., Valsaraj, K. T., "Thermodynamic Parameters for the Adsorption of Aromatic Hydrocarbon Vapors at the Gas-Water Interface", *Journal of Chemical and Engineering Data*, 2002, 47(5), pp. 1213-1219.

Raja, S., "Adsorption of aromatic hydrocarbons at gas-water interface", 2003, Thesis, 81pp., Louisiana State University, Department of Chemical Engineering.

Ramdahl, T., Schjodager, J., Currei, L.A., Hanssen, J.E., Moller, M., Klouda, G.A., and Alfheim, I. (1984) Ambient impact of residential wood combustion in Elverum, Norway *Sci. Total Environ.*, 36, 81-90.

Rayleigh L., "On the instability of jets", *London Math. Soc.*, 1879, 10:361–71.

Ravishankara, A.R., "Heterogeneous and multiphase chemistry in the troposphere", *Science*, Vol. 276, 1997, pp. 1058-1065.

Reid, J.P., and Sayer, R.M., "Chemistry in the clouds: the role of aerosols in atmospheric chemistry", *Science Progress* (2002), 85 (3), 263–296.

Reynolds S.T., Liu M.K., Hecht T.A., Roth P.M., Seinfeld J.H., “Mathematical modeling of photochemical air pollution--3. Evaluation of the model”, *Atmospheric Environment*, 1974, Vol. 8(6), pp. 563-96.

Richards, L.W., et al., Hydrogen peroxide and sulfur (IV) in Los Angeles cloud water, *Atmos. Environ.*, 17, 911-914, 1983.

Sajo, E., Raja, S., “A three-dimensional indoor aerosol transport model”, *Health Physics*, v. 82, n. 6, pp. S169 - S170, 2002.

Saxena, P.; Hildemann, L. M. Water-Soluble Organics in Atmospheric Particles: A Review of the Literature and Application of Thermodynamics to Identify Candidate Compounds. *J. Atmos. Chem.* 1996, 24, 57-109.

Saylor, J. R., and Handler, R. A., “Gas transport across an air/water interface populated with capillary waves”, *Phys. Fluids* 9 (9), September 1997.

Sayer, R.M., Gatherer, R.D.B., and Reid, J.P., “A laser induced fluorescence technique for determining the pH of water droplets and probing uptake dynamics”, *Phys. Chem. Chem. Phys.*, 2003, Vol. 5, pp. 3740–3747.

Schauer, J.J., and Cass, G. R., “Source apportionment of wintertime gas-phase and particle-phase air pollutants using organic compounds as tracers”, *Environ. Sci. Technol.*, 2000, Vol. 34, pp. 1821-1832.

Schomburg, Charlotte J.; Glotfelty, Dwight E.; Seiber, James N., “Pesticide occurrence and distribution in fog collected near Monterey, California”, *Environmental Science and Technology*, 1991, 25(1), 155-60.

Schwarzenbach, R.P.; Gschwend, P.M.; Imboden, D.M. *Environmental Organic Chemistry*; 2nd ed.; Wiley: New York, 2003.

Schwell, M. et al., “Uptake Dynamics and Diffusion of HCl in Sulfuric Acid Solution Measured in Single Levitated Micro-droplets”, *J. Phys. Chem. A* 2000, 104, 6726-6732.

Seinfeld, J.H., “*Atmospheric Chemistry and Physics of Air Pollution*”, Wiley, New York, 1986.

Seinfeld, J.H., and Pandis. S.N., “*Atmospheric Chemistry and Physics*”, John Wiley & Sons, Inc., New York, NY, 1998.

Seinfeld, J.H., “Air Pollution: A Half Century of Progress”, *Environmental and Energy Engineering*, Vol. 50, No. 6, 2004, pp. 1096-1108.

Shi, Q., Li, Q., Davidovits, P., Jayne, J. T., Worsnop, D. R., Mozurkevich, M., Kolb, C. E., "Isotope exchange for gas-phase ethanol and acetic acid at aqueous surfaces", *Journal of Physical Chemistry B*, 1999, 103, 2417-2430.

Shimono, A., Koda, S., "Laser-Spectroscopic Measurements of Uptake Coefficients of SO₂ on Aqueous Surfaces", *Journal of Physical Chemistry*, 1996, 100, 10269-10276.

Siefert, R.L., Johansen, A.M., Hoffmann, M.R., and Pehkonen, S.O., "Measurements of trace metal (Fe, Cu, Mn, Cr) oxidation states in fog and stratus clouds", *J. Air and Waste Manage. Assoc.*, 1998, Vol. 48, pp. 128-143.

Smith, G.D. et al., "Reactive uptake of ozone by oleic acid aerosol particles: Application of single particle mass spectrometry to heterogeneous reaction kinetics", *J. Phys. Chem. A*, 2002, 106, 8085-8095.

Schnelle-Kries, J. et al., "Occurrence of particle-associated polycyclic aromatic compounds in ambient air of the city of Munich", *Atmospheric Environment*, 35(1), 2001, S71-S81.

Schwartz, S.E., "Mass transport considerations pertinent to aqueous phase reactions of gases in liquid water clouds", In *Chemistry of multiphase atmospheric systems*, NATO ASI series, Springer-Verlag, Berlin, 1986, pp. 415-472.

Shi, Q., Li, Q., Davidovits, P., Jayne, J. T., Worsnop, D. R., Mozurkevich, M., Kolb, C. E., "Isotope exchange for gas-phase ethanol and acetic acid at aqueous surfaces", *Journal of Physical Chemistry B*, 1999, 103, 2417-2430.

Staudinger, J.; Roberts, P.V.A. Critical Review of Henry's Law Constants for Chemicals of Environmental Interest; *Crit. Rev. Environ. Sci. Technol.* 1981, 26, 205-197.

Subramanyam, V., "Study of Vapor-to-Particle Partitioning of Semi-volatile Organic Compounds in Urban Atmosphere", M.S. Thesis, Louisiana State University, Baton Rouge, Louisiana, 1992.

Subramanyam, V.; Valsaraj, K. T.; Reible, D. D.; Thibodeaux, L. J., "Gas-to-Particle Partitioning of PAHs in an Urban Atmosphere", *Atmos. Environ.* 1994, 28, 3083-3091.

Vieceli, J., Roeselov, M., Tobias, D. J., "Accommodation coefficients for water vapor at the air/water interface", *Chemical Physics Letters* 393 (2004) 249-255.

Sumner, A.L.; Menke, E. J.; Dubowski, Y.; Newberg, J.T.; Penner, R.M.; Hemminger, J.C.; Wingen, L.M.; Brauers, T.; Finlayson-Pitts, B.J. The nature of water on surfaces of laboratory systems and implications for heterogeneous chemistry in the troposphere. *Phys. Chem. Chem. Phys.* 2004, 6, 604-613.

Thomas, E. R., Frost, G.J., Rudich, Y., “Reactive Uptake of Ozone by Proxies for Organic Aerosols: Surface-bound and Gas-Phase Products”, *Journal of Geophysical Research*, 2001, Vol. 106, No. D3, pp. 3045-3056.

Tolocka, M. P., Saul, T. D., and Johnston, M. V., “Reactive Uptake of Nitric Acid into Aqueous Sodium Chloride Droplets Using Real-Time Single-Particle Mass Spectrometry”, *Journal of Physical Chemistry A*, 2004, 108, 2659-2665.

Ulmke, H.; Meitschke, M.; Bauckhage, K., “Piezoelectric Single Nozzle Droplet Generator for Production of Monodisperse Droplets of Variable Diameter“, *Chem. Eng. Technol.* 2001, 24, 69-70.

U. S. Environmental Protection Agency, Air Data- Monitor Summary Report, 28 2004, <http://www.epa.gov/air/data/monsum.html>.

Vacha, R.; Slavicek, P.; Mucha, M.; Finlayson-Pitts, B.J.; Jungwirth, P. Adsorption of atmospherically relevant gases at the air/water interface: Free energy profiles of aqueous solvation of N₂, O₂, O₃, OH, H₂O, HO₂ and H₂O₂. *J. Phys. Chem. A*. **2004**, 108, 11573-579.

Valsaraj, K. T. On the Physicochemical Aspects of Partitioning of Nonpolar Hydrophobic Organics at the Air-Water Interface. *Chemosphere* 1988, 17, 857-887.

Valsaraj, K. T.; Thoma, G. J.; Reible, D. D.; Thibodeaux, L. On the Enrichment of Hydrophobic Organic Compounds in Fog Droplets. *Atmos. Environ.* 1993, 27, 203-210.

Valsaraj, K. T., “Elements of Environmental Engineering - Thermodynamics and Kinetics”, 2nd ed.; CRC Press: Boca Raton, FL, 2000.

Van Ry, D., Gigliotti, C., Glenn IV, T., Nelson, E., Totten, L.A., Eisenreich, S.J., Vol. 36, No. 15, 2002, *Environmental Science & Technology*, pp.-3201

Wadia, Y.; Tobias, D. J.; Stafford, R.; Finlayson-Pitts, B.J. Real-time monitoring of the reaction of ozone with an unsaturated phospholipid at the air-water interface. *Langmuir*, 2000, 16, 9321-30.

Waldman, J.M., Munger, J.W., Jacob, D.J., Flagan, R.C., Morgan, J.J., and Hoffmann, M.R., “Chemical composition of acid fog”, 1982, *Science*, 218, 677-680.

Waldman, J.M., Munger, J.W., Jacob, D.J., and Hoffman, M.R., “Chemical characterization of stratus cloud water and its role as a vector for pollutant deposition in a Los Angeles pine forest”, *Tellus*, 1985, 37B, pp. 91-108.

Weast, R.C., “Handbook of chemistry and physics”, CRC Press Inc., Cleveland, Ohio, 1974.

West, L.M., and Feagley, S.E., "The chemical composition of atmospheric deposition collected from six Louisiana sites from 1983 to 1992", *Atmos. Environ.*, 1995, Vol. 29, pp. 1211-1217.

Wilhelmy, *Ann. Phys.*, 119, pp. 177, (1863).

Winiwarter, W et al., Organic acid gas and liquid measurements in Po valley fall-winter conditions in the presence of fog, *Tellus*, 40(B), 348-357, 1988.

Worsnop, D. R.; Zahniser, M. S.; Kolb, C. E.; Gardner, J. A.; Watson, L. R.; Van Doren, J. M.; Jayne, J. T.; Davidovits, P., "Temperature dependence of mass accommodation of SO₂ and H₂O₂ on aqueous surfaces", *J. Phys. Chem.* 1989, 93, 1159.

Worsnop, D. R., Morris, J. W., Shi, Q., Davidovits, P., Kolb, C.E., "A chemical kinetic model for reactive transformations of aerosol particles", *Geophysical Research Letters*, 2002, 29, 10.1029/2002GL015542.

Yang, J. C., Chien, W., King, M., Grosshandler, W. L., "A simple piezoelectric droplet generator", *Experiments in Fluids* (1997), 23(5), 445-447.

Zappoli, S.; Andracchio, A.; Fuzzi, S.; Facchini, M. C.; Gelencsér, A.; Kiss, G.; Krivásky, Z.; Molnár, A.; Mezős, E.; Hansson, H. C.; Rosman, K.; Zebuhr, Y., *Atmospheric Environment*, 1999, 33, 2733-2743.

Zhang, Q., Anastasio, C., "Chemistry of fog waters in California's Central Valley Part 3: concentrations and speciation of organic and inorganic nitrogen", *Atmospheric Environment* 35 (2001) 5629-5643.

VITA

Suresh Raja graduated from Boston Matriculation Senior Secondary School, Madras, India, in 1994. He then attended University of Madras from 1994 to 1998 to earn a bachelor's degree in chemical engineering. In fall 1998, he was the recipient of the graduate school award at American University, Washington, D.C. He came to the LSU graduate school in 1999 to earn a master's degree in physics and continued graduate studies in chemical engineering to earn a master's degree. He is currently a doctoral candidate at LSU.

His list of publications and presentations that resulted out of this project thus far, funded by the United States National Science Foundation include:

Raja, S., and Valsaraj, K.T., "Heterogeneous Oxidation of Naphthalene Adsorbed on the Surface of Micron-Size Water Droplets by Ozone in Air", *Journal of Air and Waste Management Association*, in press (2005).

Raja, S., Ravikrishna, R., Kommalapati, R. R., and Valsaraj, K.T., "Environmental Monitoring of Fogwater Chemistry in the Gulf Coast Urban Industrial Corridor: Baton Rouge (Louisiana)", *Environmental Monitoring and Assessment*, in press (2004).

Raja, Suresh; Valsaraj, Kalliat T. Uptake of Aromatic Hydrocarbon Vapors (Benzene and Phenanthrene) at the Air-Water Interface of Micron-Size Water Droplets. *Journal of the Air and Waste Management Association*, (2004), Vol. 54(12), 1550-1559.

Raja, Suresh; Valsaraj, Kalliat T. Adsorption and Transport of Gas-Phase Naphthalene on Micron-Size Fog Droplets in Air. *Environmental Science and Technology* (2004), 38(3), 763-768.

Raja, S.; Valsaraj, K. T.; Andrews, T.; Kommalapati, R. R.; Ravikrishna, R., "Adsorption of aromatic hydrocarbon vapors at the air-water interface and atmospheric wet deposition process", Preprints of Extended Abstracts presented at the ACS National Meeting, American Chemical Society, Division of Environmental Chemistry (2003), 43(1), 892-898.

Raja, S., "Adsorption of aromatic hydrocarbons at gas-water interface", Thesis, 81 pages, Louisiana State University, Department of Chemical Engineering, Baton Rouge, 2003.

Raja, S., Yacone, F., Ravikrishna, R., Valsaraj, K. T., "Adsorption of aromatic hydrocarbon vapors at the gas-solid and gas-water interface", Proceedings of the Air & Waste Management Association's Annual Conference & Exhibition, 95th, Baltimore, MD, United States, June 23-27, 2002 (2002), 231-240.

Raja, S., Yacone, F. S., Ravikrishna, R., Valsaraj, K. T., "Thermodynamic Parameters for the Adsorption of Aromatic Hydrocarbon Vapors at the Gas-Water Interface", J. Chem. Eng. Data, 2002, Vol. 47(5), pp. 1213-1219.